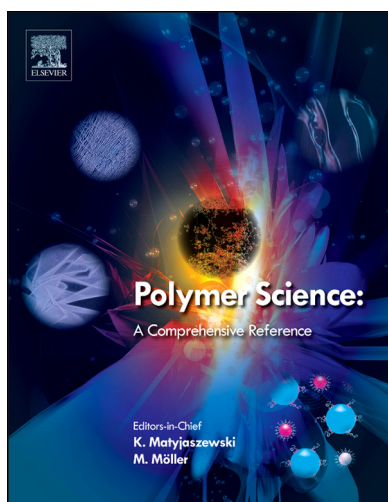


Provided for non-commercial research and educational use.
Not for reproduction, distribution or commercial use.

This chapter was originally published in *Polymer Science: A Comprehensive Reference* published by Elsevier, and the attached copy is provided by Elsevier for the author's benefit and for the benefit of the author's institution, for non-commercial research and educational use including without limitation use in instruction at your institution, sending it to specific colleagues who you know, and providing a copy to your institution's administrator.



All other uses, reproduction and distribution, including without limitation commercial reprints, selling or licensing copies or access, or posting on open internet sites, your personal or institution's website or repository, are prohibited. For exceptions, permission may be sought for such use through Elsevier's permissions site at:

<http://www.elsevier.com/locate/permissionusematerial>

Peng H, Nieuwendaal R, and Soles CL (2012) Polymer Dynamics in Constrained Geometries. In: Matyjaszewski K and Möller M (eds.) *Polymer Science: A Comprehensive Reference*, Vol 7, pp. 345–376. Amsterdam: Elsevier BV.

© 2012 All rights reserved.

7.18 Polymer Dynamics in Constrained Geometries

H Peng, R Nieuwendaal, and CL Soles, NIST Polymers Division, Gaithersburg, MD, USA

Published by Elsevier B.V.

7.18.1	Introduction	345
7.18.2	The Nature of Confinement	346
7.18.3	Techniques to Quantify Dynamics	347
7.18.3.1	Calorimetry	347
7.18.3.2	Dielectric Spectroscopy	348
7.18.3.3	Dynamic Mechanical Spectroscopy and Related Mechanical Approaches	351
7.18.3.4	Mechanical Surface Probes	353
7.18.3.5	Diffusion Experiments	354
7.18.3.6	Flow Experiments	356
7.18.3.7	X-ray Techniques	357
7.18.3.8	Inelastic Neutron Scattering	358
7.18.3.9	Fluorescence Measurements	361
7.18.3.10	Nuclear Magnetic Resonance	364
7.18.3.11	Brillouin Light Scattering	365
7.18.3.12	Modeling and Simulation	366
7.18.4	Physical Mechanisms of Confinement	368
7.18.4.1	Finite Size versus Surface Interactions	369
7.18.4.2	Chain Conformation and Molecular Mass	369
7.18.4.3	Entanglement Density	370
7.18.4.4	Cooperative and Collective Motions	370
7.18.4.5	Nonequilibrium Effects	371
References		372

7.18.1 Introduction

The widespread interest in the dynamical property of organic materials under strong states of confinement largely began with differential scanning calorimeter (DSC) measurements in the early 1990s of the glass transition and heat capacity of glass-forming liquids imbibed in a nanoporous support matrix.¹ These seminal studies evidenced reductions in the glass transition temperature (T_g) and the step increase of heat capacity that accompanies T_g for the small-molecule liquids encapsulated in controlled pore glasses with pore diameters in the 4–73 nm range, with smaller diameters leading to larger deviations. Within a few years, these finite-size studies quickly spread to polymeric systems in the form of thin films. Several manuscripts appeared almost simultaneously reporting thickness-induced deviations in the glass transition temperature of spin-cast polymer films when the film thickness dropped below a critical value. The first of these reports appeared in 1994 using spectroscopic ellipsometry^{2,3} to track the thermal expansion behavior of the polymer films as a function of thickness, identifying thickness-induced shifts in the apparent glass transition temperature. Within a few years, there were similar reports based on Brillouin light scattering (BLS),^{4,5} specular X-ray reflectivity (XRR),^{6–8} and positron annihilation lifetime spectroscopy.^{9,10} Not surprisingly, the results from the different techniques when applied to slightly different material systems did not always agree. The debates sparked a wave of literature that has continued to grow over the past two decades.

Discussions on the glass transition of confined polymer systems are often couched in the context of polymer dynamics. Macroscopically, the glass transition is associated with the

thermal softening point of the polymer. A common line of thinking has been to equate a reduced thin film T_g with an increase in the dynamic activity of the polymer or an increase of the T_g with a reduction of the polymer mobility. This connection is primarily based on the concept of time–temperature superposition (TTS) and that relaxation times at different temperatures can be directly compared by a simple shift in the timescale of the relaxation process. Under certain circumstances, it is a very reasonable assumption. However, if the nature of the motion or dynamic response becomes fundamentally different, then this line of thinking can break down. The concept of time–thickness (or some other confinement length scale) is not always valid. For example, consider a mode of polymer relaxation that involves the collective motions of several segments of the polymer chain (such as the glass transition). There is a length scale associated with this collective motion and it is feasible that the state of confinement curtails or cuts off the extent of the collective motion. Large-scale and long-range motions that involve many segments will naturally move slowly or at a low frequency. Curtailing the long-range motions by confinement would decrease mobility by suppressing the long-range motions. Any dynamic modes that remain in the polymer would naturally be shorter range and probably faster or higher in frequency. It is common to identify a T_g from a kink or a change in the temperature dependence of an observable, such as thickness or heat capacity, that is related to a dynamic process such as thermal expansion. The kink occurs when the timescale for the relaxation affecting the observable starts to change at a rate slower than the cooling or heating rate; the system enters or leaves a nonequilibrium state depending on whether it is being cooled or heated. Now, return to the

example above about the collective motion that is suppressed on the long-range, low-frequency side by the state of confinement. The remaining fast motions in the system can be cooled to lower temperatures before dropping out of equilibrium with the cooling rate. This would result in a lower apparent T_g upon confinement, despite the fact that the mobility of the system has been hindered. In this example, the simple argument of a reduced T_g equating to increased mobility is not correct. Confinement has altered the fundamental nature of the relaxation responsible for the glass transition.

The focus of this chapter is to review the different methods that have been used to quantify the dynamics in polymers under strong states of confinement. We have purposely limited the scope of this review to include only those measurement methods which directly measure polymer dynamics and ignore, for the sake of length, those that measure an indirect property that can be related to a dynamic process such as T_g . For example, we include inelastic neutron scattering in this review because a single measure of the energy gained or lost by a neutron scattered from a confined polymer can tell you what dynamic motions are present in the polymer. As a counter example, we do not address techniques such as specular XRR or spectroscopic ellipsometry which can quantify the thickness of a thin film, despite the fact that the temperature dependence of the thickness can also be used to interpret either the coefficient of thermal expansion or the thin film T_g , both properties that are influenced by polymer dynamics. Moreover, as mentioned above, it is well recognized that within this vast body of literature focused on the dynamics of polymers under confinement, there are many unresolved conflicts and disagreements between the different techniques, measurements, and systems. We make no attempt to unify this body of sometimes controversial or conflicting literature into a single picture. Over the past two decades, several review articles and book chapters have attempted to do this.^{11–15} Rather, in this review, we focus squarely on the measurements and the physics behind the measurements. Our intent is to help the reader better understand what is being measured by each technique and then point them to several of the leading or major references in that area. To the best of our knowledge, such a review has been lacking in the scientific literature.

7.18.2 The Nature of Confinement

There are many ways in which polymers can be placed in strong states of confinement. Before delving into the different ways in which polymer dynamics can be measured under confinement, we should discuss the different ways in which polymers can be confined. The most commonly encountered and well-defined geometry is the planar film. It is straightforward to spin-cast smooth, planar films onto any number of supporting substrates. If the substrate is atomically smooth, it is generally possible to create polymer films with almost no additional roughness using the spin-coating technique. The thickness of the film is readily controlled by changing either the concentration of the polymer in solution or the spin-casting rate. The thin film approach is attractive because the thickness can easily be quantified using techniques such as XRR, ellipsometry, or profilometry; in these situations, there is very little ambiguity as to what the length scale of confinement is. Here, we refer to this

geometry as ‘thin film confinement’. The schematic in Figure 1 depicts the concept of thin film confinement. The thin film confinement case can be further classified by the nature of the confining interface. Supported thin films are left on the substrate, which is generally more rigid than the polymer itself. Free-standing thin films are somehow released from the substrate and placed on a holder that suspends them without other materials touching the film.

The other extreme is to confine a polymeric material inside a porous cavity or support. There are many examples of nanoporous support media, including zeolites, Vycor, controlled pore glasses, anodic aluminum oxide (AAO) membranes, and porous templates made by vitrifying self-assembled surfactants or block copolymers. Here, we refer to this as ‘nanopore confinement’. In all these examples, the porous support is usually a glassy or ceramic-like material that is significantly harder than the polymer. This creates rigid confinement in three dimensions, whereas thin film confinement often has a free surface as one of the confining walls. A cartoon of nanopore confinement geometry is provided in Figure 1. For most measurements, the dynamics of the rigid porous support media are negligible compared to the soft polymer inside the pore. One of the biggest advantages of the nanopore confinement route is that the amount of confined polymer can be significant, making measurements straightforward. The porosities of the confining media are often on the order of 30% by volume, meaning that a few grams of the support media contain several hundred milligrams of the confined polymer. This makes measuring the response of the confined material much easier than the thin film case where a square centimeter of a 10 nm thick film will contain approximately 1×10^{-7} g of polymer. The signal-to-noise ratio is usually significantly better in nanopore confinement cases in comparison to thin films. The difficulty with nanopore confinement is usually getting the polymer inside the pores. This is usually done by some sort of a liquid infiltration approach, and viscous polymer melts often have a hard time imbibing into the nanoporous support media. Contamination and cleaning of the porous support media can also be a challenge. A wide range gas or solvent vapors, including water, can spontaneously liquify via capillary condensation mechanisms inside these small pores.

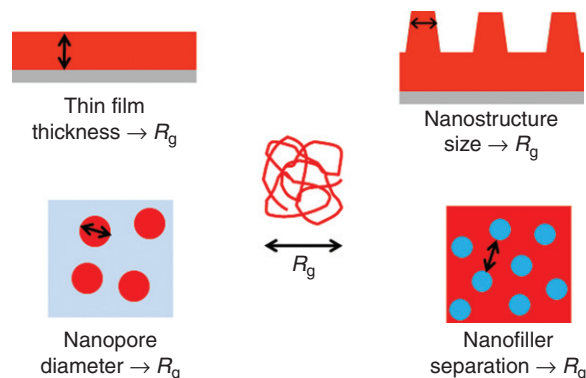


Figure 1 The coil in the center of the panel is intended to represent the length scales of a single coil in an amorphous polymer melt, nominally the radius of gyration (R_g). The other cartoons depict the different confinement geometries discussed, where the length scales of confinement begin to approach the macromolecular dimensions.

An approach that circumvents the difficulties of filling nanoporous supports with viscous polymer fluids is to generate a composite material where nanoparticles are blended into the polymer. At reasonably high loadings the average distance between the particles, between which the polymer is 'confined', becomes comparable to the particle size. Here, we refer to this approach as 'nanofiller confinement' as depicted in [Figure 1](#). This is a potentially easy way to create a high density of confined polymeric material. As the filler is the minor phase, signal-to-noise issues are generally not an issue when measuring the dynamics in these systems. Difficulties can arise when trying to quantify the precise length scales of the confinement; a distribution of confining length scales exists. One also has to worry about the uniformity or quality of the dispersion of the filler particles. Nanoparticles often have a tendency to aggregate or flocculate; achieving well-dispersed samples can be difficult. This is especially true when clay particles are used as nanoscale fillers. It is very difficult to exfoliate the clay uniformly in the composite sample.

The last type of confinement routinely encountered is 'nanostructure confinement'. This refers to physically limiting the material to an object whose dimensions are on the nanoscale. Some common examples of this include particles or powders whose diameters or sample volumes reach the nanoscale. Other less common examples include structures (see [Figure 1](#)) that have been fabricated using any number of nanofabrication schemes, such as nanoimprint lithography, optical lithography, e-beam lithography, focused ion beam milling, or self-assembly processes. One of the biggest advantages of this approach is that any effects from a confining support or medium can be, to a first approximation, ignored as it is a very clean form of confinement. However, free-standing nanostructures or nanoparticles often tend to be very unstable. Small environmental changes can easily lead to irreversible changes (usually coalescence) of the nanoscale structures.

In addition to the different geometries, one must also consider the contact mechanics of confinement. The confining interfaces can be hard inorganic materials that are stiffer or less dynamically active, soft and compliant materials that are more dynamically active than the polymer, or free surfaces with vacuum, air, or some other gaseous environment present at the interface. On top of these considerations, the interactions between the confining and polymer surfaces can be attractive or wetting, repulsive or nonfavorable, or something in between that resembles a neutral interface. All these considerations, as we discuss below, must be considered and have an impact on the dynamics of the confined polymer systems.

7.18.3 Techniques to Quantify Dynamics

Now that we have discussed the different ways in which polymers can be confined by their environment, we shift our attention to the techniques that are used to quantify the dynamics of the polymer within the confining media. Our emphasis in this section is primarily in discussing the physics of the measurements in order to provide the reader with the insight to interpret the existing literature independently. We attempt to provide the reader with several of the major and most seminal works related to the different measurement techniques, but fully realize that our extensive reference list is not

exhaustive. We also try to summarize some of the more general conclusions that have come from the community using these techniques to quantify polymer dynamics under confinement. Over the past several years, there have been several review articles about dynamics in confinement and we point the reader to these reviews as a valuable resource for developing a deeper understanding of this topic.^{11–15} There has yet to be a review dedicated to the measurement science side of this topic, and this is the focus of this chapter.

7.18.3.1 Calorimetry

Calorimetry quantifies the heat capacity of a material and is one of the oldest and most established ways to quantify the dynamics in polymeric materials. The connection to dynamics comes through the fact that the heat capacity C is a frequency (ω)-weighted integral over the density of states ($g(\omega)$) for the various vibrations and molecular motions that occur within the polymer material:

$$C \propto \frac{\partial}{\partial T} \int \omega g(\omega) d\omega \quad [1]$$

By measuring how much heat can be put into or extracted from a material as a function of temperature, one can quantify the integrated density of states. The spectrum of motions that contributes to the heat capacity is broad, including everything from the localized group vibrations, to skeletal vibrations of the polymer backbones, to the relaxation and dissipative motions above the glass transition temperature in the molten polymer. The localized group vibrations such as CH_2 stretching, CH_2 wagging, C–O stretching, or C–C stretching are high-frequency motions (typically on the order of 10^{13} Hz) that are also small in amplitude. These are the modes typically quantified in either Fourier transform infrared (FTIR) or Raman spectroscopy. The skeletal excitations tend to be less dependent on specific moieties along the polymer chain and are more related to longer-wavelength, intermolecular excitations. These acoustic-like and collective modes typically extend from the terahertz and gigahertz frequencies downward toward the zero frequency limit. There are also a host of relaxation or dissipative processes that occur over these same timescales in most polymer liquids and solids. The heat capacity C is an integral over all these motions and therefore a direct indicator of polymer dynamics.

From the heat capacity alone, it is generally impossible to separate the time and length scales of all the contributing motions. However, the direct frequency weighting generally suggests that the higher-frequency motions are the dominant contributors to the measured heat capacity. This is evidenced by the fact that there have been reasonably successful attempts to invert the vibrational spectrum of crystalline polymers, such as polyethylene, using a normal mode analysis and the vibration force constants from infrared and Raman spectroscopy.¹⁶

In polymer science, heat capacity is typically measured using a DSC where reference and sample cells are independently controlled at an identical temperature. The difference in the energy required to maintain each of these cells at their temperature set points and the mass of material in the sample cell is used to calculate the heat capacity and specific heat. Most DSCs require about 1 to 10 mg of material to obtain a reasonable signal-to-noise ratio for a heat capacity measurement. The standard DSC

cell has a 6.5 mm diameter sample pan, meaning that a polymer film (of this diameter) would have to be approximately 1 μm thick to obtain a reasonable signal in a DSC measurement. This is much too thick to observe confinement effects in polymers. However, it is possible to observe confinement effects via DSC by using a three-dimensional confining media such as polymers imbibed into a nanoporous support or a highly filled nanoparticle-polymer composite where the diameter of the pores or the distance between the particles reaches the length scales for confinement effects. The concept here is that the confining media, usually a rigid support, does not contribute significantly to the heat capacity compared to the relatively soft polymers which are dynamically more active. There are several examples in the literature where systems both filled with nanoparticles and imbibed into nanoporous supports have been used for calorimetry studies of polymers under confinement. With the nanoparticles,^{17–25} these experimental works generally show that if the interactions between the nanoparticle and the polymer are attractive or favorable, the polymer becomes immobilized at the particle interface. This results in decreased polymer mobility as evidenced by an increase of T_g or decrease of the heat capacity of the polymer with increased particle loading. If the interactions between the polymer and the particle are repulsive or nonadhering/nonwetting, the polymer T_g typically decreases with particle loading. The results are very similar for confinement in a nanoporous matrix.^{13,26–31} For pores bigger than 7 nm in diameter, most people see a counterbalance between adsorption and confinement effects. If strong interactions exist between the pore wall and the polymer, a reduction in the polymer dynamics is evidenced. However, confinement effects in the center of the pore can facilitate motions within the polymer. In general, though, when the pore size drops below 5 nm they start to see a reduction in the step increase of the heat capacity at T_g which directly reflects reduced molecular mobility.

There have been a few attempts to quantify confinement effects in nanoscale polymers by accumulating large quantities of confined material within a conventional DSC pan. One such strategy has been to spin-cast several thin (on the order of tens of nanometers) polymer films onto silicon wafer supports and then transfer the material, either by scrapping or by floating, off the support and into the DSC pan.^{32,33} A similar approach was to use a microtome to generate multiple thin film slabs that could be collected for analysis in a standard DSC pan.³⁴ These methods generally reveal a decrease in the apparent glass transition with increasing confinement. An interesting approach to obtain polymer nanopowders has been to freeze-dry or spray-evaporate large quantities of a polymer dissolved in a dilute solution whose concentration is far below the chain overlap concentration.^{35–37} This process results in powders that are reported to be either single chain or nearly single chain species. These nanoparticle powders are a form of confinement and, with this approach, it is possible to produce enough of the material to obtain a reasonable heat capacity signal in a standard DSC instrument. There have been reports of either an increase³⁵ or a decrease³⁶ in the apparent T_g of the material over the bulk using this method. These types of sample preparation schemes, however, are usually tedious, time consuming, and not widely implemented.

Recent advances in nanocalorimetry have helped to make quantitative confinement studies more feasible. The enabling concept of nanocalorimetry has been to significantly reduce the

thermal mass of the heating elements and the temperature sensors in the sample and reference cells. This has been accomplished by using photolithography and nanofabrication techniques to integrate heating elements and thermocouples into a supported membrane of either silicon or silicon nitride which is on the order of 200 nm thick. The advantage of this approach is twofold. First and foremost is the fact that the thermal mass of the cell is significantly reduced which leads to increased sensitivity when trying to quantify the small amount of heat exchanged with a nanoscale sample. Using the nanocalorimeter approach, it is now possible to measure the heat capacities and T_g s in polymer films as thin as just a few nanometers. The second advantage is that the low thermal mass of the heater/sensor enables extremely large temperature scanning rates. While conventional DSC instruments have a maximum heating rate of 60 K min^{-1} , nanocalorimeters can heat and/or cool at rates as high as 10⁶ K min^{-1} . This allows one to quantify nonequilibrium and rate-dependent processes. It is also possible to implement fast oscillatory variations of the temperature on top of a slower linear ramp in the nanocalorimeter configuration. With this approach, the complex heat capacity can be separated into its real (in-phase) and imaginary (out-of-phase) components, a technique now referred to as AC nanocalorimetry. Commercial instruments capable of combining extremely fast temperature scales with complex heat capacity analysis at frequencies between 1 Hz and 50 KHz have recently become available.

The pioneering works in the field of thin film nanocalorimetry have come primarily from the research group of Professor L. H. Allen. In particular, they have seminal works on using nanocalorimetry to quantify thickness-induced deviations in the glass transition temperature of thin polymer films.^{38–44} Other major contributions have come from the research group of Professor Christoph Schick, including a spin-off company that sells commercial nanocalorimeters.^{45–55} What is somewhat surprising is that nearly all these thin film nanocalorimeter studies do not evidence the apparent thickness-induced shifts of the glass transition temperature for polymer films as thin as a few nanometers. This often contradicts the plethora of other techniques discussed throughout this chapter which evidence more dramatic deviations. The explanation for this discrepancy is unclear. It should be noted that the nanocalorimeter technique has been extremely successful in quantifying finite-size shifts in the melting temperatures in crystalline polymer and metallic thin films, as predicted by the Gibbs–Thompson effect; the technique appears to produce reliable data. The lack of agreement between the nanocalorimetry measurements and the other methods with respect to the glass transition phenomenon remains part of the mystery of the dynamics of thin polymer films. For a better understanding of the state of this field, we refer the reader to a recent comprehensive review.⁵³

7.18.3.2 Dielectric Spectroscopy

Dielectric spectroscopy, also called impedance spectroscopy, measures the equivalent capacitance and resistance of a material as a function of frequency. An AC electric field is applied to a sample sandwiched between two parallel plate electrodes. This alternating field induces small displacements of the electric dipoles in the system that affect both the rate at which the

capacitor charges and the final charge state through the permittivity or the extent of dipole alignment. By knowing how the capacitance and resistance of this equivalent circuit responds as a function of the AC frequency, through the signal attenuation and phase lag factors, one can define the complex dielectric constant ε^* of the material. ε^* is a frequency-dependent, complex parameter that can be further broken down into its real and imaginary components, $\varepsilon^*(\omega) = \varepsilon'(\omega) + i\varepsilon''(\omega)$, through the Kramers–Kronig relation. This is analogous to dynamic mechanical experiments that apply a sinusoidal stress to a material and monitor the resulting strain oscillations which are related through the complex compliance. There are several classic texts that address these types of dynamic measurements and a deeper treatise is beyond the scope of this text.^{56–58} For now, it is sufficient to note that ε' is the real or in-phase portion of the dielectric constant, while ε'' is the imaginary or loss component. The ratio $\varepsilon''/\varepsilon'$ is defined as the classic $\tan \delta$ loss factor. If the characteristic motion of a dipole in the sample is slower than the applied frequency, dielectric spectroscopy sees it as static. As the applied frequency decreases, eventually it reaches the point where the timescales of the motion of the dipole and the applied frequency are similar. This results in noticeable phase lag in the dielectric response and a resulting maximum (peak) in the $\tan \delta$ relaxation peak spectrum.

It is also possible to perform dielectric measurements in the time domain, albeit with less accuracy compared to impedance analysis in the frequency domain. In this approach, the sample is treated as a capacitor and a step function in the electric field is applied to the sample. From the time-domain response of the sample, primarily through the transient charge or discharge currents for the equivalent capacitance of the sample, one can extract the instantaneous or unrelaxed (ε_u) dielectric constant and, after a sufficient period of time, the relaxed (ε_r) dielectric constant. In the time domain, these dielectric constants are real (not complex) values, but ε_u is somewhat analogous to ε' , while ε_r reflects the amount of loss. It is possible to Fourier transform the time evolution of the dielectric constant ($d\varepsilon/dt$) to obtain a complex dielectric function that can be compared with the traditional frequency-domain dielectric measurements. A typical time-domain experiment is the so-called thermally stimulated depolarization current (TSDC) measurement whereby the sample is electrically polled at elevated temperature and then cooled to a lower temperature at which the polled dipoles are frozen in. The recovery of the dipoles to their unpolled state is then observed while slowly heating the sample. The mechanical analog to these time-domain dielectric measurements would be creep experiments where the time-dependent displacements are recorded in response to applying a constant load.

The utility of dielectric spectroscopy comes from the wide range of timescales which can be probed seamlessly using a single type of probe. Broadband dielectric measurements are possible over a frequency range of approximately 10^{-6} – 10^{12} Hz when a series of different dielectric spectrometers are utilized. The fact that a single measurand is used over this entire frequency range facilitates the tracking of a single relaxation process or molecular motion over a wide range of temperatures, providing a broad picture of the entire relaxation spectra in a self-consistent way. Most measurement techniques are sensitive not just to different timescales, but also to different aspects of the polymer dynamics. With dielectric spectroscopy,

the measurements are most sensitive to those structural elements that have large dipole moments, such as a carbonyl group. In contrast, the dynamics of a methyl group which gives a very large signal in inelastic neutron scattering have almost no signal in dielectric spectroscopy. Even if a broad range of timescales can be stitched together using an ensemble of measurement techniques, each will likely be sensitive to different physical phenomena. In this respect, broadband dielectric spectroscopy is extremely unique and versatile because it can be used to self-consistently study a wide range of time and temperature scales. It should be clarified that several different types of dielectric techniques are needed to access the entire frequency range of 10^{-6} – 10^{12} Hz; it cannot be done in one simple measurement. **Figure 2** shows a typical variation of ε' and ε'' over the broadband dielectric spectroscopy range and indicates the different types of instruments and sample geometries that are required to access these frequencies.⁵⁹ Please note that all the techniques identified in **Figure 2** are simple parallel plate geometries as described above; this is a simplification for illustrative purposes and the concepts are similar for the nonplanar geometries.

It is also important to understand the nature of the dipoles in a polymeric material that the dielectric spectroscopy will be sensitive to. The dipole moment is a vector quantity, possessing a well-defined direction. According to Stockmayer,⁶⁰ polymers can be grouped into three major classifications according to the nature of their dipole moments. Type A polymers have fixed dipoles that point in the direction parallel to chain backbone. Usually these polymers, such as poly(ethylene oxide) (PEO), have a well-defined dipole built into the main chain of the polymer. For type A polymers, there is a well-defined relationship between the radius of gyration of the polymer chain and the polarization. Fluctuations in this polarization can be used to quantify low-frequency breathing modes of the polymer coil or other collective motions that involve large portions of the polymer chain. These normal modes are often related to the terminal relaxation time or the timescale for the polymer to relax an entanglement constraint. In contrast, type B polymers have rigid or fixed dipoles that are situated orthogonal to the main chain axis. In these systems, there is no correlation between the net dipole moment and the chain contour. Fluctuations of the dipole moment in a type B polymer reflect segmental motions. Most synthetic polymers fall predominantly into this type B classification. The last classification scheme is type C which refers to polymers whose dipoles reside in flexible side chains that can easily change their orientation relative to the backbone director. One classic example of a type C polymer is poly(vinyl methyl ether), whose dipole is at an angle normal to the backbone and spins around on the axis with which it is connected to the backbone. In order to understand the nature of a dynamic relaxation process in dielectric spectroscopy, it is critical to know what dipole in the system is responsible for the relaxation and what is the orientation of geometry of that relaxation relative to the polymer chain.

Broadband dielectric spectroscopy has been utilized in many forms to study the dynamics of polymers under strong states of confinement. These include all the major modes of confinement discussed previously, including thin film, nanoporous, nanofiller, and nanostructure confinements. This is a testament to the utility of broadband dielectric spectroscopy. It is relatively straightforward to design a sample configuration

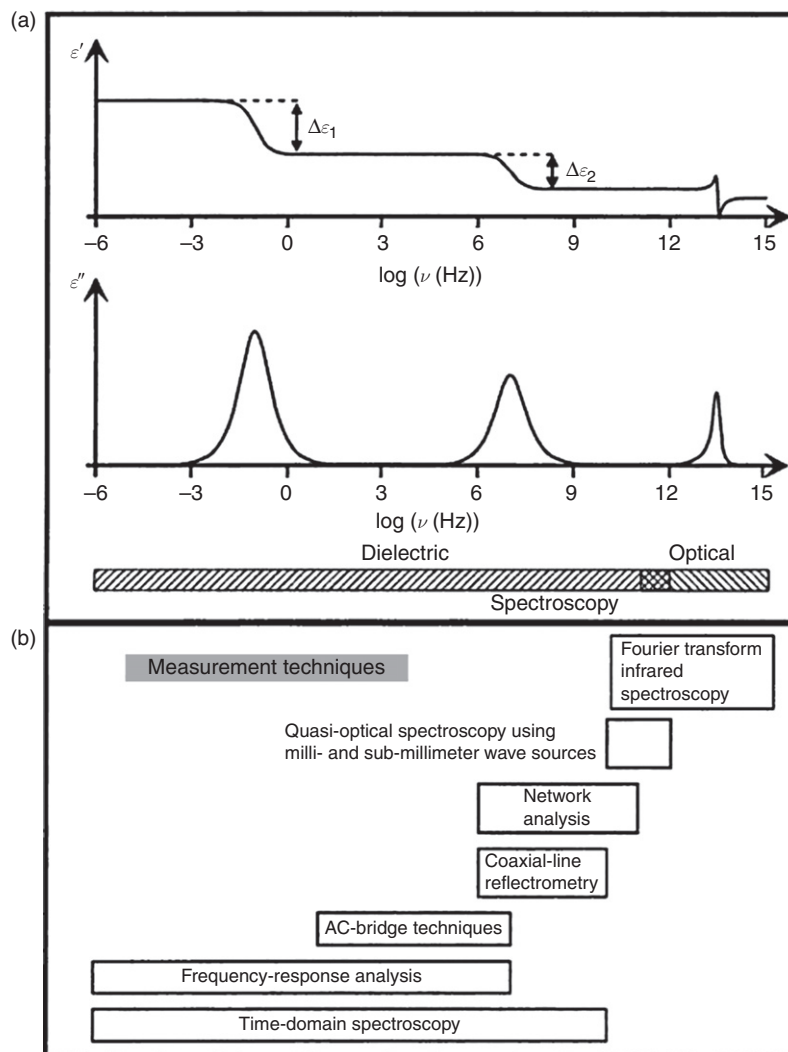


Figure 2 (a) A typical variation of ϵ' and ϵ'' over the frequency range of 10^{-6} – 10^{12} Hz that is nominally probed by broadband spectroscopy. (b) The different types of dielectric instruments mapped to the frequency ranges they probe. Reproduced with permission from Kremer, F.; Schonhals, A. *Broadband Dielectric Spectroscopy*; Springer: Berlin, Germany, 2003, p. 36.⁵⁷

that will yield a measurable signal-to-noise ratio. However, there are also caveats that must be considered for polymeric materials in each of these highly confining environments. For thin film confinement, one must always be cognizant of the dielectric strength or breakdown voltage. The field strength varies inversely with the film thickness for a planar sample confined between two planar electrodes. Most polymers start to exhibit dielectric breakdown at a field strength of approximately 1 MV cm^{-1} which can be achieved in a 10 nm film at a voltage of just 1 V. In many cases, the electrodes are deposited on the thin film samples using metal evaporation techniques. This can lead to a rough interface between the polymer and the evaporated metal. Roughness on a 10 nm film can lead to local asperities, where the effective thickness between the electrodes is much less than 10 nm, and significantly higher local field strengths. With thin film dielectric measurements, one must always be concerned about possible nonlinear effects, dielectric breakdown, or local shorts between the electrodes. Unfortunately, the voltage applied across the sample or an

evaluation of the field strength is almost never reported in the dielectric literature on confined polymer systems.

Interfacial polarization effects are another source of concern when interpreting the dielectric spectra in confined polymer systems. By their nature, highly confined polymer systems intrinsically possess a large fraction of interfacial material. One must be aware of how these interfacial effects can show up in the quantification of the complex dielectric function. There are several processes which contribute to the frequency and temperature dependence of $\epsilon^*(\omega)$. These include (1) the fluctuation of the molecular dipoles due to molecular motions, (2) the motion of mobile charge carriers in the system, and (3) the separation of charges or dipoles induced at a dielectric interface. These interfacial dipoles include the requisite interfaces between the electrodes and the sample as well as any internal interfaces within a heterogeneous sample itself. Of these possible contributions, it is important to separate out potential artifacts that may not be related to the dynamics of interest to properly interpret $\epsilon^*(\omega)$. This can be a significant

challenge, especially in the nanoporous or nanofiller confinement effects where the large surface-to-volume ratio has the potential to introduce conducting species through adsorption or large numbers of surface dipoles. A recent text on this topic is a valuable resource for interpreting dielectric spectra in confined polymer materials and addressing the issues of interfacial polarization.^{61,62}

The body of literature on using dielectric techniques to study polymers in confinement is now quite vast and it is certainly beyond the scope of this chapter to provide a comprehensive review of this work. We strongly recommend an excellent textbook edited by Kremer and Schonhals that contains several chapters relevant not only to the fundamentals of broadband dielectric spectroscopy, but also to the dynamics of polymers in confinement.⁵⁷ This is an excellent text for the fine details. Briefly discussing some of the major themes in this field, dielectric spectroscopy has been applied to all three states of confinement discussed here, namely nanofiller confinement,^{63–67} thin film confinement,^{54,68–102} and nanoporous confinement.^{27,29–31,79,86,96,103,104} The dielectric community has been very active studying dynamics under confinement. The references provided herein are not intended to be a comprehensive list, but certainly include most of the seminal works. A general theme that appears to be emerging in these works is that the impact on the polymer dynamics depends on the nature of the confinement. Strong interactions with rigid entities, including nanoparticles, supporting substrates, or the walls of porous supports, will lead to hindered dynamics. When these effects dominate, one sees an increase in T_g or a slowing down of the alpha relaxation in dielectric spectroscopy. However, pure confinement effects which alter the packing or configuration of the polymeric molecules relative to the bulk typically result in faster dynamics. This is evidenced by a decrease in the T_g or a speeding-up of the dielectric alpha relaxation. In general, there is a competition between these two effects, as discussed nicely by Kremer and Schonhals.^{27,29–31,105} The basis for the argument is depicted schematically in Figure 3 for T_g measurements from Alba-Simionesco and co-workers.¹⁰⁶ They have systematically studied a host of different materials in controlled pore glasses with nominal pore diameters of 2.5, 5, 7.5, and 20 nm. For several systems, they find that confinement effects lead to facilitated motion for pore diameters approximately 5–7.5 nm. In these systems, the dynamics are faster than the bulk. However, in smaller pores, the adsorption effects dominate and the overall dynamics of the polymer are slower than bulk. What is interesting is that the confinement effects are most pronounced for the dielectric alpha relaxation processes; the dielectric beta process which is faster and typically represents local side group or sub- T_g relaxations is, in general, less strongly affected by confinement. It is also generally true that the strengths of all the dielectric relaxations typically decrease under confinement relative to the bulk, regardless of whether the dynamics have sped up or slowed down. This generally suggests that the number of relaxation species is decreased. As discussed previously, type A polymers that have a well-defined dipole in the direction of the backbone can exhibit a normal mode or breathing mode that reflects fluctuations on the scale of the radius of gyration of the chain. There have been several studies focusing specifically on how this normal mode responds to confinement, most often in thin film

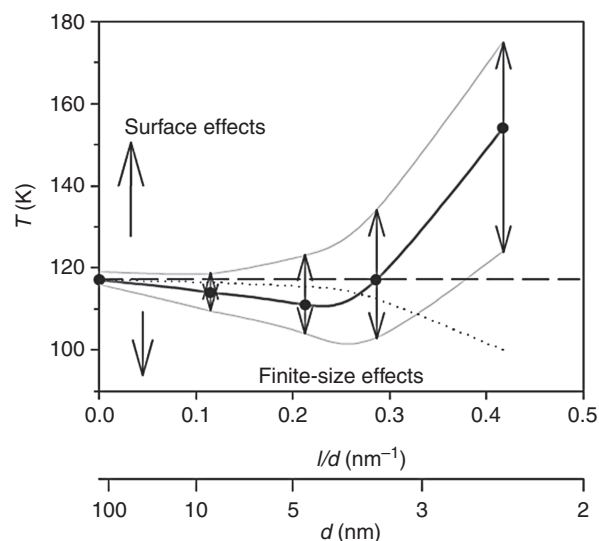


Figure 3 The T_g of toluene confined in nanopores vs. the inverse of the pore diameter d . The average T_g s defined by the peak of the heat capacity derivative are indicated by the filled circles. The arrows represent the widths of the transition region, while the dashed line refers to the T_g of bulk toluene. Reproduced with permission from Alba-Simionesco, C.; Dosseh, G.; Dumont, E.; *et al. Eur. Phys. J. E* **2003**, *12*, 19.¹⁰⁶

studies,^{69,71,80,81,92,93} but also in nanopores.^{27,31,57} These studies show that the normal mode is strongly affected by confinement, more so than the alpha mode, which nominally makes sense: slower and larger-scale motions are naturally affected by confinement more readily.

7.18.3.3 Dynamic Mechanical Spectroscopy and Related Mechanical Approaches

Mechanical approaches to characterize the polymer viscoelastic and dynamic properties in bulk polymers include dynamic mechanical analysis (DMA), stress relaxation, and creep and recovery. Beyond the brief introduction below, readers are referred to common textbooks on polymer mechanical properties and viscoelasticity for detailed description on this topic.^{58,107,108} Among the mechanical techniques, DMA methods are quite versatile and can incorporate a range of sample geometries and mechanical loading scenarios. In many ways, DMA methods are a mechanical analog to dielectric spectroscopy. A sinusoidal stress is applied to a sample in a range of configurations, including tension, compression, shear, or bending. If the characteristic molecular motion in the sample is much slower or faster than the applied frequency, the observed strain is largely in phase with the stimulus. When the timescales of the molecular motion and the applied frequency are similar, the polymer molecules can adapt their configurations on a timescale comparable to the applied load, which leads to a phase lag in the strain response. The complex modulus is expressed as an in-phase component, the storage modulus, and an out-of-phase component, the loss modulus. The ratio of the loss modulus to the storage modulus is defined as $\tan \delta$ and is often called the damping. A common measurement is to hold the frequency constant and scan the temperature to find the thermal transition temperature such as T_g . In general, the

moduli and damping are measured against temperature and load frequency. Unlike dielectric spectroscopy, a DMA instrument only covers a narrow frequency window. Typical frequency ranges accessible by DMA instruments are limited from approximately 10^{-5} to 10^2 Hz over a wide range of temperatures. TTS allows stitching the data over a wide range of temperatures and frequencies. A thermal transition can be identified when the storage modulus decreases in log scale against a linear temperature scale at a fixed frequency. Such decrease is also accompanied by a peak in the loss modulus and $\tan \delta$. The $\tan \delta$ peak in the plot against frequency in log scale at a fixed temperature, however, is often discussed using the concept of relaxation time distribution. A change in any of the three aspects of the $\tan \delta$ peak, namely, position, width, and amplitude, signals a change in the dynamic behavior of associated motion. Although the majority of DMA measurements focus on segmental motions and the glass transition behavior, DMA is sensitive to motions at a wide range of length scales, from local molecular motions in glassy solids to viscous flow in low-viscosity liquids. Traditionally, a DMA instrument is best suited for high-compliance (rigid solids) solids, whereas rheometer is needed for liquid samples. In practice, a higher-compliance instrument is needed to analyze the solid materials, whereas a more sensitive instrument is required for the liquids. While their names are different, the principle of operation is the same. In the context of confined polymers, DMA is more appropriate.

One can also perform stress relaxation or creep measurements under static stress or strain loading to probe the relaxation processes in polymeric materials. In the stress relaxation experiment, the stress is monitored with time after a stepwise strain is applied; in creep measurements, the time-dependent strain is measured after a stepwise stress is applied. These measurements are slow and typically extend for several decades in time, usually plotted as the log-log evolution of modulus versus time for stress relaxation or compliance versus time for creep. The relaxation time or retardation time is typically identified as the middle point of the viscoelastic region where the modulus strongly decreases and compliance strongly increases, respectively. The principle of Boltzmann superposition makes it possible to express the time-dependent moduli and compliances in terms of one another. In that sense, stress relaxation measurement and creep measurement are equivalent. However, the relaxation time and retardation time are often not identical, albeit in the same order of magnitude. In addition, the stress relaxation (or creep) measurement at different temperatures can also be superpositioned to cover many decades of time duration. Using TTS, the stress relaxation data can also be presented on a semilog plot of modulus versus temperature at a fixed arbitrary time. Such a plot looks very similar to the semilog plot of storage modulus versus temperature at a fixed arbitrary frequency from the DMA measurement. However, stress relaxation and creep are only sensitive to molecular motions that cause polymer chain conformation changes, such as segmental motions and viscous flow. Therefore, these two techniques cannot characterize the side group motions that appear in DMA as lower-temperature transitions. Nonetheless, for the same segmental motion observed by these three techniques, the temperature shift factor for TTS is expected to be the same.

Systems confined by nanoparticles (i.e., nanocomposites) are very convenient for mechanical testing; the measurement techniques are exactly the same as those used for the neat polymer. A vast body of literature contains a number of different trends with respect to the change of storage modulus, loss modulus, and $\tan \delta$ with the increase of nanofiller loading.^{109–113} For example, the $\tan \delta$ position can be the same as the bulk or can shift to higher and lower temperatures with the added nanofillers. The interaction between the polymer and the filler appears to be the key factor influencing the dynamic properties of the polymer matrix. It is generally argued that when the interactions are strong, polymer molecules close to the rigid inorganic fillers are constrained and the $\tan \delta$ peaks associated with T_g and other thermal transitions shift to higher temperatures.^{111,113–116} In some cases, a new $\tan \delta$ peak at an elevated temperature is assigned to the interface layer attached to the inorganic fillers.^{110,117,118} The $\tan \delta$ peak has also been found broadened,^{114–116,119} indicating that the polymer dynamics become more heterogeneous. On the other hand, there are reports that $\tan \delta$ does not change with nanofillers, even with change of filler and polymer interaction.^{112,119,120} One should keep in mind that a majority of the nanocomposite systems in literature are complicated. For one, many of the polymer matrices are thermoset or semicrystalline, such as epoxy and polypropylene. Moreover, additives such as surfactants that are often used to help the filler disperse into the polymer matrix could also contribute to the change in the polymer dynamics. For example, the new $\tan \delta$ peak at a higher temperature in a composite is assigned to the chemically bound polymer to the filler surface via the additive.¹²¹ In general, it is wise to use multiple techniques to better understand the dynamics of confined systems and this is particularly easy with nanofilled systems because nominally bulk measurement techniques can be used. For example, it is trivial to perform DSC measurements on the same samples that are used for DMA and help verify the interpretation.

DMA measurements have also been used to quantify systems under both nanopore and thin film confinement. It turns out that mesoporous materials, for example, Vycor glass, that have constant loss modulus are excellent hosts for DMA measurement on organic liquids, despite the fact that modulus of the porous host is significantly stiffer than the liquid. By analyzing the dynamic complex elastic susceptibility of molecular glass-forming liquids confined in these rigid nanometer-sized pores, Koppensteiner and co-workers identified two relaxation peaks, one of slowed dynamics for the layer of material at the pore interface and another of faster dynamics for the material at the center of the pores.¹²² Free-standing thin films are mechanically too weak to be subjected to the DMA measurement. However, DMA measurements have been performed on thin polymer films supported on a polyimide substrate.¹²³ Here, the loss modulus was calculated from the Takayanagi parallel model⁵⁸ in which the dynamic strain is the same for the thin film and the substrate. The results indicated that the glass transition peak is broadened, supposedly due to the surface and the interface regions, with a higher-temperature peak emerging when the interfacial interactions are strong.¹²³

One unique DMA-like measurement is called surface forces apparatus.^{124–127} In this measurement, the sample is sandwiched in-between two atomically smooth parallel plates typically made of mica. Using such smooth plates creates a

confining space down to a couple of nanometers in thickness. Sinusoidal shear forces are applied by a piezoelectric element. A second sensor piezoelectric element is used to detect the resulting response. Using this setup, the viscosity, storage, and loss modulus of the confined liquid can be measured. The viscosity of the confined liquid is found to be increased by orders of magnitude than the bulk.^{124,125} Likewise the relaxation times in confined liquid and polymer melts can be orders of magnitude longer than the bulk.^{124–126} These effects occur when the film thickness approaches 5–10 times the molecular diameter of the polymer chain and are attributed to a layering alignment of the molecules parallel to the interfaces. Similar results are widely predicted by computer simulations as discussed below.

Recently, a series of innovative creep measurements performed on free-standing thin polymer films have been reported by McKenna and co-workers.^{128,129} Thin polymer films of different thicknesses are first placed on a rigid substrate patterned with an array of micron-sized holes that go through the entire substrate. Subsequent annealing promotes good adhesion of the polymer film to the substrate and the periphery of the holes. Pressurized air is applied to the bottom of the substrate to induce a 'bubble' in the polymer film over the hole. Atomic force microscopy (AFM) is then used to track the contours of the bubble as a function of time and thereby determine the creep strain. The resulting compliance versus time curves of the thin films agree with the bulk response in the glassy relaxation regime, indicating a bulk-like T_g and dynamics in the glassy region. However, the compliance in the rubbery region is thickness dependent and approximately an order of magnitude lower than the bulk value for the thinnest films studied. Such a stiffening response is discussed in terms of altered chain conformation or entanglement density for polymers under thin film confinement.^{128,129}

7.18.3.4 Mechanical Surface Probes

Since its invention in the 1980s, the AFM has been widely used for imaging, measuring, and manipulating matter at the nanoscale. The miniaturized nature of the AFM tip, which interacts with a small volume of material, is particularly well suited for studying polymer surfaces and thin films. In the AFM (see Figure 4) a sharp tip located at the end of a cantilever is used to probe the sample surface. The three most common operating modes include contact, noncontact, and tapping; readers are

referred to comprehensive books and review papers regarding the details and applications of AFM on polymer research.^{130–132} As shown in Figure 4, the mirror on the top surface of the cantilever reflects a laser light onto a position-sensitive photodiode detector. This optical lever is very sensitive to deflections and/or torsions or vibrations of the cantilever as the tip interacts with the sample. If the stiffness of the cantilever is known, these signals can be used to quantify the forces, in both the vertical and the lateral directions, applied to the sample surface. Feedback between the z -axis piezoelectric stage below the sample and the photodiode detector helps control and maintain the vertical force of the tip on the sample surface. The lateral piezo-drivers define sizes of the scanning area as well as a range of scan speeds by moving the sample horizontally. In some AFM designs, the piezoelectric scanners are located on the scanning head such that the cantilever is moving while the sample substrate is stationary.^{133–135} Other designs have the cantilever mounted on a stationary (in the x - y plane) bimorph actuator that only enables motion in the z -direction and the sample stage is moved in-plane by piezoelectric scanners.¹³⁶ Since the focus of this chapter is the dynamic behavior, we do not dwell on measurements that use the AFM tip simply as an indentation tool to obtain the hardness or modulus, even though such modulus measurement when performed as a function of temperature can be used to identify the surface T_g . Rather, we focus on measurements of the surface properties that are dependent on the tip oscillation frequency and scanning speed. Such measurement results are directly tied to the polymer dynamic properties. For these measurements, the AFM is always operated in the contact mode.

Dynamic measurements of a polymer surface can be done by moving the AFM tip either perpendicularly or laterally to the surface. In force-modulated scanning force microscopy (FM-SFM)^{136–143} and AFM adhesion measurement (AFMAM),^{144,145} the AFM tip moves vertically against the sample surface; in shear-modulated scanning force microscopy (SM-SFM)^{134,135,146,147} and lateral force microscopy (LFM),^{133,134,137,148–152} the tip moves parallel to the surface. In FM-SFM, also referred to as scanning viscoelasticity microscopy (SVM), the cantilever tip is mounted on the piezoelectric bimorph actuator which has a resonance frequency of approximately 1–10 kHz. The modulated force is detected by the deflection of the cantilever; thus, the modulus of the surface can be calculated by an indentation model. Frequency response analyzers can be used to track the phase behavior between the input sinusoidal voltage used to drive the actuator and the sinusoidal response of the cantilever deflection. Using the same framework as traditional DMA analysis, Kajiyama and co-workers were able to calculate a storage modulus E'' , a loss modulus E' , and a corresponding $\tan \delta$ (E''/E') using the AFM. Their data suggest that the surface is more mobile than the bulk for low molecular mass polymers, with a lower T_g and a lower activation energy for the glass transition.^{136,138–143}

AFMAM measurements have been used to quantify the pull-off force when detaching the tip from the polymer film, from which an adhesion force F_{ad} is determined. F_{ad} has been defined as the maximum pull-off force, corresponding to the maximum deflection of the AFM tip in the pull-off curve. These measurements have been performed at AFM tip oscillation frequencies ranging from 30 Hz to 50 kHz and also as a function of temperature. The results show that at a certain frequency, F_{ad} increases with the temperature as the glassy

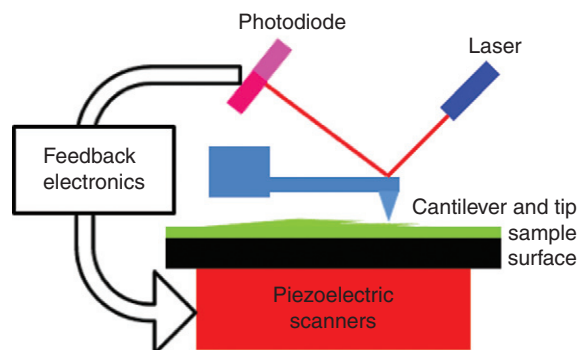


Figure 4 The schematic depicting the major components of a typical atomic force microscope. See the related text for discussion.

surface turns rubbery. On the other hand, at a fixed temperature, F_{ad} also depends on the 'pecking' (frequency) rate of the tip: at lower frequency, the surface is more rubbery. Such behaviors resemble those observed in traditional DMA, from which master curves can also be constructed following the Williams–Landel–Ferry (WLF) scaling behavior. The T_g and the shift factors obtained in this approach on thin polymer films were consistent with bulk-like behavior.^{144,145}

With SM-SFM measurements, the cantilever tip is sinusoidally modulated in the lateral direction while in contact with the polymer surface. Using a small vertical load and small lateral modulations, the probing depth of the SM-SFM can be on the order of 1 nm, enabling substrate-independent measurements down to film thicknesses of a few nanometers.¹⁴⁶ Typically, the cantilever is driven at a constant amplitude by the piezoelectric drivers. At low temperatures, the tip does not slip across the sample surface, which generates large elastic torsional stresses in the cantilever. When the sample surface goes through glass transition and the polymer becomes more mobile, the tip is able to deflect (slip) across the surface; the polymer creeps under the lateral load applied through the AFM tip. The slip amplitude can be indirectly deduced from the decreased cantilever torsion. The T_g is indicated by the discontinuity in the slope of the amplitude response, that is, the onset of creep. This creep-like response is, of course, expected to be dependent on the tip oscillation frequency. Master curves can be constructed with measurements at different temperatures and tip oscillation frequencies. These types of measurements have shown that the surface dynamics are largely the same as the bulk.^{134,146,147} However, this technique has also been used to evidence a relatively thick layer (200 nm) near the interface of a rigid solid substrate with reduced mobility and a higher T_g . Surprisingly, though, this trend reversed in the 10 nm closest to the substrate; there was evidence for enhanced mobility and a reduced T_g .¹³⁵

LFM is another widely used AFM technique to laterally probe the polymer surface, sometimes referred to as friction force microscopy (FFM). In this mode of operation, the AFM tip slides across the polymer surface at a range of scanning speeds. The friction and adhesion force with the surface cause the cantilever to twist, and the friction force is measured from the torsion of the sliding cantilever. The frictional behavior of polymeric solids is closely related to their dynamic viscoelastic properties.¹⁴⁹ The friction force depends on both the temperature and the scanning speed. The scanning rate dependence of the lateral force corresponds to the frequency dependence of the loss modulus E'' . Master curves can be constructed with measurement at different temperatures and scanning speeds. The results based on this technique reflect the controversies commonly seen in the field of polymer dynamics in thin films and confined geometries. There are multiple observations of polymer surfaces and thin films with either bulk-like behavior or enhanced mobility.^{133,134,136,137,142,149,151,152}

The AFM techniques above focus on the mechanical properties of the polymer surface. To a great extent, they are DMA measurements using the small AFM tips. Besides these mechanical approaches, there are other AFM-based techniques utilizing the small tip to probe the thermal and dielectric properties of the polymer surface. For example, AFM with a conductive tip operated in the noncontact mode can be used to measure local dielectric properties.⁹⁰ The basis behind this measurement is

that fluctuations in the sample polarization beneath the tip produce proportional variations in the cantilever resonance frequency. This is essentially a dielectric measurement with a nanometer-sized electrode. In another AFM-based technique called scanning thermal microscopy, the scanning tip also serves as a heating element.¹⁵³ The probe power will increase as the surface goes through the glass transition. These measurements are purported to be sensitive to the local heat capacity of the polymer; however, the measurements can be complicated. The contact area with the tip and the sample are poorly defined and can change as the probe penetrates into the sample. The tip deflections can be used to measure the local thickness expansion; the polymer thin film T_g is found to be strongly dependent on the polymer and substrate interaction.^{153,154} It is important to consider both the elastic properties and the heat capacity of the supporting substrate with these measurements; both can affect the nature of the thermal softening transition nominally identified with the glass transition.¹⁵⁴ The measurements are also sensitive to how the heat is dissipated in the thin film to the surroundings and supporting substrate.

7.18.3.5 Diffusion Experiments

There are several reports in the literature using diffusion experiments to probe changes in the polymer dynamics under confinement. These experiments generally track either the diffusion of the polymer chains themselves or the diffusion of small probe molecules dissolved in the polymer matrix. The diffusion of an entire chain involves center of mass movements and is a direct measurement of polymer dynamics. The time-scale for these events, depending over what length scale the diffusion occurs, is usually in the order of seconds and longer. In general, two different schemes have been used to measure the diffusion of whole chains in thin film confinement. The first scheme measures the in-plane motion of molecules within a single-layer thin film, while the second measures out-of-plane movement of molecules in the perpendicular direction in a bilayer or multilayer thin film structure. The diffusion of small probe molecules in a polymer film is related to polymer dynamics in an indirect way. It is understood that the local motions of the polymer, such as the beta-relaxation, control the rate at which the small molecules move through the polymer.¹⁵⁵ To measure the diffusivity of small-molecule probes in a polymer thin film, the probe molecules can be either diffusing from outside into the film (such as in moisture-uptake measurement) or moving inside the film after already being dispersed in the polymer matrix.

Some of the first diffusion studies in confined polymers involved measuring the fluorescence of small-molecule dyes or additives. The change in the fluorescence intensity offers a sensitive technique to study diffusion. More details of these measurements are given in Section 7.18.3.9; only a brief description is presented here. Fluorescence recovery after photobleaching (FRAP) measurements have proven to be useful for measuring the in-plane diffusion of the dye species.^{156–158} Thin polymer films can easily be doped with fluorescent dyes, as a blended additive, a functionalized end group, or a substituent attached to the main chain as a fluorescent side group. Selected areas of the film are bleached and the recovery of fluorescence intensity due to the diffusion of nonbleached molecules into the bleached area can be used to calculate the diffusion coefficient of

polymers¹⁵⁸ or small molecules.¹⁵⁷ Another technique utilizes the fluorescence nonradiative energy transfer (NRET) process to measure the diffusion of small-molecule chromophores in polymer thin films. The concept here is that diffusion of the chromophores from one polymer layer into another layer with tethered 'donor' moieties lowers the fluorescence intensity in the bilayer structure.¹⁵⁹ In fluorescence NRET, an excited 'donor' species transfers its energy to an 'acceptor' species (e.g., the chromophores), resulting in a decrease of the donor fluorescence intensity.

Bilayers are widely used to study the interdiffusion of polymer thin films in the direction perpendicular to the plane of the film. The composition gradient between the bilayers can be made initially very sharp by transferring discretely made single-layer films into a bilayer stack. The diffusivity can be obtained by tracking the composition profile across the interface of the layered structure before and after thermal annealing. Using this approach, it is trivial to vary the thicknesses of the different films in the bilayer to explore the thin film confinement effects. Most of these studies rely on one of two techniques to measure the composition profile across the interface: either neutron reflectivity^{160–163} (NR) or dynamic secondary ion mass spectroscopy (DSIMS).^{163–166} Both these techniques take advantage of the fact that a contrast between the two layers can be obtained by selectively deuterating one of the layers; the assumption that replacing hydrogen with deuterium in the polymer does not alter the diffusion behavior is generally a reasonable one. Both NR and DSIMS are very sensitive to the difference between H and D, providing a high-resolution way to track the mixing of the two layers as diffusion proceeds. A brief description of the two techniques is given below. Figure 5 also summarizes some typical NR results for confined polymer films.

NR uses a highly collimated beam of neutrons to measure thin film structure. In terms of theory, it is quite similar to XRR, which uses X-rays instead of neutrons. For both X-rays and neutrons, the refractive index of a material is generally slightly less than 1. When the incidence angle is below some critical

value θ_c , total external reflection is measured from the flat sample surface. Beyond θ_c , there are oscillations in the reflected intensity versus the incident angle, attributed to the neutron scattering length density (or electron density) profile of the film. When reflected beams from the top surface and the buried interfaces interfere constructively or destructively, periodic patterns emerge. Fitting the reflectivity curve yields film thickness, roughness, and scattering density profile through the thickness of the film, from which the composition profile of the layered structure is obtained. XRR measurements are usually not sensitive to the scattering length density difference between the deuterated and hydrogenated versions of the material, but they are very important for verifying the total film thickness and surface roughness in the NR models.^{160,161} For more details about the two reflectivity techniques, readers are referred to a book by Roe.¹⁶⁷ In DSIMS, the film surface is sputtered by a focused beam of ions (typically Ar⁺) and the secondary ions ejected from the sample surface are measured with a mass spectrometer to determine the elemental, isotopic, and molecular composition. The DSIMS instrument erodes the sample at a well-controlled and calibrated rate. By knowing the elemental composition as a function of sputtering time, one can reconstruct the elemental composition as a function of depth in the sample.¹⁶⁸ Using this approach, one can track the degree of mixing, as initially discrete bilayer samples interdiffuse. It is important to realize that the depth resolution of the NR techniques is better than 1 nm, whereas that of DSIMS is closer to 10 nm. However, samples with a total thickness greater than 200 nm are generally not possible to measure with NR, while DSIMS in principle does not have an upper thickness limit. It should also be noted that NR is a nondestructive technique such that one sample can be measured after subsequent annealing steps. DSIMS is a destructive technique and only one measurement can be made per sample.

A common and largely noncontroversial theme that has emerged is a slowing down of the diffusive processes in thin film, especially when the chains are in contact with the

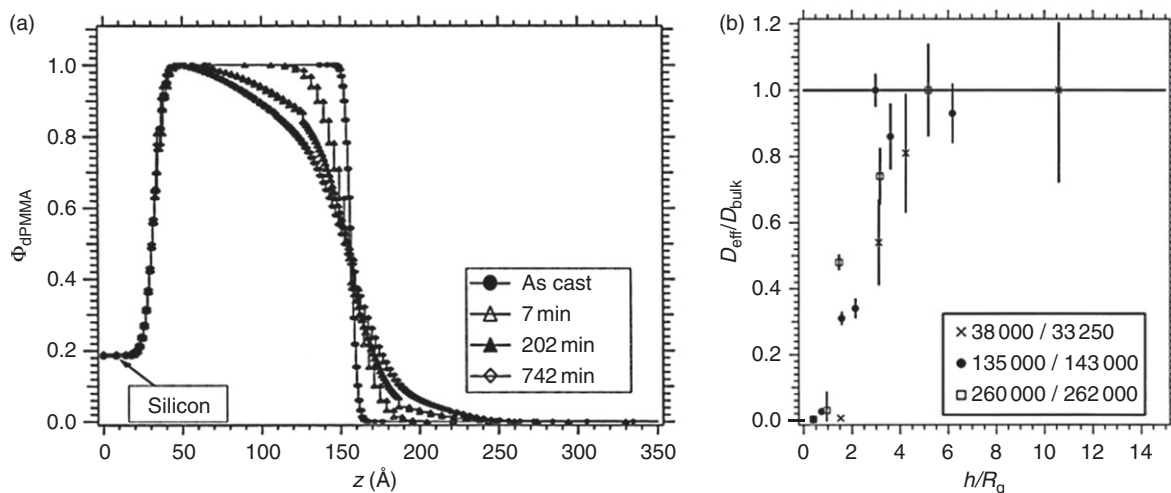


Figure 5 (a) A typical interdiffusion profile obtained by NR for a bilayer sample of deuterium-substituted poly(methyl methacrylate) (PMMA) (dPMMA) on normal hydrogenated PMMA, both of comparable molecular mass. The composition profile is shown as the volume fraction of dPMMA across the bilayer interface. Upon annealing, the interface broadens as the two layers are mixed. From the width of the interface one can extract an effective diffusion coefficient as plotted in (b). These experiments show that the intermixing slows down significantly when the thickness of the dPMMA under the layer is approximately 5 times the R_g of the bulk material. Reproduced with permission from Lin, E. K.; Kolb, R.; Satija, S. K.; Wu, W. L. *Macromolecules* **1999**, *32*, 3753.¹⁶¹

substrate. For films nominally less than an R_g thick or when essentially all the polymer molecules are in contact with a solid substrate interface, the effective diffusion constant can be 2 orders of magnitude less than that of the bulk.^{160,164} This significantly reduced mobility is often attributed to the chain conformations being distorted parallel to the substrate and/or numerous contacts per chain with the attractive surface. However, there are discrepancies on how far the substrate effect reaches, ranging from 3–4 R_g s thick to more than 10 R_g s.^{158,161,168,169} The molecular mass dependence of the diffusion coefficient is also debated,^{164,165,169} leading to different models interpreting the reduced diffusivity in polymer thin films. These interdiffusion measurements also raise the questions regarding the existence of a mobile surface layer. Two DSIMS measurements reveal opposite results, one stating the surface diffusivity is less than the bulk,¹⁶⁵ while the other stating the surface mobility is higher than the bulk.¹⁶³

In the small-molecule probe diffusion measurements, the observations are more controversial. FRAP measurements have shown that the relationship of the dye–probe diffusion coefficient in the thin film and in the bulk is temperature dependent; below a certain temperature, the diffusivity in the thin film is higher than the bulk, and above that temperature, the opposite is found.¹⁵⁷ NRET measurements also reveal a complicated response of the small molecule's mobility in polymer thin films.¹⁵⁹ On the other hand, simple mass uptake and film thickness measurement show that the water diffusivity in polymer thin films is substantially smaller than that in the bulk.^{170–172}

7.18.3.6 Flow Experiments

For macroscopic films (i.e., films thicker than a few microns), the free energy is given by the sum of capillary and gravitational energies;¹⁷³ the film is stable and surface undulations (and structures) will decay with time under the Laplace pressure given by the surface tension and radius of curvature. For microscopically thin films, the long-range van der Waals forces, that is, interaction between the top and bottom surfaces of the film, dominate the free energy. The stability is then controlled by the balance between the Laplace pressure and the disjoining pressure, $A/(6\pi h^3)$, where A is the difference between the Hamaker constants for solid–liquid and liquid–liquid interactions.^{174,175} When the solid–liquid interaction is stronger, that is, on a wetting surface, the film is stable and thickness fluctuations decay for all wavelengths. When the liquid–liquid interaction is stronger, that is, on a partial wetting surface, thermal fluctuations at the polymer–vacuum interface can spontaneously become amplified if the disjoining pressure is more dominant than the Laplace pressure. In this regime, fluctuations can grow and impinge on the substrate. Depending on the curvature of the free energy with film thickness, spinodal decomposition patterns and holes have been observed.^{176,177} It is worth mentioning here that the treatment of polymer films as liquids in the above is only valid at temperatures higher than T_g , when the modulus of the polymer film can be ignored and the self-relaxation time of the polymer molecules is much faster than the timescale involved in the capillary waves. In addition, the presence of air bubbles, dust particles, and other defects (or simply externally applied puncture) can also lead to hole formation by heterogeneous nucleation and ensuing rupture of the thin film. A key difference between the chain diffusion and

these flow-related studies in thin polymer films is that the flow is driven by surface tension (and other forces), which may result in high shear strain rates and corresponding nonlinear viscoelastic behavior.

The change in the film surface profile and the breakup (or generally speaking, dewetting) of thin films provide a means to study the dynamics of polymer thin film. Clearly, this type of flow involves the entire macromolecular chain movement and it reflects the mobility at long timescale in the order of tens of seconds and beyond. This mobility is of considerable technological interest, because it concerns the thermomechanical stability of polymer thin films and nanostructure. Film rupture is studied with both supported and free-standing geometries; from the timescale for rupture, one can quantify the dynamics for films of varying thicknesses.^{177–179} Another approach has been to template patterns in the surface and then monitor how quickly the patterns decay as a function of time and length scale of the patterns. These patterns can be irregular rough surfaces, nanoparticle-induced patterns, or very regular patterns created by lithography techniques such as nanoimprint lithography.^{180–183} The evolution of the surface structure as a function of annealing time and temperature is usually measured with AFM or optical methods.^{179–181,184} Scattering methods have also been used to quantify the surface wave;¹⁷⁶ more on this topic will be given in Section 7.18.3.7. The early stage of spinodal dewetting can also be studied by X-ray or NR where a change in the reflectivity curve reflects hole formation/growth and surface/interface roughening.^{185,186} If the surface structures are periodic, such as line-space gratings, both laser light and X-ray diffraction measurements have been used to quantify the kinetics of the decay process.^{187,188} In the case of hole growth in free-standing films, a method using gas flow rate to measure the hole growth has been developed.¹⁸⁹

The kinetics of the flow behavior is determined by the viscoelastic properties of the confined polymer films/nanostructures. Viscosity is often the focus of the measurement; surface tension is usually regarded as the driving force, but residual stress in some cases is not negligible and can even dominate.^{182,187,190} We will address the effect of the residual stress toward the end of this section; the bulk of the discussion below focuses on cases where surface tension is deemed to be the primary driving force. Theoretically, spinodal decomposition of polymer thin films can be used to study their dynamics; the growth rate in amplitude of a characteristic wavelength is dependent on the viscosity.^{174,175,191} However, a limited number of studies have focused solely on the scaling relationship between the spinodal pattern and the film thickness, not revealing thickness-dependent dynamics behavior.^{176,177,192} On the other hand, heterogeneous hole growth is a more convenient subject to investigate the polymer dynamics. Once a hole is formed in the polymer thin film, the driving force for hole growth is 2γ for suspended films and $|S|$ for supported films where S is the spreading coefficient defined as $S = \gamma_s - \gamma_{SL} - \gamma$ and the three γ terms represent the surface tensions of the substrate, substrate–film interface, and the film, respectively.¹⁹³ For a nonwetting surface, S is negative and gives rise to a Laplace pressure $|S|/h$ (or $2\gamma/h$ for suspended film) that drives the hole growth in a film of thickness h . The viscous dissipation inside the film and at the substrate/film interface can be calculated from the observed radial flow from the hole edge. Balancing the energy released from the hole growth with the viscous

dissipation, the viscosity can be calculated from the hole growth rate. For suspended films, the hole diameter grows exponentially with time, $R \propto \exp(t/\tau)$, with the rise time $\tau \propto \eta h/\gamma$ ¹⁹⁴ for a supported film, the hole diameter growth rate is constant, with $\partial R/\partial t \propto |S|h^{1/2}/\eta$.¹⁹⁵ Another related dewetting measurement deals with polymer films shrinking on a liquid substrate.¹⁹⁶ In the absence of friction at the edge of the film, the entire film shrinks at elevated temperature owing to the Laplace pressure $|S|/h$ on the surrounding edge. The film can be viewed under uniaxial extension along the film surface normal direction. The steady-state extensional viscosity can then be calculated from the strain rate, resulting in $\eta = |S|/(\partial h/\partial t)$.

For polymer surface profile evolution with time and temperature, the physics is well described by the Navier–Stokes equation, a staple tool for liquid behavior.¹⁷³ When the film thickness is larger than the wavelength (or $qh \gg 1$, wave vector $q = 2\pi/\lambda$), the relaxation time of the surface capillary wave is approximated by $\tau \approx \eta h/(\pi\lambda)$.^{188,197} This simple relationship has been used to quantify the viscosity of both polymer surfaces and polymer thin films.^{184,197,198} Another capillary wave theory leads to a more complicated relationship between the relaxation time and the wavelength of the surface wave.^{199,200} However, the change to a polymer surface profile, such as the recovery of a bumpy surface from a templating process, is not always modeled as capillary waves. This is justified when such change occurs at or below the bulk T_g . The viscosity at such low temperatures is presumed to be so large that viscous flow is not possible. Thus, the interpretation of those results rarely invokes viscosity. Instead, when the surface profile change happens at the temperatures below the bulk T_g , it is often regarded as a form of relaxation and the polymer dynamics are thought to be accelerated at the polymer surface. Still, the results from related measurements question this simple argument.^{180,184} The authors point out that the interpretation of recovery from a textured polymer surface requires information on the local strain and stress states; surface tension might not be the only driving force for the recovery. One study demonstrates that polymer surface dimples formed at different conditions show drastically different recovery kinetics below the bulk T_g .²⁰¹

Among these measurements focused on viscosity, some report a reduced viscosity with decreased film thickness,^{179,196,199} while others report that the thin film and surface viscosity are bulk like.¹⁸⁶ Shear thinning is an important issue as it can explain both the reduced effective viscosity^{178,202} and the hole growth with rim formation.^{203,204} Residual stress is another key as it has been shown time and again that it can affect the hole growth and flow behavior in general.^{205–207} It has been widely regarded that spin-coated thin polymer films are ‘highly metastable’,²⁰⁸ and large residual stresses persist.^{95,206} It is also noted that spin-coating can lead to oriented, nonequilibrium conformations of the polymer chains.²⁰⁹ The residual stress adds to the driving force of hole growth. Residual stress has been clearly shown to result in apparent viscosity that appears to be reduced from their bulk values.^{182,184,187,190} In fact, a recent study showed that the residual stress cannot be completely removed from a constrained film on a solid substrate.²¹⁰

In addition to the above measurements on thin polymer films, there are also reports on polymer flow through nanometer-sized channels or gaps. Capillary forces appear to be able to draw polystyrene (PS) melt into anodized aluminum

oxide membranes with channels 15 nm in diameter. The filling rate is used to calculate the viscosity, which shows weaker dependence on the molecular mass than the bulk behavior.²¹¹ In another report, the resistance to the squeezed flow into a 36 nm gap is found to be smaller for higher molecular weight PS than for the lower molecular weight counterparts.²¹² Both cases demonstrate that confinement of polymer chains to spaces smaller than the molecular coil size may greatly affect the center of mass mobility.

7.18.3.7 X-ray Techniques

Generally speaking, X-ray techniques are not used to study polymer dynamics. Most X-rays interact elastically with a material, with the electrons in the material scattering the incident photons. X-ray scattering techniques are well suited to probe structure in matter due to the elastic nature of the scattering and the commensurability of the X-ray wavelengths with the structures encountered in materials. X-rays can be inelastically scattered by material, where the scattered X-rays either gain or lose energy depending on the dynamics of the atoms in the material, but these techniques are not widely implemented for polymeric materials and are beyond the scope of this chapter. An X-ray technique that is very relevant to polymer dynamics in thin confined films is X-ray photon correlation spectroscopy (XPCS). There are some interesting studies that use XPCS in studying the polymer melt surface wave and nanocomposites.^{197,213–215} XPCS applies the same principles of dynamic light scattering in the X-ray regime. A sample is illuminated by a coherent X-ray beam which results in a speckle pattern in the scattered beam. This speckle pattern contains the information about the relative positions of the atoms or particles responsible for the scattering. If the particles or atoms in the beam are dynamically active, the speckle pattern will fluctuate with time. The dynamic information of the particles is derived from an autocorrelation of the speckle intensities as a function of time recorded in the scattering experiment. The second-order autocorrelation curve is generated from the intensity trace as follows:

$$g_2(q, \tau) = \frac{\langle I(t)I(t+\tau) \rangle}{\langle I(t) \rangle^2} \quad [2]$$

where $g_2(q, \tau)$ is the autocorrelation function of the intensity I at a particular wave vector, q , and delay time, τ . At short time delays, the correlation is high because the particles or surface waves do not have a chance to move to a great extent from the initial state; $I(t)$ and $I(t+\tau)$ are similar for short time intervals. As the time delays become longer, the correlation decays, because the two signals become increasingly different from each other. The Siegert equation relates the second-order autocorrelation function with the first-order autocorrelation function $g_1(q, \tau)$ as follows:

$$g_2(q, \tau) = 1 + \beta [g_1(q, \tau)]^2 \quad [3]$$

where the parameter β is a correction factor that depends on the geometry and alignment of the X-ray beam in the scattering setup. $g_1(q, \tau)$ contains the relaxation dynamics of the system. Typically, XPCS measurements are sensitive to dynamic processes on the order of 10^{-2} – 10^6 Hz and length scales on the order of 0.1– 10^4 nm. A review paper supplies details of the method and data reduction.²¹⁶

In nanofilled systems, the X-ray scattering contrast comes from the electron density difference between the polymer matrix and the nanoparticle, such as silica. The dynamics of the polymer matrix will cause the position of the nanoparticles to fluctuate. A good analogy is the movement of small particles in a suspension due to Brownian motion. The relaxation of polymer matrix is found to be very complicated and heterogeneous. Indeed, stretched exponential functions that are commonly used in bulk polymers, $f(q,t) = \exp[-(t/\tau)^\beta]$ with $\beta < 1$, were not able to describe the correlation function and the polymer matrix behavior.²¹³

XPCS measurements have been very effective at quantifying the surface wave dynamics in polymer thin films above their T_g . If the incidence angle of the X-ray beam is kept below the critical angle for total external reflection, the X-rays are not able to penetrate into the thin polymer film and all the scattering results from waves across the polymer surface.¹⁹⁷ This, of course, requires that the polymer be sufficiently above its glass transition such that the capillary waves are dynamically activated. The off-specular diffuse scattering from the polymer surface is recorded as a function of time with a two-dimensional charge-coupled device (CCD) camera. Such off-specular diffuse scattering is different from the specular XRR. In XRR, the specular reflection only reveals information in the direction of the sample surface normal, such as film thickness and roughness. The diffuse in-plane scattering intensity is usually much weaker than the specular intensity, but its intensity is greatly enhanced in total external reflection, allowing time-resolved measurement. In such a mode, the scattering from the film–substrate interface is negligible, and only fluctuations of the polymer–vacuum interface are probed. As addressed in the previous section, the polymer melt surface fluctuation should decay as a single exponential. Fitting of the first-order autocorrelation function gives the relaxation time, from which the viscosity is calculated. A series of measurements revealed that polymer films thicker than $4R_g$ yield thin film viscosities in agreement with the bulk viscosity.^{197,214,215} However, thinner films show suppressed dynamics and enhanced viscosity relative to the bulk.²¹⁵ In such strong thin film confinement, the polymer surface cannot be regarded as a viscous liquid; to interpret the XPCS data, a shear modulus has to be included due to what has been interpreted as a pinning of the polymer chains to the substrate.²¹⁵

XPCS is a time-resolved X-ray diffuse scattering experiment. However, even simple diffuse X-ray scattering has been used to study the polymer thin film.^{192,217,218} When a molten polymer thin film is quenched to temperatures well below T_g , the surface waves at the elevated temperature are presumed to be frozen into the now glassy film. This allows for diffuse scattering measurements even above the critical angle for total external reflection in spite of the weak intensity. The polymer thin film surface behaves like a capillary wave when the interaction between the film and the substrate is weak.¹⁹² Unusual nonliquid-like behavior emerges under strong confinement due to strong interactions at the polymer–substrate interface.^{217,218}

7.18.3.8 Inelastic Neutron Scattering

Neutron scattering is a powerful tool for characterizing the structure and dynamics of soft materials like polymers. Neutrons are similar to light and X-rays in terms of their utility

in scattering for materials science, but with several distinct advantages that make neutrons well suited for characterizing polymeric materials. Cold neutrons, like those found in most neutron scattering facilities, have wavelengths on the order of 1–10 Å. As with X-rays, these length scales are on par with the typical interatomic or intermolecular distances in materials, which make diffraction and small-angle scattering measurements feasible; neutrons are excellent structural probes, comparable to X-rays in the parameters they can quantify. Classic diffraction experiments can be used to probe interatomic or intermolecular distances, crystal structures, and radial distribution functions. Small-angle scattering experiments can be used to probe larger ensembles or aggregate structures such as particles, heterogeneities, agglomerates, and crystal domains with length scales nominally in the 1 nm to 1 μm range. It is also possible to perform reflectivity experiments using neutrons to characterize the thickness, vertical density or composition profile, and roughness of a given polymer film with thickness in the range of approximately 1–200 nm. Neutron diffraction, scattering, and reflectivity are hence powerful structural probes for polymeric materials and thin films.

The X-rays in most scattering experiments have energies on the order of a few kilo electron volts. This is at least 6–7 orders of magnitude greater than the typical solid- and liquid-state excitations that occur in most polymeric materials. Most X-rays scatter or penetrate polymers with very little change in the energy of the incident beam. In contrast, cold neutrons have energies typically in the millielectron volts range, which are on the same order of magnitude as the activation energies for many of the solid-state excitations, molecular relaxations, and dynamic processes that occur in polymeric materials. This is coupled by the fact that hydrogen-containing materials scatter neutrons strongly; hydrogen has the largest scattering cross section of all the elements for neutron scattering. This is unlike X-ray scattering where the scattering length density of a material increases with the atomic number Z . Hard materials like ceramics or metals typically do not scatter neutrons strongly at all, whereas polymers and organics that are rich in hydrogen scatter strongly. The combination of a large scattering cross section with incident beam energies that are comparable to the intrinsic excitation energies means that polymeric materials scatter neutrons with large changes in the energy of the incident neutron beam. Using energy-sensitive neutron detectors, it is easy to quantify the energy gain/loss from the scattered neutrons. From energy and angular dependencies of the scattered neutrons, it is possible to determine the time and length scales of the dynamic processes in the polymers. This is the basis for inelastic neutron scattering.

The neutron scattering cross section of an element can be broken into its coherent and incoherent components (there is also an absorption cross section which is unrelated to scattering which we will not address here). The cross section reflects the number of neutrons scattered per second from the element divided by the intensity of the incident neutron beam. For coherent scattering events, there is a spatial correlation between the scatterings from different nuclei of the same type (with the same scattering length density). These spatial correlations allow us to determine the Van Hove or the pair–pair correlation function, that is, the spatial correlations between the different atoms. For incoherent scattering events, this spatial correlation

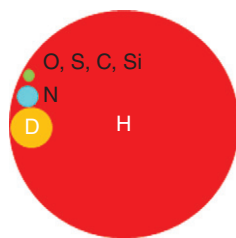


Figure 6 A series of spheres scaled to the corresponding incoherent neutron scattering cross section of some of the elements commonly encountered in polymeric materials. As discussed in the text, H has the largest incoherent neutron scattering cross section of any of the elements. Inelastic neutron scattering experiments to quantify dynamics, which rely on incoherent scattering, are strongly biased toward the motions of the hydrogenous groups.

is lost and there is no relation between scattering events between different pairs of atoms. However, the energy gained or lost by the scattered neutron is still perceivable. By converting the energy exchange into the time domain, one can determine the self-correlation function. This tells us at a time t (defined by the energy exchange) how far the nucleus has moved from its initial position at $t = 0$. From the energy and angular dependence of the incoherent scattering, one can determine the time and length scale of the relaxations or other dynamic motions in a polymeric system. In the discussion above, we mention that hydrogen has the largest scattering cross section of all the elements. This cross section is nearly all incoherent; the coherent scattering from hydrogen is negligible. **Figure 6** displays a series of circles whose areas are scaled proportionally to the incoherent scattering cross section of the nuclei they represent. From this representation, it is apparent that inelastic neutron scattering is primarily sensitive to the dynamics of the hydrogen-containing chemical groups or

moieties. As most polymers are hydrocarbons, their incoherent scattering is very strong. Inelastic neutron scattering is one of the most direct methods to quantify the time and length scales of polymer dynamics.

The dynamic processes and relaxations that occur in polymers span a broad range of time and length scales. It is generally not possible to access the full phase space of time and length scales of these processes in a single inelastic neutron scattering experiment. Different types of experiments are sensitive to different regions of this phase space, as illustrated in **Figure 7**. With respect to polymer dynamics in confinement, the three primary techniques that have been utilized thus far include neutron spin echo (NSE) spectroscopy, backscattering (BS) spectroscopy, and time-of-flight (TOF) spectroscopy. The different principles of operation for these different spectrometers are beyond the scope of this review. Here, the primary focus is in on the time and length scale of the dynamics probed by each spectrometer. The NSE is sensitive to the slowest motions of the three spectrometers. It is most sensitive to dynamic processes on a timescale of 10^{-7} – 10^{-10} s, placing it in the micro- to nanosecond range. To place the NSE technique in context, most solid-state NMR instruments are sensitive to dynamic processes on the order of a microsecond and slower. As larger objects tend to move slower, NSE is also sensitive to the longer-range motions; length scales on the order of 1–100 nm are common in NSE experiments. At these length scales NSE can be used to monitor diffusive motions of polymer chains or large-scale collective motions that span across tens to hundreds of atoms. By comparison, BS measurements are sensitive to slightly faster and shorter range motions. Most backscattering spectrometers are only sensitive to those motions faster than a nanosecond (slower motions appear as static or elastic scattering) at length scales that are comparable to most wide-angle X-ray diffraction experiments. This includes molecular and atomic displacements nominally in the 1–30 Å

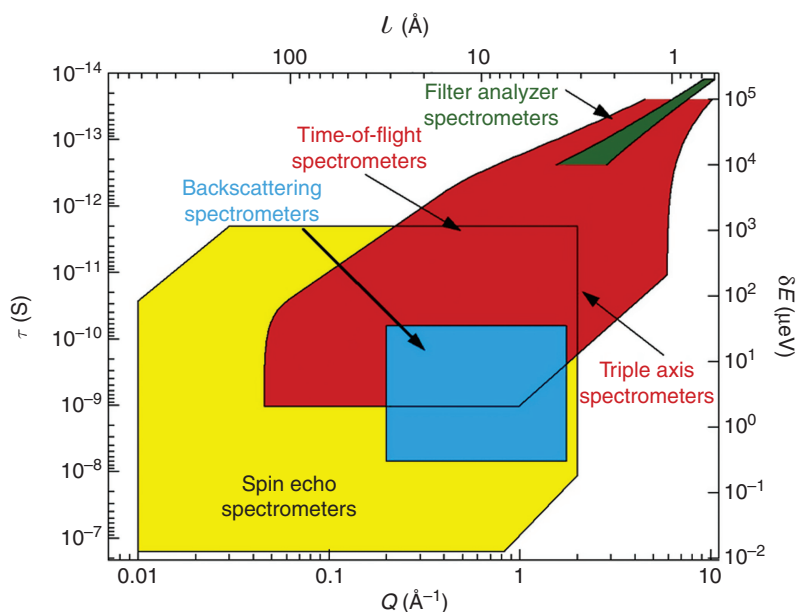


Figure 7 This figure maps out the length and energy scales that are accessible with the different inelastic neutron scattering techniques. In the text, we have limited our discussion to the time-of-flight (TOF) spectrometers, backscattering (BS) spectrometers, and spin echo spectrometers.

range, which include not just atomic vibrations but also some of the segmental motions. In polymers, these often include side group motions, such as methyl rotations or crank shaft motions of chain segments. The TOF spectroscopy is sensitive to the fastest dynamics of the three instruments and to dynamics on the order of picoseconds and faster and over comparable length scales as in the BS instrument. At these timescales, the dynamical processes probed in TOF experiments are typically atomic or molecular vibrations. Many of the same modes seen in infrared or Raman spectroscopy are also evidenced by TOF spectroscopy. Yet, unlike infrared or Raman, there are no optical selection rules in neutron scattering as to which modes are visible; the closest equivalent would be the scattering cross section. In this respect, TOF can be regarded as more sensitive to the vibrational and high-frequency relaxation processes of the hydrogenous moieties in the sample. To properly interpret experimental neutron scattering data for polymers under strong states of confinement, it is important to remain cognizant of the time and length scales of the motions that the spectrometer is sensitive to.

Inelastic neutron scattering processes are typically weak in comparison to elastic scattering events. The intensities of elastically scattered neutrons (no energy exchange) are often 3–4 orders of magnitude greater than those observed in inelastic scattering. To obtain a reasonable signal-to-noise ratio, most inelastic scattering experiments typically require 50–100 mg of the polymer sample in the neutron beam. This condition is not met with a single thin polymer film. As we discuss later, there have been several attempts to stack multiple thin films together to obtain a sufficient scattering intensity, but sample preparation is a challenge. However, inelastic neutron scattering on highly confined polymer systems achieved by either the nanoparticle or the nanopore confinement schemes is straightforward. The hard confining media, either the particles or the porous support media, often have scattering cross sections significantly smaller than the hydrocarbon polymers. The inelastic scattering signal from the confining media is significantly weaker and to a first approximation can be treated as neutron transparent. The inelastic neutron scattering of a poly (methyl methacrylate) confined by adding large volume fractions of alumina nanoparticles is still dominated by the polymer. This is further facilitated by the fact that dynamics of the hard material, such as the aluminum sample can or alumina nanoparticles, are often negligible in comparison to the soft polymers. Nevertheless, it is always a good idea to estimate the volume fractions of the hard confining material and the soft polymer, calculate the relative scattering length densities of the two phases, and obtain a quantitative estimate of their relative contributions to the inelastic scattering. It is also important to correct the experimental scattering data for the background signal from the confining media, but this is made easy by the fact that the polymer generally scatters strongly and with considerably more dynamic processes in comparison to the confining media.

The first inelastic neutron scattering measurements on polymers under strong states of thin film confinement were performed by Soles and co-workers on a variety of systems. In reality, these pioneering measurements were not truly 'inelastic' in that they did not quantify the change in energy of the scattered neutrons.^{219–225} Rather, they monitored confinement-induced changes in the elastic scattering intensity

as a function of temperature and wave vector and used the Debye–Waller formalism and a harmonic oscillator approximation to convert the q dependence of the elastic intensity changes into a mean square atomic displacement $\langle u^2 \rangle$; these measurements could tell when a molecular motion became fast enough to appear within the energy resolution window of the spectrometer (approximately a nanosecond), but they could not tell how fast they were moving within that window. Nevertheless, these measurements showed a strong suppression of $\langle u^2 \rangle$ for films thinner than approximately 100 nm. The magnitude of the suppression depended upon the sub- T_g or side group molecular mobility within the system. Systems with higher mobility in the glassy state were more strongly suppressed, while systems with little mobility below segmental mobility below T_g showed little suppression below T_g . Above T_g where molecular mobility is generally significantly higher, all systems showed substantial suppression of mobility with decreasing thickness. This was interpreted in terms of an effective stiffening of the polymer film. Surprisingly, there was no correlation with these direct measurements of molecular mobility and the apparent T_g measured by other techniques. Overall, the level of mobility decreased regardless of whether the apparent T_g , as measured by a kink in some other temperature-dependent property, increased or decreased. The authors also effectively correlated these suppressed mean square atomic fluctuations to a slowing down of the reaction-diffusion transport processes responsible for performance of photoresists in semiconductor fabrication.

Shortly after these initial Debye–Waller measurements of the elastic scattering intensities in thin polymer films, several researchers developed methods to quantify the full inelastic scattering spectra. In the original measurements by Soles and co-workers,^{219–225} the polymer films were supported on Si wafers, cleaved into smaller pieces, and placed in the neutron scattering cell. Since Si is essentially transparent to neutrons, the scattering was dominated by the polymer films, despite the fact that most of the sample cell contained Si. However, the amount of polymer was not sufficient to resolve the inelastic scattering processes that were several orders of magnitude lower in intensity (and thus the use of the Debye–Waller approximation). This problem was solved by several other groups who used aqueous floating techniques to lift the polymer films off the thick Si wafers and then transfer them to much thinner aluminum foils or meshes.^{225–232} Using this approach, they were able to increase the amount of polymer film in the neutron beam by almost an order of magnitude. Since aluminum is also essentially transparent to neutrons, this enabled a full quantification of the inelastic neutron scattering spectra as a function of film thickness. These new results proved to be fully consistent with the previous Si-supported films and revealed a suppression of $\langle u^2 \rangle$ for films thinner than approximately 100 nm which was interpreted as an effective stiffening of the film. The additional information provided by the inelastic spectra help identify the nature of this dynamic suppression or stiffening. The frequency of the Boson peak, a collective many-atom vibrational mode with an energy of approximately 1–5 meV in most glassy materials, was largely unchanged by the state of thin film confinement. Rather, the dynamic suppression showed up in the anharmonic or relaxation processes of the material that occur on the nano to picoseconds time-scale. These measurements revealed that the dynamic

suppression of motions parallel to the plane of the film was less significant than that perpendicular to the film.²³² They also revealed that the magnitude of this dynamic suppression did not appear to depend on the molecular mass of the polymer film.²²⁷

There have also been numerous inelastic neutron scattering studies on polymer dynamics in strong states of nanopore confinement. There are a wide variety of porous confining media available that are made of inorganic and hard materials. These materials are attractive for inelastic neutron scattering studies because (1) the porous media is often transparent to neutrons and (2) even if there is some inelastic scattering from the porous media it is typically much more rigid and dynamically dead than the soft polymers. These porous confinement studies can be largely separated into two groups: channels and spherical pores. Most of the porous channel work leverages the increasing availability of porous AAO membranes which have well-defined pore sizes packed in a hexagonal array, extending for several microns to make thick, porous membranes (although there have also been a few using similar porous silicon substrates). One can readily fill the membrane by utilizing capillary forces which merely require placing a polymer melt on the surface of the membrane. Most of the studies in this field have focused on PEO in porous AAO. The first published example in this field reported an increase in $\langle u^2 \rangle$ of the PEO over the bulk state for confinement in 33 nm diameter pores for temperatures between T_g and T_m .²³³ These increased dynamics were attributed to a disruption of the crystallinity of the PEO in the nanopores. The dynamics of amorphous PEO in the rubbery state are significantly more active than crystalline PEO below its melting temperature. However, subsequent measurements on a range of pore sizes from 40 nm down to 13 nm in diameter seem to generally support a reduced mobility of the PEO with increasing confinement.^{234–238} The emerging notion is that near the wall of the pore a layer of tightly bound PEO forms while the molecules in the center pore can display more bulk-like dynamics. However, these measurements are not without controversy. One of the most recent reports indicates that the PEO displays bulk-like behavior even in an 18 nm pore.^{236,237} It should also be emphasized that measurements have used a range of spectrometers, including TOF, BS, and NSE. Together, these instruments will quantify timescales that include the high-frequency local atomic displacements that would be affected by interactions with the pore surface, intermediate Rouse modes of several statistical segments between entanglement junctions, and the larger-scale and slower reptation motions. What is somewhat surprising is that it looks like the longer timescale dynamics measured by NSE, on the verge between Rouse- and reptation-like, are largely unchanged by confinement whereas the higher- Q , higher-frequency modes in BS and TOF tend to show the most signs of suppression. This notion could be consistent with an immobilized, surface layer of molecule around the periphery of the pore and a mobile population of molecules in the center.

Most of the work on polymers confined in three-dimensional pores have come from Schonhals and co-workers on poly(methyl phenyl siloxane) (PMPS) and poly(dimethyl siloxane) (PDMS) imbibed in controlled pore glasses. They have a series of publications on these systems which generally show a slowing down of the high-frequency

dynamics of the methyl groups and other hydrogenous groups of the polymer as the pore size systematically decreases from 7.5 down to 2.5 nm.^{29–31} At very low temperatures, deep in the glassy state, the onset of the methyl rotors does not seem to be strongly affected by confinement. However, above T_g there is a clear decrease in the anharmonic motions that would give rise to translational motions as the state of confinement increases. This reduced mobility in the confined polymer is supported by a transition from VFT-type dynamics in the bulk and large pores to Arrhenius behavior in the smallest pores and a subsequent decrease in the step change of heat capacity at the calorimetric T_g . Polymer mobility seems to be strongly suppressed in three-dimensional nanopores.

7.18.3.9 Fluorescence Measurements

Fluorescence techniques are widely used to quantify the dynamics of polymers in strong states of confinement. Most of these measurements have been on polymers under thin film confinement, but recently there have been a few extensions to nanoparticle confinement as well.^{239,240} These optical techniques are attractive because they are relatively easy to implement in the laboratory setting and versatile in their capabilities. Several different types of fluorescence measurements have been used to quantify the dynamics of thin polymer films, each sensitive to slightly different physical parameters, time-scales, and length scales. Here, we briefly review the more common approaches.

The most straightforward and widely implemented method is to monitor the fluorescence intensity as a function of temperature. A fluorescence detector or fluorimeter is used to quantify the fluorescence intensity coming from the thin polymer film while it is exposed to an excitation source. To maximize the signal intensity at the detector, one usually first looks at the complete spectrum of fluorescence emission of the film and sets the detector to selectively monitor the wavelengths for one of the stronger emission peaks. It is then straightforward to configure the polymer film, typically supported on a quartz or glass substrate, in a thermally controlled environment and record the emission intensity as a function of temperature. Typically, the fluorescence intensity decreases as the temperature increases and one encounters a kink or change in the temperature dependence at the calorimetric glass transition temperature of the polymer. The convention has been to ascribe shifts in this kink with decreasing film thickness as changes in the apparent glass transition of the thin polymer film. This approach has largely been championed by the Torkelson research group and they have amassed an extensive body of literature on using these methods to study confined and thin polymer films.^{89,159,239–261}

There are many possible explanations as to why the fluorescence intensity is temperature dependent. Fluorescent chromophores generally exhibit a reduction in their fluorescence intensity with increasing temperature due to the increased thermal energy and the concomitant increase in the rate of the nonradiative decay of the chromophore from the excited state back down to the ground state. Shortened excited states lead to a decrease in the fluorescence intensity with increasing temperature. That the temperature dependence of these decay processes is different above and below T_g seems reasonable, given the fact that polymer dynamics in the two

regimes are very different. However, very little is known about the mechanisms by which this occurs. One cannot easily assign a dynamic time or length scale to these observations, since the processes are complex and poorly understood. In fact, the nature of the response is not always the same. Generally, the temperature dependence of the intensity decay becomes stronger above T_g , but there are a few examples of where it becomes weaker.^{242,244,245} It has been suggested that the transition to a weaker thermal dependence above T_g occurs when the thin films have strong interactions with the substrate, implying increased rigidity of the polymer in the rubbery state,²⁴² but it has also been shown that the effect can be induced by switching the covalent attachment point of the chromophore from a chain end to a side group.²⁴⁵ There are also examples of fluorescence intensities that increase with increasing temperature, making the interpretation complicated.²⁴⁵ These counterintuitive responses suggest a very complicated connect to the level of polymer dynamics in the film. We refer the readers to a recent manuscript which describes in detail the nature of some of these anomalies.²⁴⁵ Nevertheless, time- and temperature-dependent fluorescent measurements have proven to be a valuable tool in inferring thickness-dependent changes in the dynamics of thin polymer films from changes in their apparent glass transition temperatures. There are numerous examples of where the apparent glass transitions determined by this approach are consistent with other complementary measurements.^{242–246,254,261} One of the general themes that emerge in this literature is that the thin film T_g increases for films supported on substrates with favorable interactions and decreases on substrates where the interactions are unfavorable. These effects typically set in when the film thickness drops below approximately 50 nm.

These temperature-dependent fluorescence intensity measurements have been extremely powerful in extracting distributions in the apparent glass transition temperature in thin polymer films. There has been a long-standing debate in the polymer thin film community about the nature of the dynamics at the various interfaces of the film (e.g., free surface or substrate) in comparison to the center of the film. Theoretical predictions by de Gennes suggested that chains at the free surface of a thin film exhibit enhanced mobility and that the focus should be on determining the distribution of T_g s and mobilities through the thickness of the film. Fluorescence intensity measurements effectively addressed this issue by specially designed multilayer films.²⁴⁶ An extremely thin, 12–14 nm thick, chromophore-labeled PS film was spin-cast on a salt crystal and then floated off into a water bath. The labeled PS film was then picked up and laminated onto chromophore-free PS films that were about 1 order of magnitude thicker. Several variations of the multilayer films were made. There were bilayers where the dye-labeled thin film was either at the free surface or at the bottom in contact with the supporting substrate as well as trilayers of varying thicknesses where the dye-labeled PS was located in the center of the film. By monitoring the temperature dependence of the fluorescence intensity of just the dye-labeled marker layer at its various locations, the authors could extract a distribution of apparent T_g s through the thickness of the multilayer composite. These measurements revealed strong negative deviations of the apparent T_g near the free surface, but no deviations near the rigid supporting substrate. When the total thickness of the

multilayer samples decreased below approximately 50 nm, the authors saw apparent T_g reductions across the stack, but generally stronger ones near the free surface. These measurements were also extended to multilayer films where the different layers consisted of immiscible polymers to show that apparent surface T_g reductions could be eliminated by changing the underlayer.²⁶¹ This implies collective molecular motions across the interface. However, shifts in the apparent glass transition temperature are not true measurements of polymer mobility; shifts in a temperature-dependent kink do not necessarily capture overall changes in the polymer dynamics. Torkelson and co-workers addressed this issue by using a known sensitivity of the fluorescence intensity to isothermal physical ageing.²⁶² In the early 1990s, they showed that physical ageing increases the fluorescence intensity in a well-defined manner. Using this phenomenon and the selectively labeled multilayer samples, they were able to extract physical ageing rates as function of location through the thickness of the film.^{258,259} These measurements revealed that the physical ageing rates were reduced by a factor of 2 at the free surface and by a factor of 15 near the supporting substrate. These results suggest retarded relaxations of the polymer at both the free surface and the substrate. It is striking that apparent T_g reductions were observed for this same system at the free surface but not the substrate interface. The relation between the apparent T_g and the actual dynamics is not always straightforward.

We have yet to discuss the chromophores used in these temperature-dependent fluorescence measurements. There are three possible schemes for obtaining fluorescence measurements in thin films: freely doped films, labeled films, and intrinsic fluorescence. Freely doped films are typically the easiest samples to prepare, but also the most problematic to interpret. For this approach, trace amounts of a fluorescent small molecule such as pyrene, anthracene, or dispersed red 1 are added as a free dye to the spin-casting solution. The concentrations of these dyes are usually kept well below 1% by mass of the polymer in the solution. As the film is spin-cast and dried, the dye molecules are entrapped in the film. The idea is that if trace amounts are used, the dye will not adversely affect the intrinsic properties of the polymer matrix itself. This approach is very easy in that chemistry is not required. As long as a cosolvent can be found for the polymer and the dye, films can be cast. However, one should verify that the probe molecules are not altering the dynamics of the polymer by their presence. The biggest problem with this approach, however, is in the interpretation. Interfacial partitioning of the dye molecules is a big concern. There will always be a slight preference for one of the two components (dye and polymer) to be at an interface or phase separate into domains and this may affect the results; the fluorescence response might be biased toward one of the substrates or a dye-rich region (depending on loading). There can also be a tendency for the small probe molecules to sublime from the film, especially at elevated temperatures, which will give reproducibility errors in the fluorescent intensities. Quantifying the amount and distribution of the free probes in the thin films is not a trivial task.

Many of these concerns can be diminished or alleviated by using polymers with chromophores or dyes covalently attached to the chain as an end group, a side group, or segment inserted into the main chain itself. Typically, these labels are added in very low concentrations so that they do not affect the dynamics

or nature of the neat polymer. Their incorporation into the polymer chain keeps the dye molecules well dispersed. The addition of the entropic contributions of the polymer to their free energy of mixing keeps them well dispersed and less susceptible to surface energy effects. This also solves the problems with dye sublimation. Using this approach, one can exact precise control over where the dye molecules are located along the chain, reducing the ambiguity in the measurement. There are also the innovative measurements that we discussed earlier of selectively incorporating very thin layers of dye-labeled polymers at specific locations within a thicker film to probe the dynamics in different regions of the film.^{258,259} The biggest complexity with this approach is the complication that custom polymers must be synthesized or labeled. This is often a non-trivial task. It is also known that the fluorescence response of a dye molecule can depend on the way in which it is incorporated into a thin film. The thickness-dependent responses of chromophore, one freely doped into a polymer and the other covalently attached to that same polymer, can be completely different.²⁴⁵ Furthermore, covalently attached chromophores can also behave very differently if they are attached to different locations of a polymer, such as a side group versus a terminal end group.²⁴⁵ This makes interpretation of the molecular mechanisms of confinement difficult. However, they are quite useful for identifying thickness trends within a given system.

There are also several temperature-dependent experiments that rely upon the intrinsic fluorescence of the polymer. The number of polymers that exhibit intrinsic fluorescence makes these experiments limited, especially since this type of fluorescence is generally weak and not amendable for thin film measurements. These types of experiments are preferred when possible because they are not complicated by interpretations about where or what the dye is doing in the polymer. However, these measurements also come with their own set of concerns. It is generally understood that the fluorescent intensity coming from a polymer is dependent on the refractive index and absorption coefficients of the polymer, which are also temperature dependent. However, estimates indicate that this effect is not greater than a few percent on the measured intensities.²⁴⁵ There are also reports that the fluorescence intensity can change isothermally with physical ageing of the polymer.^{258, 259, 262} This should be considered when comparing different heating or cooling rates for the fluorescence intensity measurements. *In situ* ageing affects might affect the measurements for very slow ramp rates. It has also been shown that presence of dissolved diluents or small molecules can have very pronounced effects on the apparent T_g s measured by fluorescence intensities.^{244,252,257} Diluents have been shown effective at eliminating thickness-induced changes in the apparent T_g and the presence of sorbed gases, water vapor, and/or residual casting solvents might influence the results as well.

A more detailed understanding of the dynamics in thin polymer films can be obtained by switching from temperature-dependent fluorescence intensity measurements to quantitative measurements of the fluorescence lifetimes. The ability to measure a well-defined lifetime assigns a specific timescale for the polymer dynamics being probed. There are many different variations of these fluorescent lifetime measurements, often differing in the timescales being probed. On the fast end of the spectrum, there are several examples of measuring the fluorescence lifetime of the excited state of a dye molecule either

blended into or covalently attached to the polymer chain. The excited state of the chromophore is typically generated with a fast laser pulse (typically on the order of a nanosecond full-width half maximum (FWHM)) of a single wavelength laser which induces a fluorescent excited state followed by a time-dependent monitoring of the fluorescent decay. Granick and co-workers used this approach, coupled with a chromophore whose optical dipole was aligned parallel to the chain axis, to study the relaxation anisotropy in thin PS films.²⁶³ There are also examples of where two photon processes, such as second harmonic generation (SHG), can be used to excite the chromophore. It is generally understood that the lifetime for the excited states and the fluorescent lifetimes would be greatest in a vacuum; inside a glassy or rubbery polymer, the long-lived fluorescent lifetimes are cut short by interactions with the chromophore and the surroundings. In this way, the fluorescent lifetime is sensitive to the dynamic fluctuations in their surrounding environment, that is, the polymer environment. Often, these lifetimes are on the order of tens to hundreds of nanoseconds in most polymeric environment. However, it is dangerous to overgeneralize these timescales as they depend on the size and nature of the chromophore. There are examples using SHG excitation in combination with an electric field where the susceptibility of the excited state fluorescence took several hundred seconds to recover, although these results were somewhat complicated by the presence of an electric poling field.²⁵⁰ Nevertheless, there have been direct comparisons between the temperature-dependent fluorescent measurements described above and the lifetime measurements here that reveal similar apparent glass transition in thin polymer films.²⁵⁷ The advantage of the lifetime measurements is that the timescale is well defined.

It is also possible to use fluorescent techniques to quantify diffusive processes in thin polymer films. Fluorescence NRET methods have been utilized to quantify movements on the order of 1–10 nm of chromophores in thin polymer films. NRET occurs when a donor chromophore that has been excited into its fluorescent state transfers its energy to an acceptor chromophore through a coulombic dipole–dipole interaction. As these interactions fall off as $1/R^6$, where R is the separation between the donor and the acceptor, these interactions are limited to separations of just a few nanometers. The terminology in this field can be somewhat confusing and other names for essentially the same process include Forster resonant energy transfer (FRET) or sometimes called fluorescent resonant energy transfer (also FRET); all these processes are essentially the same mechanism. The basic concept of these measurements is to measure how long it takes for the excited donor chromophore to transfer its energy to the acceptor. By knowing the timescale and the Forster radius for the donor–acceptor pair, one can estimate a diffusion coefficient over the length scale of a few nanometers. This, of course, requires labeling the polymers with suitable donor and acceptor molecules. The time for energy transfer can be quantified by monitoring either the loss of fluorescence in the acceptor chromophore or the onset of fluorescence in the acceptor, if applicable. Hall and co-workers were successful in extending these NRET-diffusive measurements out over much longer length scales by assembling bilayer polymer films where each half of the bilayer is only labeled by the donor or the acceptor. With this approach, the timescale for interdiffusion of the two layers could be tracked

over several minutes by monitoring the onset of the NRET effect as the two layers became intimately mixed.¹⁵⁹

FRAP methods can also be used to quantify chain mobility or tracer molecule mobility in confined polymeric systems. FRAP experiments utilize a fluorescent dye molecule, either as an additive or as a label on a polymer chain, whose emission is irreversibly bleached by exposure to an intense laser light. An initial 'writing' step creates spatial variations in the fluorescence emission by selectively exposing specific regions of the film to the intense incident radiation. The regions exposed to this light lose their fluorescence, while the unexposed regions remain fluorescent. A second 'reading' operation occurs by flood-exposing the film to a uniform film of the same wavelength light at a significantly reduced intensity. It is important that the intensity of this reading beam is not sufficient to induce photobleaching of the chromophore. This will create fluorescent patterns, defined by selectively exposed regions, in the as-bleached samples. Diffusion in the film is tracked by monitoring the fluorescent intensity in the bleached regions. With time, the active dye molecules can diffuse back into the bleached regions, leading to a recovery of fluorescence. By knowing how long it takes for steady-state fluorescence to recover into the bleached regions and the length scale of the bleached patterns, one can calculate an in-plane diffusion coefficient for the dye-labeled species. The time and length scale of these FRAP measurements are primarily defined by the periodicity of the pattern bleached into the film or material. The larger the length scale of the bleached patterns the longer it will take for active chromophores to diffuse back into the bleached regions and recover the fluorescence. Depending on the size of the patterns, this will be as short as hundreds of nanoseconds to as long as several hours. This timescale will also depend on the temperature and the viscosity in the polymer film. Typically, the bleached patterns are periodic line-space gratings. These can be achieved by passing the incident light through a shadow mask such as chrome lines on a quartz substrate. This method is well suited for pattern periodicities on the order of a micron or larger, probing diffusion over similar length scales. Frank and co-workers used this approach, with a pattern periodicity of 4 μm , to document a 50% decrease in the self-diffusion coefficient of dye-labeled PS chains for films thinner than 150 nm.¹⁵⁸ This length scale was significantly larger than the nominally 50 nm length scale for many of the reported T_g deviations in thin PS films. It is also possible to generate periodic optical patterns through interfering laser beams. Tseng and co-workers used this approach to also probe the mobility of dye-labeled PS in thin film over similar length scales, but unlike Frank *et al.*,¹⁵⁸ they reported a significant increase in the self-diffusion coefficient for films thinner than 100–300 nm.^{156,157} The source of the discrepancy for these measurements is believed to be segregation of the fluorescent dye to the surface where the polymer mobility is enhanced.¹⁵⁷ It should be possible to probe significantly smaller length scales using the FRAP techniques using interfering laser beams to generate the bleaching patterns; diffusion length scales on the order of 100 nm or smaller should be feasible, although reports in the literature have yet to be seen. Lastly, it is important to note that this approach creates bleached patterns in the plane of the film. Recovery of the fluorescence requires in-plane diffusion of the active chromophores, which is one significant advantage of this technique. Most methods, including all the

other fluorescent methods discussed thus far, cannot distinguish between in-plane and vertical dynamic processes.

7.18.3.10 Nuclear Magnetic Resonance

Solid-state nuclear magnetic resonance (NMR) can be used to study molecular dynamics (MD) in confined polymeric systems. Since the NMR relaxations generally occur in the micro to millisecond time regime, NMR is uniquely suited to study the dynamics that occur under various levels of confinement since critical relaxation times that relate to confinement (Rouse modes, disengagement times, and Kuhn segment fluctuations) also occur in this time regime. We refer the reader to more comprehensive surveys on dynamics of organic materials using solid NMR.^{264,265}

The formal theory of Bloembergen, Pound, and Purcell (BPP) has long been established to describe the relaxation of nuclear magnetization by the coupling of the nuclear spins to stochastically fluctuating local magnetic fields with spectral density around the Larmor frequency (and its second harmonic).²⁶⁶ Indeed, for several decades now, BPP theory has been utilized to describe the fluctuations that occur in polymers in the 10^3 – 10^8 Hz frequency regime, generally by measuring relaxation times over a range of temperatures and magnetic field strengths. In this spirit, various parameterized models have been established to describe specific spectral density functions that might be observed in polymeric systems.²⁶⁷ BPP theory is also very useful for interpreting the strongly coupled ^1H NMR line-shape since motional narrowing of the line is generally observed for higher densities of fluctuations in the megahertz regime. Indeed, ^1H NMR line-shape analysis has been utilized to qualitatively describe the motions of polymers confined in multiple geometries,²⁶⁸ to complement other variable temperature relaxation studies that have been performed on confined systems.^{269,270}

Deuterium NMR is a powerful method for probing specific molecular motions; a very comprehensive review was given some time ago.²⁷¹ Since the deuterium nucleus is a quadrupole, it is sensitive to electric field gradients and, hence, behaves as a second-rank tensor making the ^2H resonance of each nucleus sensitive to orientation. In the case of polymers with molecular motions much slower than the theoretical NMR linewidth (<10 kHz), the resultant ^2H NMR line-shape is a Pake doublet with a splitting that is directly proportional to the quadrupolar coupling constant. However, polymers that have molecular motions on similar timescales as the ^2H linewidth (10 kHz to 10 MHz) can induce interesting changes in the ^2H NMR line-shape which can be directly related to specific molecular motions. As a result, the ^2H line-shape can be utilized to understand specific molecular motions that occur in polymers; it has been utilized for a number of confined polymeric systems for just that purpose.^{272–283}

One quite robust method that can probe relaxations over quite a broad range of frequencies is field cycling NMR relaxometry.²⁸⁴ In this method, high-field (several Tesla) polarized magnetization is inverted or saturated and the recovery of the magnetization occurs in a cycled magnetic field over a variable time interval such that the longitudinal relaxation time (T_1) can be measured in various field strengths; recall that nuclear magnetic relaxation is sensitive to spectral density around the Larmor frequency, which is in turn proportional to the field

strength via the relation $\omega = \gamma B_0$, where ω is the Larmor frequency (rad s^{-1}), γ is the gyromagnetic ratio ($\text{rad s}^{-1} \text{T}^{-1}$), and B_0 is the magnetic field strength (T). Since the magnetic field can be cycled over quite a large range of values (10^{-5} –1 T), the corresponding range of Larmor frequencies is considerably large as well (10^3 – 10^8 Hz). Hence, the longitudinal relaxation time (T_1) measured via field cycling NMR can be used to probe relaxations occurring over several decades in time (10^{-3} – 10^{-8} s). As a result, field cycling NMR has been demonstrated in numerous polymeric systems in multiple geometries of constraint.^{285–292} Of specific note has been the work of Kimmich and colleagues, who have utilized the technique on a confined PEO melt in a solid methacrylate matrix, polyfluoropolyether (PFPE) thin films sandwiched between Kapton foil, and PFPE melts in confined silica glass (Vycor) nanopores.²⁹³

Another method that has been growing attention as of late is multiple quantum magic angle spinning (MQMAS) NMR due to the ease of implementation into standard solid NMR spectrometers. In MQMAS, a (nonobservable) higher-order quantum coherence is prepared, which is then allowed to evolve over a variable mixing time, and is subsequently reconverted into a (detectable) single-quantum coherence state. A veritable library of pulse sequences have been developed which can populate higher-order coherence states. However, we only mention the most highly used sequence, back-to-back (BABA), utilized in double-quantum NMR due to its ability to be implemented in experiments which rely on fast magic angle spinning (MAS) (> 25 kHz). In double-quantum NMR, residual dipolar couplings are measured between specific spin pairs by monitoring the growth of double-quantum intensity during the excitation time. The strength of this residual dipolar coupling is taken at several temperatures, which can then be used to construct the orientational autocorrelation function over four decades in time by utilizing the time–temperature superposition:

$$\tau_c(T) = \frac{\zeta(T)N_e^2 b}{kT} \quad [4]$$

where N_e is the number of statistical (Kuhn) segments in an entangled unit, $\zeta(T)$ is the friction coefficient, and b is the tube width in the Doi–Edwards model. The calculated orientational autocorrelation function is very informative of the dynamics that result from constraint, as has been shown by a number of recent studies.^{294–297}

7.18.3.11 Brillouin Light Scattering

BLS is the inelastic scattering of an incident optical wave field by the thermally excited elastic waves or acoustic phonons that naturally exist in all solids. These phonons set up periodic or wave-like modulations of the dielectric constant or index of refraction of the materials which are viewed as a moving diffraction grating by the incident light. BLS refers to the scattering of a coherent beam of laser light (photons) from these transient, propagating elastic waves (phonons). Concepts such as the conservation of momentum and energy apply to this scattering process. For an elastic wave in the material traveling with a wave vector \mathbf{q} and frequency $\omega(\mathbf{q})$, conservation of momentum means

$$\mathbf{k}_s - \mathbf{k}_i = \pm \mathbf{q} \quad [5]$$

where \mathbf{k}_i is the wave vector in the incident light and \mathbf{k}_s is the wave vector of the scattered light. Likewise, the scalar conservation of momentum dictates that

$$\omega_s - \omega_i = \omega(\mathbf{q}) \quad [6]$$

where ω_s is the frequency of scattered light, ω_i is the frequency of the incident light, and $\omega(\mathbf{q})$ is the \mathbf{q} -dependent frequency of the elastic wave in the medium. This is an inelastic scattering process. The plus signs in the preceding equations correspond to ‘anti-Stokes’ events where phonons are annihilated and the scattered photons gain energy, whereas the minus signs refer to ‘Stokes’ events where phonons are created and the scattered photons lose energy. In the typical BLS experiment, it is straightforward to quantify the frequency of the scattered mode and therefore the shift in frequency from the incident light $\Delta\omega$. By treating the scattering in a BLS experiment as a Bragg reflection of the incident light by the moving optical diffraction grating that is generated by the elastic wave and taking advantage of the simplification that $|\mathbf{k}_s| \approx |\mathbf{k}_i| = k$, one can arrive at the relationship

$$v = \frac{\lambda_0 |\Delta\omega|}{4\pi n \sin(\phi/2)} \quad [7]$$

where v is the velocity of the acoustic mode in the material, $\phi/2$ is the Bragg angle, λ_0 is the wavelength of the incident photon, and n is the index of refraction. From the frequency of the incident and scattered light in a BLS experiment, it is straightforward to calculate the velocity of the propagating acoustic mode.

There are many different types of elastic modes in a solid. The longitudinal acoustic (LA) type modes have their unit polarization vectors parallel to the wave vector \mathbf{q} describing their propagation, whereas transverse acoustic (TA) modes are perpendicular. To properly interpret the nature of these different modes, one must take into account several factors, including the geometry of the sample, whether it is optically transparent (bulk modes) or opaque (surface modes), and the angular dispersions of the modes. Generally speaking though, the velocity of the different modes can be predicted by the elastic stiffness tensors of the material. Specifically,

$$v_{\text{LA}} = \sqrt{C_{11}/\rho} \quad [8]$$

$$v_{\text{TA}} = \sqrt{C_{44}/\rho} \quad [9]$$

where v_{LA} is the velocity of the LA mode, v_{TA} is the velocity of the TA mode, ρ is the material density, and C_{11} and C_{44} are the elastic stiffness constants. C_{44} is directly the shear modulus (often denoted as G) of the material. From C_{11} and C_{44} , it is also straightforward to calculate Young’s modulus E , bulk modulus K , and Poisson’s ratio σ of the material through the following equations:

$$E = \frac{C_{44}(3C_{11} - 4C_{44})}{C_{11} - C_{44}} \quad [10]$$

$$K = C_{11} - 3/4 C_{44} \quad [11]$$

$$\sigma = \frac{1 - 2C_{44}/C_{11}}{2(1 - C_{44}/C_{11})} \quad [12]$$

In other words, monitoring the velocities of the thermal phonons allows for a direct measure of the material stiffness. As the temperature increases and a polymeric material softens, there is a concomitant slowing down in the velocity of the phonons traveling through the material. For a more detailed description of the acoustic properties of materials and the BLS measurement techniques, we refer the reader to several relevant texts.^{298–300}

While BLS events are inelastic in nature, the frequency shift of the light scattered by the phonons are typically 4–5 orders of magnitude smaller than the central frequency of the incident. It can be a challenge to detect such small, weak frequency shifts which are usually on the order of 30–40 GHz at most; extremely sensitive detection methods are required. These frequencies mean that BLS measurements probe the elastic properties of the material on a nanosecond time frame. This is usually much faster than the mechanical methods that are used to quantify analogous properties. For most BLS measurements, a tandem Fabry–Perot interferometer is used to isolate these small, weak frequency shifts from the strong elastic scattering. Tandem Fabry–Perot interferometers, as described by Sandercock, bounce the reflected light off a series of multi-pass mirrors whose positions are precisely controlled by piezoelectric actuators. The positions of the mirrors can be controlled, through micrometer displacements, to only allow selective wavelengths to pass through the optical path. By scanning the position of the mirrors, one can monitor the intensity of the reflected light off the central frequency as a function of wavelength or frequency shift $\Delta\omega$, thereby identifying the different acoustic modes. As the intensity of the inelastic BLS events is very weak and the calibration of the interferometer mirrors is very sensitive to events like thermal fluctuations, these are very difficult measurements. The detectors usually operate in the single-photon counting regime. The signal-to-noise ratio is made worse by the required use of extremely thin polymer films, where the amount of material contributing to the scattering is limited. When studying thin polymer films, one must also be aware of the wavelength of the acoustic phonons being probed relative to the film thickness. It is easy to get into the regime where the wavelength of the acoustic mode is comparable or greater than the thickness of the film. In this limit, the acoustic modes typically show softening in a free-standing mode whereas stiffening is observed for supported films on rigid substrates.³⁰⁰ In this limit, the modes tend to probe more of the properties of the substrate of surrounding media rather than the polymer itself.

Despite these difficulties, some of the initial and most seminal measurements of T_g shifts in confined polymer films have come from the temperature dependence of the LA modes in thin polymer films. In an analogous manner to a mechanical modulus measurement, the LA mode shows a pronounced softening upon heating past the glass transition temperature of the polymers. Some of the first T_g reduction measurements in thin polymer films performed as a function of decreasing film thickness were evidenced by temperature-dependent BLS measurements. These include T_g depressions in both supported and free-standing films.^{4,5,301,302} In general, these measurements reveal the most dramatic reductions in T_g observed for the free-standing films, a somewhat decreased reduction for films supported on a substrate, and a more diminished reduction for supported films with a rigid capping layer. The authors generally observed that these deviations from the bulk-like response of the polymer set in for film thicknesses thinner than approximately

50 nm. Subsequent BLS measurements showed that these thin film deviations were largely independent of chain length for molecular masses less than approximately 350 kg mol^{-1} ; however, significantly larger chains did show T_g depressions at noticeably larger film thicknesses.^{303–305} The molecular mass independence for the lower molecular masses was rationalized by the length scale of the film approaching the natural size of the cooperatively rearranging regions (CRRs) for the glass; the chain dimensions of the low molecular mass polymers were smaller than the CRRs. The transition to a molecular mass dependent T_g shift for the larger chains nominally coincides with the mean square end-to-end distance of the polymer coil being compressed by the film thickness.

More recently, there have been several extensions of BLS measurement to a wide range of confined polymer systems. These include but are not limited to more detailed studies of thin polymer films,^{306, 307} materials confined to the domains of a phase-separated diblock copolymer morphology,^{308, 309} periodic one-dimensional multilayer polymer systems,^{310–313} colloidal polymeric nanoparticles,^{314–316} and lithographically fabricated polymer nanostructures.^{317–319} These more complicated states of confinement significantly complicate the analysis of the BLS data. Typically, the focus is on how the nature of sample geometry or periodicity influences the propagation or dispersions of the different modes and less on how the dynamical properties of the material change. As was originally shown by Sandercock using the simplest thin film geometry, confinement of the mode to a physical structure with dimensions approaching the wavelength of the thermal phonons leads to a quantization of that mode.³²⁰ In this limit, the frequency or velocity of the mode is a function of both the material properties and the physical size. A change in size could be erroneously interpreted as a change in modulus. It is straightforward to determine film thickness independently via a variety of techniques, making thin film BLS measurements generally reliable. However, it becomes difficult to extract dynamical changes in the material properties for more complicated structures where there is uncertainty in shape and possibly even material properties. The two effects can be convoluted.

7.18.3.12 Modeling and Simulation

Modeling and simulation have played a critical role in advancing our understanding of polymer dynamics under strong states of confinement. With experimental measurement techniques in polymer science, the biggest challenge is often to assign a molecular mechanism to the observable of the experiment. For example, how does a shift in the apparent T_g of a thin PS film as evidenced by a change in the temperature dependence of the fluorescence intensity of a chromophore dye relate to a molecular process in the polymer film? What is the cause of the observed effect? This can be a difficult question to answer and is precisely why this review focuses on describing to what the different experimental methods are sensitive. The advantage of modeling and simulation is that they have the potential to directly reveal the reverse of this causal relationship; they can be used to show how a molecular mechanism or specific process leads to the change in an experimentally measured property. This has proven to be an extremely useful tool in understanding the dynamics of polymer systems under confinement. As described throughout this review, polymer

confinement is a field with a significant amount of conflict and contradiction between the different experimental methods and measurement. We have yet to arrive at a completely unified understanding of how confinement affects polymer dynamics. In the face of this conflict, modeling and simulation have played a critical role in leading the experimentalists to devise new measurements and better refine their interpretation. There is a vast body of literature utilizing modeling and simulation to understand the behavior of polymer systems under confinement. Since the molecular mechanisms or specific processes are explicit in these computational methods, it is beyond the scope of the text to provide a comprehensive review of this vast body. Rather, in the following, we provide a short synopsis of some of the different methods and emphasize some of the important parameters or limits. We refer the reader to several excellent review articles for a more comprehensive description of the simulation methods typically encountered in polymeric materials in general.^{321–324} In this review, we limit the scope to those studies relevant to confinement.

The use of simulation to predict a property or response for a confined polymer requires a realistic and reliable model for the system. Depending on the properties of interest, there are several different types of models that one can use, with different levels of complexity. The most physically and chemically accurate model takes into account a large number of interaction parameters, leading to computationally intensive simulations. The trade-off quickly becomes sacrificing electronic, atomic, and molecular specificity in the models to enable larger-scale simulations. Real polymers are intrinsically large molecules, containing hundreds to thousands of atoms per molecule. To accurately model or predict the dynamical response of a polymer system over longer time and length scales, one needs to account for the many-body interactions between hundreds to thousands of polymer chains, which becomes computationally intensive. With the computing resources available today, one must still sacrifice specificity in the model to predict larger-scale properties that result from many-body dynamics.

At the most basic and complex level is the quantum mechanical models that take into account all the nuclear and electronic degrees of freedom of the system. These utilize the quantum mechanical wave functions of the exact atoms in the polymer to solve the Hamiltonian operator and 'predict' parameters like bond strengths, torsional potentials, and both intermolecular and intramolecular interaction potentials from first principles. These quantum mechanical models lead to the most detailed and complicated descriptions of the polymer system. They can be used to predict not only the high-frequency, local atomic vibrations and modes in the chain, but also qualities such as chemical reactions and electrical properties. A more simplified approach comes from classical atomistic models where the quantum effects are ignored and the parameters like bond strengths, torsional potentials, and intermolecular and intramolecular interactions are simply assigned reasonable values. This helps simplify subsequent simulations, enabling the modeling of larger-scale or more complicated systems. However, the utility of these classical atomistic models depends strongly on the quality of the model; considerable efforts are spent in trying to validate and refine the force fields and interaction parameters in the model. These atomistic models are typically used to predict dynamics and local atomic fluctuations on the picosecond timescale and

angstrom to tens of nanometers length scale. At these length scales, the motions start to become more collective in nature.

The next level of simplification comes from essentially ignoring the hydrogen atoms in the system and treating chemical moieties such as a methyl or methylene group as a single united atom with a single effective force field. This reduces the complexity of the system and allows the prediction of a slightly larger-scale response. Depending on the computing power of the type of simulation method used, united atom models are typically useful for predicting polymer dynamics on the nano to micrometer length scale, over timescales from approximately nano to microseconds. Further simplifications are made possible by coarse graining the system in different ways. This could be restricting the number of sites available through lattice or off-lattice locations, or introducing coarser binning of the chain into multi-carbon atom beads or repeat units, the so-called bead-spring models. These coarser grain models start to lose molecular specificity, such as hydrogen bonding, specific dipole interactions, or bond stiffness effects, but enable one to increase the size of the system and number of molecules that can be efficiently simulated. They typically use simplified Lennard-Jones (LJ) potentials to describe the nonbonded interactions between particles. This is needed to predict larger-scale dynamics on the scale of Rouse- or reptation-type motions.

At the largest length scales, field theoretic and continuum mechanics models are able to predict the equilibrium structure of multicomponent systems and macroscopic flow response of a polymer system. However, these models do not contain molecular detail. They are based either on a phenomenological description of the free energy of the system, such as the Flory-Huggins or Landau free energies, or on actual hydrodynamic parameters such as viscosity.

There are also several different kinds of simulation methods that can be used to predict the response of polymers under confinement. The so-called *ab initio* methods are used with the quantum mechanical models to minimize the free energy Hamiltonian and find the optimum configuration of the local bond lengths, orientations, and inter and intramolecular configurations. In most of these methods, the electronic states of the polymers are accounted for and the simulations are the most complicated. *Ab initio* methods are able to accurately predict the response of a polymer from first principles on a timescale on the order of femto to picoseconds at sub-angstroms to nanometer length scales. They are the most detailed and local form of simulation. The next level up in terms of time and length scale is the MD simulation technique. The MD simulation method entails solving the classic equations of motion for all the particles in the system. The atoms, molecules, or particles move under the action of conservative forces that are additive and symmetric, derived from the interaction potentials or force fields that are inputs for the model. MD methods can be implemented with full atomistic, united atom, and particle-based models; the technique is quite generic in this respect. To extract dynamics, the MD technique integrates the time rate of change in the momentum in the system and equates that sum of the forces acting on it. The time and length scale probed by MD methods depend on the details of the model. Full atomistic simulations are more local while coarse grained simulations reach longer time and length scales. General speaking MD methods probe dynamics on timescales of a femto- to tens of nanoseconds, up to length scales of tens

to hundreds of nanometers. Given the nature of the MD method, it is straightforward to impose a small distortion (strain or stress) to the system and watch how the system re-equilibrates. However, MD methods are generally poor at establishing what that initial equilibrium structure is.

Both the MD and the *ab initio* methods minimize the free energy of the system by watching the system move across the potential energy surface into the lowest energy configuration. With these path integral methods, it is easy for the system to get caught in a local minimum that is not representative of the actual system. To circumvent these problems, Monte Carlo (MC) simulation methods are routinely applied to polymeric systems. With the MC approach, the system is randomly placed in a large number of different possible configurations. The total free energy of the system is calculated for each possible configuration and statistical mechanics are used to calculate the probability for each of the different possibilities. This approach is generally much better at establishing the equilibrium structure and less likely to get caught in nonphysical local energy minima. For this reason, MC and MD methods are often integrated together when simulating polymer dynamics. MC methods can be used as an annealing technique to establish what the equilibrium chain conformation is. Once equilibrium is reached, MD methods can be used to better quantify dynamics. Solving the equations of motion is admittedly superior for quantifying the dynamic behavior over the equilibrium statistical mechanics approach. However, one can also establish transition probabilities for moving between different states to predict kinetic or dynamic processes using MC simulations. The quality of these data is highly dependent on the validity of the update criterion for when a transition is allowed. These update criteria are phenomenological, because real polymers do not randomly 'hop' between different configurations, and therefore need to be validated. For dynamical process, MC methods extend the accessible timescales out to the microsecond range and the length scales to approximately micrometer. Again, the exact time and length scale depend on the nature of the model being used. Atomistic classical models tend to be more local and detailed than the coarser united atom or bead-spring models.

The molecular insight into polymer dynamics under confinement is essentially lost when moving to these coarser-grained models. Polymers begin to feel strong states of confinements at length scale of approximately 100 nm or less. Simulation methods that treat the entire system as an effective medium do not provide insight into why the dynamics are changing. There are a host of simulation techniques that are suitable for larger-scale systems, including lattice Boltzmann methods, field theoretic simulations, dynamic density functional theory methods, multiscale simulations, and finite element methods. However, these techniques are rarely used to study polymers under confinement unless they are coupled with other simulation methods³²⁵ and beyond the scope of this review. Most of the simulations of polymers under confinement are MC and/or MD in nature, using fully atomistic, united atom, or bead-spring representations of the polymers. The *ab initio* methods generally focus on time and length scales too local for polymer dynamic studies. However, Grant Smith and co-workers have been very successful in incorporating quantum mechanically accurate force fields into their atomic MD simulations of confined polymers.^{326–329}

The body of literature on using modeling and simulation to quantify the dynamics of confined polymer systems is considerable. While our references are far from exhaustive, this body of literature includes studies on thin film,^{88,104,282,325,330–352} nanoparticle,^{329,353–357} and volumetric or nanopore^{358–360} states of confinement. There are also a large number of publications focusing on the structure and dynamics of polymers near free surface and solid interfaces that are also relevant to understanding polymers in confinement.^{327,328,361–371} There have been several recent reviews summarizing the common themes that have emerged from this body of research.^{323,333,347} It is now generally recognized that density profile of the chain segments near a surface or interface experiences an interfacial layering effect.^{323,327,332,347,351,355,367,369,372} This layering is a natural consequence of the geometric constraint of chain segments near the surfaces since they are forced to predominantly lie parallel to the interface. This results in a layering effect, with a layer thickness equal to the molecular diameter of the polymer chain that extends to approximately 5–10 molecular diameters into the film. At longer length scales, the disorder in the amorphous material randomizes the system and the density profile becomes uniform. For most polymer chain diameters, this layered interfacial region is no more than 5–10 nm thick. Considering that a thin film will have two interfaces, these length scales are reasonably consistent with experimental thin film studies that report deviations in dynamic properties for films thinner than approximately 50 nm. It should be noted that this layering is purely a geometric effect and occurs near free surfaces, surfaces with strongly attractive interactions with the chain segments, and surfaces with weak or repulsive interactions with the chain segments.

The nature of the interactions with the surface, however, does have a significant impact on the change of the polymer dynamics on confinement. For both the nanoparticle and thin film states of confinement, it has been shown that dynamics of the polymer are facilitated or speed up near a surface with repulsive or weak interactions, whereas the dynamics slow down near a strongly interacting surface.^{323,328,334,342,344,345,348,353,355–357} This has been shown for both the high-frequency local mean square displacements of the atoms vibrating in their potential energy wells, the so-called caged motions, and the larger-scale anharmonic or diffusive motions where the atoms or particles jump out of the cages established by their nearest neighbors. For chain segments near a free surface, it is generally observed that the overall polymer dynamics are facilitated.^{342,343,364} However, it has been shown that segmental motions near the surface can be anisotropic. Diffusive motions perpendicular to the free surface tend to slow down whereas motions parallel to the surface are facilitated.^{336,347,364,365} Simulation and modeling have also been helpful in developing and validating various theoretical descriptions or arguments for the origins of confinement effects, including mode coupling theory,^{88,324,333,348–350,352,360,373,374} the coupling model,^{337,338,341,375,376} dynamical heterogeneities,^{282,327,328,343,346,377} or CRRs.^{104,340,342,358,378}

7.18.4 Physical Mechanisms of Confinement

Now that we have discussed some of the different ways in which polymer dynamics can be quantified under strong states of confinement, we briefly turn our attention to the

interpretation or analysis of the data. As have alluded several times through this text, the community still does not have a comprehensive and predictive understanding of the dynamics of polymers under confinement. The literature still contains contradictions and there are definitely gaps in our understanding of this complicated topic. A unified and predictive understanding of polymer dynamics in confinement is still beyond our reach. For a detailed understanding of the state of this field, we refer the reader to several competent reviews on this topic.^{11–15} In this section, we identify some of the key physical mechanisms or fundamental questions that are actively being discussed within this community. These are the key topics of interest in this field and subject of the current debates. We can bring some of these concepts to the reader's attention, but unfortunately we cannot answer all the outstanding questions.

7.18.4.1 Finite Size versus Surface Interactions

A topic of considerable debate right now in the confinement community relates to the difference between true finite-size effects versus interface- or surface-driven interactions. In this context, a finite-size effect would result from the low or reduced dimensionality of the system. For polymeric molecules, these are typically a confinement-induced change in the configuration of the macromolecule, a loss of configurational entropy in the confined system, or change or frustration in the density or packing of the molecules in the confining space. These would be changes that if present in the 'bulk' material would lead to dramatically different properties. The other emerging school of thought is that most of the 'confinement' effects are really just surface effects. This concept appears consistent with a number of experimental observations that the polymer dynamics near a rigid interface with favorable or attractive interactions are hindered whereas the mobility near an interface with repulsive or nonfavorable interactions is facilitated. However, in practice it is difficult to clearly distinguish between these two schools of thought. It is reasonable to expect that the conformation of a macromolecule near an interface that has either strongly attractive or repulsive interactions with the surface is different from the bulk where the molecules are essentially bathed in a neutral environment. Likewise, there is also the issue of the extent of the surface interactions. How far away from the interface do surface interactions propagate? It is difficult to cleanly separate these schools of thought. To illustrate this by an example, one of the classically recognized confinement effects is reduction of the melting temperature in nanosized crystals. Crystalline nanoparticles can have melting temperatures several hundred degrees lower than their bulk counterparts, commonly referred to as the Gibbs–Thompson effect; this is considered a fundamental finite-size effect. However, in reality, the lower melting point comes from the increased chemical potential of the system that arrives from the dominance of the surface energy and radius of curvature in the free energy of the system; it is also fundamentally an interfacial effect.

Another issue that has received considerable attention is the difference between free-standing, supported, and capped (rigid contacts on both sides) thin films. It is now widely believed that the mobility of the polymer near an air interface is greater than that near an interface with a more rigid material. There are several different examples of how relaxations near a free air

surface proceed at a faster rate than those in the bulk material. This is largely consistent with the thin film T_g literature which seems to indicate that the T_g depressions in a free-standing film are more significant than those in either a supported or capped film. Quite often, the theoretical predictions of enhanced chain end segregation near a free surface are invoked to describe this observation and there have been dynamic AFM measurements of the polymer viscosity as a function of molecular mass that support this argument; higher molecular mass chains have fewer chain ends to segregate and less significant reductions in the surface viscosity over the bulk. There have also been theoretical predictions by de Gennes of enhanced chain slide or reptation motions near the free surface of the polymer.³⁷⁹ His theory predicts a decrease in the T_g of the thin film when the thickness of the film approaches the natural dimensions of the polymer coil. However, contrary to these predictions of enhanced mobility near a free surface, XRR and positron annihilation lifetime spectroscopy measurements always show a reduced thermal expansion coefficient as the film thickness decreases. Inelastic neutron scattering measurements also support this notion of reduced mobility in thin films, regardless of the nature of the interface. A comprehensive understanding remains elusive.

7.18.4.2 Chain Conformation and Molecular Mass

Intuitively, polymers are very intriguing materials to study under confinement. The R_g of a single polymer coil, depending on its molecular mass, can be anywhere from a few up to 30 or 40 nm for high molecular mass polymers. These are very large length scales compared to the fundamental structural units of other types of materials. For this reason, it is intuitive to think that finite-size or confinement effects occur at much larger length scales in polymers relative to other types of materials. To a first approximation, this notion seems to be true. Seminal measurements by Dalnoki-Veress and co-workers^{14, 380} showed that reductions of the apparent glass transition temperature in PS films were somewhat independent of molecular mass, becoming significant for films nominally thinner than 50 nm for polymers below a critical molecular mass of approximately 378 kg mol^{-1} . At this molecular mass, the R_g of the polymer is certainly becoming comparable to the thickness at which the deviations are evidenced. Furthermore, for larger molecular masses the onset of the apparent thin film T_g systematically shifted to thicker films with increasing molecular mass. These data, presented in **Figure 8(a)**, strongly suggest that under certain circumstances the length scale of the unperturbed molecule relative to the film thickness is an important factor in establishing the glass transition of the thin film. However, **Figure 8(b)** also shows the experimental data and Gibbs–Thompson melting point reductions of tin nanoparticles as a function of particle diameter.³⁸¹ What is striking in this plot is that the melting point suppressions do not become dramatic until the radius of the particle drops below 50 nm. This is almost exactly the same length scale for the T_g reductions in the lower molecular mass PS films in **Figure 8(a)**. Concepts of macromolecular length scales do not apply to gold atoms. It is actually quite remarkable that the length scale of 50 nm shows up repeatedly in a range of material systems for the onset of finite-size deviations. The nature of this is not clear but it is clear that perturbations of chain conformation are not

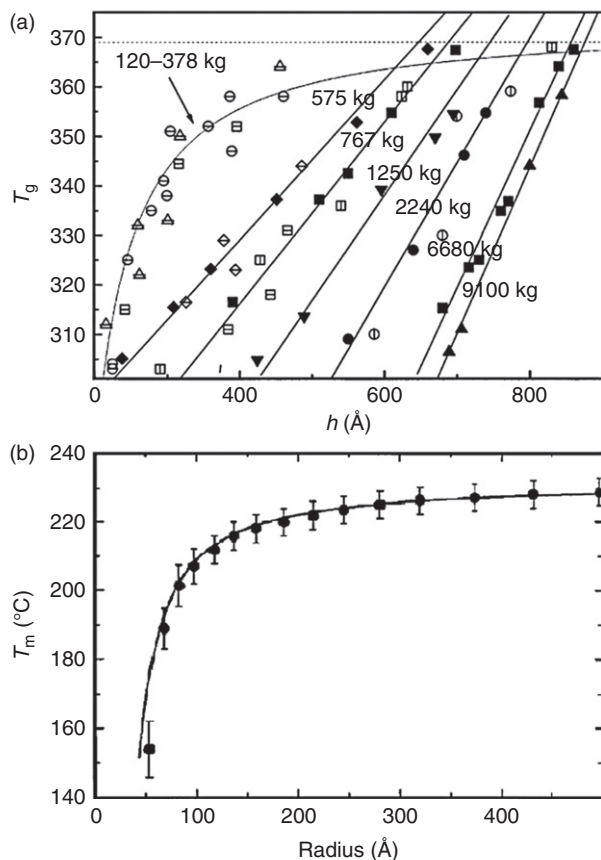


Figure 8 (a) Measured T_g values for free-standing PS films with M_w from 120 to 9100 kg mol⁻¹. Reproduced with permission from Wu, W. L.; Vanzanten, J. H.; Orts, W. J. *Macromolecules* **1995**, *28*, 771.⁶ (b) Measured melting temperature of tin nanoparticles as a function of their particle diameter. The solid line is a modified Gibbs–Thompson model. Reproduced with permission from Lai, S. L.; Guo, J. Y.; Petrova, V.; et al. *Phys. Rev. Lett.* **1996**, *77*, 99.³⁸¹

required. It appears that for extremely large chains, conformational distortions might be an issue, but for shorter ones it is not required to evidence finite-size effects.

To help clarify these issues, there have been attempts to measure the R_g of the polymer under different states of confinement. Several simulations have predicted that R_g changes in thin films upon confinement, generally leading to a flattening of the coil in the thickness direction and nominal spreading of the coil in plane.^{332,382–386} Experimentally, there have been attempts to quantify the R_g in thin films using small-angle neutron scattering. Early reports did indeed evidence this flattening of the random coil in stacks of thin films that were cast on water.³⁸⁷ However, Jones and co-workers found that the R_g in the plane of the film remained bulk-like, even in films whose thickness was less than unperturbed dimensions of the coil.^{388–391} The state of thin film confinement did not flatten the random coil configuration of the molecule. Similar measurements were repeated with PS imbedded in the nanochannels of an AAO membrane. Even when the diameter of the pore became significantly less than the unperturbed dimensions of the polymer coil, the R_g remained bulk-like.²¹¹ There really only appear to be two possible explanations for these observations. The first relates to the true nature of a random walk in a

polymer coil. Most people assume that the geometry of the coil can be approximated by a sphere in three dimensions. This is actually not true and early works show that the random walk of a linearly connected chain leads to high aspect ratio ellipsoids or cigar-shaped objects.³⁹² It is within the realm of possibility that the ellipsoids simply lay down in the plane of the film or align themselves down the axis of the AAO nanopores. These molecular orientations would not require distortions of the coils. The cigars could still be randomly oriented in the plane of the film and could explain why transmission ‘sans’ measurements reveals an R_g that is still very close to the bulk value.

7.18.4.3 Entanglement Density

The explanation of the R_g measurements above does not strongly relate to dynamics. However, there is a second possible explanation that would have an impact on the dynamical response of the polymer. It is well known that dynamic properties like flow, viscosity, and other relaxation processes are influenced by the entanglement density of a polymer. Entanglements are constraints that resist viscous flow. The observation above of an average chain diameter in the plane of the film that does not flatten out and expand with decreasing film thickness also suggests that interfaces of the film act as reflecting interfaces. When a random walk approaches an interface, it simply changes directions and reflects back on itself. We know that chains of an amorphous polymer are highly entangled and interpenetrating. This has to be true to generate the well-understood intermolecular entanglement junctions that are evidenced in rheological experiments. If in extremely thin films the chains are forced to fold back in on themselves, the result would be that intermolecular penetration and entanglements are lost.^{393,394} This is an attractive concept, depicted schematically in Figure 9, to explain dynamic observations where increased molecular mobility is evidenced in thin films. However, it is difficult to quantify the degree of entanglement in a thin polymer film as quantitative rheology measurements are difficult. There are now a few measurements starting to address this issue. Si and co-workers recently used the degree of necking in the thickness direction that occurs in a polymer film under tensile deformation to predict a reduced thin film entanglement density.³⁹⁵ These measurements were supported by Rowland and co-workers who saw a decreased resistance to viscous flow of the polymer melt under a nanoscale punch in high molecular mass polymers when the thickness of the film became less than the R_g of the polymer. However, recent bubble inflation^{128,129,396} and surface forces apparatus^{69,126} measurements of polymer melts evidence a ‘stiffening’ in very thin films that would seemingly not support a reduced entanglement density. A clear understanding of the nature of the entanglement density in confined polymer systems remains an issue of debate.

7.18.4.4 Cooperative and Collective Motions

The notion of collective or cooperative motions in glasses and liquids has been around for many years, stemming back to the original Adam–Gibbs theory.³⁹⁷ Their concept is based on the argument that configurational entropy is required for diffusive motions in a polymer. There are CRRs of molecules or polymer segments in a melt that grow in upon cooling and make

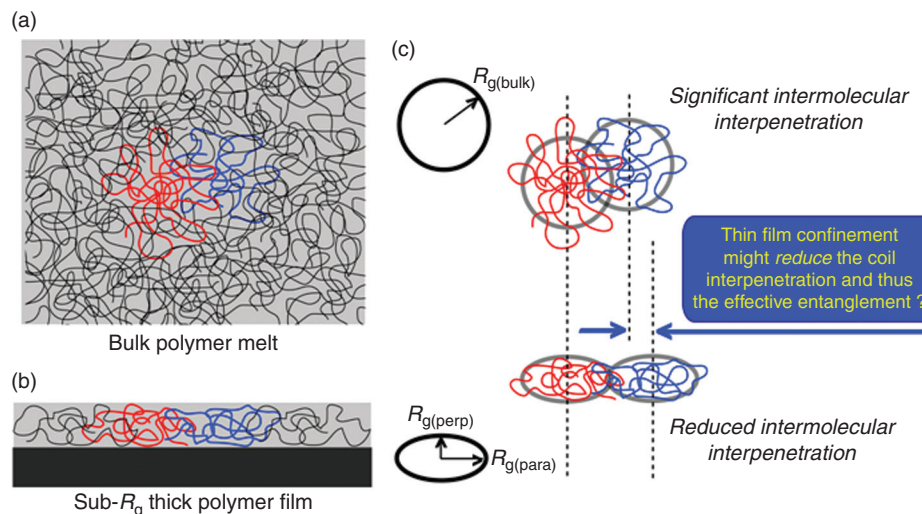


Figure 9 (a) A sea of interpenetrating macromolecular coils in a bulk polymer melt. (b) For thin films with total thickness below the radius of gyration, R_g , the coils do not appear to spread laterally, and $R_{g(\text{para})} \approx R_g > R_{g(\text{perp})}$. This implies that the interpenetration of coils decreases. (c) The coil shape and relative position of an arbitrary pair of nearest-neighbor coils in the bulk and thin films.

configurational transitions more difficult. When the CRRs grow to be the size of the entire system, there is no configurational entropy left since the system is frozen. There have been several attempts to quantify the size of the CRRs in bulk polymer system using different models and measurements such as calorimetry,^{398–401} NMR,^{402–405} and dielectric spectroscopy;⁸⁴ typically estimates of the CRRs are on the order of 1–7 nm in diameter at the glass transition. It is then natural to think about this model in terms of confinement where the length scales of the system at a given temperature can approach the size of the CRRs, thereby affecting the dynamics of the system.^{23,25,63,84,90,104,110,142,225,241,243,244,246,256,261,304,340,358,373,375,376,380,400,401,406–413}

If the size of the system becomes smaller than the CRRs, then the extent of the CRRs become saturated and additional cooling is not as effective at suppressing dynamics as compared to the bulk. In this case the dynamics over the bulk would be enhanced. We note that estimated CRR length scales of approximately 1–7 nm are much smaller than the approximately 50 nm length scales for the apparent T_g deviations in thin polymer films. However, the CRR length scales are much more consistent with the dynamic confinement effects when the polymer is confined either by nanoparticles (especially when the particles are sheet or flake-like particles like clay) or in a nanoporous matrix.

It is also common to discuss the physics of polymer glasses and liquids in terms of spatially heterogeneous dynamics (SHDs). Modeling and simulations have shown that the dynamic processes are highly localized and collective.^{414–416} The dynamic processes of a disordered glass or liquid are dominated by a small fraction of the atoms, segments, or molecules that execute collective motions. These SHDs often have string-like shapes and, like the CRRs from the Adam-Gibbs theory, grow in length as the system is cooled. Theoretical comparisons have suggested that the CRRs and SHDs are largely equivalent.^{417,418} As with the CRRs, the natural question here is how the length scales of confinement in turn affect the SHDs and the dynamic response of the polymer. These efforts include theoretical predictions,^{419–421} computer simulation and modeling,^{327,328,360} and experimental

methods.^{67,90,213,231,232,278,280,289,295,297,410} One interesting development here has been computer simulations that suggest both thin film confinement and the addition of diluents or plasticizers to bulk materials effectively reduce the level of SHD.³⁴⁰ This, when combined with experimental observations that the deviations apparent in the T_g of thin polymer films can be eliminated by the addition of plasticizers to the film, seems to suggest that the SHDs are indeed important.^{244,257}

7.18.4.5 Nonequilibrium Effects

As mentioned several times throughout this review, there has been difficulty in building consensus on the effects of confinement on polymer dynamics. This can in part be traced to the fact that a wide range of nonequilibrium or nonintuitive responses have made the interpretation more difficult. There is still a large amount that we do not understand regarding polymer dynamics under strong states of confinement and this has undoubtedly complicated the interpretation. Some of the earliest reports in this field suggested that spin-cast thin polymer films are metastable states,²⁰⁸ exhibiting isothermal expansion even deep in the glassy state. Since these early results, there have been others identifying confined polymers as metastable^{95,377,422} or nonequilibrium^{180,240,399,408,423,424} systems. This can lead to a nonintuitive response of the material such as an apparent negative thermal expansion coefficient or a film that expands upon cooling.^{206,231,425–428} There are a number of reports now indicating that both the thermal^{95,117,135,206,303,429} and processing²⁴² history of the samples will have an impact on the dynamical properties. People are starting to pay more attention to how parameters like residual solvent^{206,207,290,423,430,431} and/or residual stress^{187,190,205–207,256,423,432–437} impact the response of the material. The bottom line is that there are many complications in highly confined systems relative to bulk polymers. We do not fully understand the nature of these complications at this time. This is precisely why this review has focused primarily on the different types of measurement and the aspects of the

polymer dynamics to which they are sensitive. To help unravel the mystery of polymer dynamics under confinement and help resolve many of the existing controversies, it is important to better understand the physics behind measurement. This chapter is intended to be a resource for those seeking such an understanding.

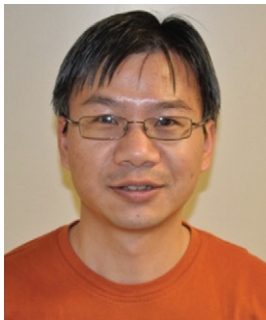
References

- Jackson, C. L.; McKenna, G. B. *J. Non-Cryst. Solids* **1991**, *131*, 221.
- Keddie, J. L.; Jones, R. A. L.; Cory, R. A. *Europhys. Lett.* **1994**, *27*, 59.
- Keddie, J. L.; Jones, R. A. L.; Cory, R. A. *Faraday Discuss.* **1994**, *98*, 219.
- Forrest, J. A.; Rowat, A. C.; Dalnoki-Veress, K.; et al. *J. Polym. Sci., Part B: Polym. Phys.* **1996**, *34*, 3009.
- Forrest, J. A.; Dalnoki-Veress, K.; Stevens, J. R.; Dutcher, J. R. *Phys. Rev. Lett.* **1996**, *77*, 2002.
- Wu, W. L.; Vanzanten, J. H.; Orts, W. J. *Macromolecules* **1995**, *28*, 771.
- Wallace, W. E.; Vanzanten, J. H.; Wu, W. L. *Phys. Rev. E* **1995**, *52*, R3329.
- Orts, W. J.; Vanzanten, J. H.; Wu, W. L.; Satija, S. K. *Phys. Rev. Lett.* **1993**, *71*, 867.
- Xie, L.; Demaggio, G. B.; Frieze, W. E.; et al. *Phys. Rev. Lett.* **1995**, *74*, 4947.
- DeMaggio, G. B.; Frieze, W. E.; Gidley, D. W.; et al. *Phys. Rev. Lett.* **1997**, *78*, 1524.
- Tsui, O. K. C.; Russell, T. P. In *Anomalous Dynamics of Polymer Films*; Tsui, O. K. C., Ed.; World Scientific: Singapore, 2008; p 267.
- Roth, C. B.; Dutcher, J. R. *J. Electroanal. Chem.* **2005**, *584*, 13.
- Alcoultabi, M.; McKenna, G. B. *J. Phys.: Condens. Matter* **2005**, *17*, R461.
- Forrest, J. A.; Dalnoki-Veress, K. *Adv. Colloid Interface Sci.* **2001**, *94*, 167.
- Forrest, J. A. *Eur. Phys. J. E* **2002**, *8*, 261.
- Barnes, J.; Fanconi, B. *J. Phys. Chem. Ref. Data* **1978**, *7*, 1309.
- Ash, B. J.; Schadler, L. S.; Siegel, R. W. *Mater. Lett.* **2002**, *55*, 83.
- Ash, B. J.; Siegel, R. W.; Schadler, L. S. *J. Polym. Sci., Part B: Polym. Phys.* **2004**, *42*, 4371.
- Ash, B. J.; Siegel, R. W.; Schadler, L. S. *Macromolecules* **2004**, *37*, 1358.
- Bansal, A.; Yang, H. C.; Li, C. Z.; et al. *J. Polym. Sci., Part B: Polym. Phys.* **2006**, *44*, 2944.
- Bansal, A.; Yang, H. C.; Li, C. Z.; et al. *Nat. Mater.* **2005**, *4*, 693.
- Pham, J. Q.; Mitchell, C. A.; Bahr, J. L.; et al. *J. Polym. Sci., Part B: Polym. Phys.* **2003**, *41*, 3339.
- Sargsyan, A.; Tonoyan, A.; Davtyan, S.; Schick, C. *Eur. Polym. J.* **2007**, *43*, 3113.
- Sen, S.; Xie, Y.; Bansal, A.; et al. *Eur. Phys. J. Special Topics* **2007**, *141*, 161.
- Srivastava, S.; Basu, J. K. *Phys. Rev. Lett.* **2007**, *98*, 165701.
- Park, J. Y.; McKenna, G. B. *Phys. Rev. B* **2000**, *61*, 6667.
- Schönhals, A.; Goering, H.; Schick, C. *J. Non-Cryst. Solids* **2002**, *305*, 140.
- Schönhals, A.; Goering, H.; Schick, C.; et al. *Eur. Phys. J. Special Topics* **2007**, *141*, 255.
- Schönhals, A.; Goering, H.; Schick, C.; et al. *Eur. Phys. J. E* **2003**, *12*, 173.
- Schönhals, A.; Goering, H.; Schick, C.; et al. *Colloid. Polym. Sci.* **2004**, *282*, 882.
- Schönhals, A.; Goering, H.; Schick, C.; et al. *J. Non-Cryst. Solids* **2005**, *351*, 2668.
- Koh, Y. P.; McKenna, G. B.; Simon, S. L. *J. Polym. Sci., Part B: Polym. Phys.* **2006**, *44*, 3518.
- Koh, Y. P.; Simon, S. L. *J. Polym. Sci., Part B: Polym. Phys.* **2008**, *46*, 2741.
- Wang, X. R.; Zhou, W. S. *Macromolecules* **2002**, *35*, 6747.
- Mi, Y. L.; Xue, G.; Lu, X. L. *Macromolecules* **2003**, *36*, 7560.
- Rong, W. R.; Fan, Z. Y.; Yu, Y.; et al. *J. Polym. Sci., Part B: Polym. Phys.* **2005**, *43*, 2243.
- Bernazzani, P.; Simon, S. L.; Plazek, D. J.; Ngai, K. L. *Eur. Phys. J. E* **2002**, *8*, 201.
- Efremov, M. Y.; Olson, E. A.; Zhang, M.; Allen, L. H. *Thermochim. Acta* **2003**, *403*, 37–41.
- Efremov, M. Y.; Olson, E. A.; Zhang, M.; et al. *Thermochim. Acta* **2004**, *412*, 13.
- Efremov, M. Y.; Olson, E. A.; Zhang, M.; et al. *Rev. Sci. Instrum.* **2004**, *75*, 179.
- Efremov, M. Y.; Olson, E. A.; Zhang, M.; et al. *Phys. Rev. Lett.* **2003**, *91*, 085703.
- Efremov, M. Y.; Olson, E. A.; Zhang, M.; et al. *Macromolecules* **2004**, *37*, 4607.
- Efremov, M. Y.; Warren, J. T.; Olson, E. A.; et al. *Macromolecules* **2002**, *35*, 1481.
- Kwan, A. T.; Efremov, M. Y.; Olson, E. A.; et al. *J. Polym. Sci., Part B: Polym. Phys.* **2001**, *39*, 1237.
- Adamovsky, S.; Schick, C. *Thermochim. Acta* **2004**, *415*, 1.
- De Santis, F.; Adamovsky, S.; Titomanlio, G.; Schick, C. *Macromolecules* **2006**, *39*, 2562.
- Huth, H.; Minakov, A. A.; Schick, C. *J. Polym. Sci., Part B: Polym. Phys.* **2006**, *44*, 2996.
- Huth, H.; Minakov, A. A.; Serghei, A.; et al. *Eur. Phys. J. Special Topics* **2007**, *141*, 153.
- Minakov, A.; Morikawa, J.; Hashimoto, T.; et al. *Meas. Sci. Technol.* **2006**, *17*, 199.
- Minakov, A. A.; Adamovsky, S. A.; Schick, C. *Thermochim. Acta* **2005**, *432*, 177.
- Minakov, A. A.; Schick, C. *Rev. Sci. Instrum.* **2007**, *78*, 073902.
- Minakov, A. A.; van Herwaarden, A. W.; Wien, W.; et al. *Thermochim. Acta* **2007**, *461*, 96.
- Schick, C. *Eur. Phys. J. Special Topics* **2010**, *189*, 3.
- Serghei, A.; Huth, H.; Schick, C.; Kremer, F. *Macromolecules* **2008**, *41*, 3636.
- Zhou, D.; Huth, H.; Gao, Y.; et al. *Macromolecules* **2008**, *41*, 7662.
- Riande, E.; Diaz-Calleja, R. *Electrical Properties of Polymers*; Marcel Dekker: New York, NY, 2004.
- Kremer, F.; Schönhals, A. *Broadband Dielectric Spectroscopy*; Springer: Berlin, Germany, 2003.
- McCrum, N. G.; Read, B. E.; Williams, G. *Anelastic and Dielectric Effects in Polymeric Solids*; Dover: New York, NY, 1991.
- Kremer, F.; Schönhals, A. In *Broadband Dielectric Spectroscopy*; Kremer, F.; Schönhals, A., Eds.; Springer: Berlin, Germany, 2003; Vol. 1, p 35.
- Stockmayer, W. H. *Pure Appl. Chem.* **1967**, *15*, 539.
- Schönhals, A.; Kremer, F. In *Broadband Dielectric Spectroscopy*; Kremer, F.; Schönhals, A., Eds.; Springer: Berlin, Germany, 2003, p 59.
- Steeman, P. A. M.; van Turnhout, J. In *Broadband Dielectric Spectroscopy*; Kremer, F.; Schönhals, A., Eds.; Springer: Berlin, 2003, p 495.
- Anastasiadis, S. H.; Karatasos, K.; Vlachos, G.; et al. *Phys. Rev. Lett.* **2000**, *84*, 915.
- Boucher, V. M.; Cangialosi, D.; Alegria, A.; Colmenero, J. *Macromolecules* **2010**, *43*, 7594.
- Napolitano, S.; Wubbenhorst, M. *J. Phys. Chem. B* **2007**, *111*, 9197.
- Prevosto, D.; Lucchesi, M.; Bertoldo, M.; et al. *J. Non-Cryst. Solids* **2010**, *356*, 568.
- Wong, H. C.; Sanz, A.; Douglas, J. F.; Cabral, J. T. *J. Mol. Liq.* **2010**, *153*, 79.
- Bauer, C.; Bohmer, R.; Moreno-Flores, S.; et al. *Phys. Rev. E* **2000**, *61*, 1755.
- Cho, Y. K.; Watanabe, H.; Granick, S. *J. Chem. Phys.* **1999**, *110*, 9688.
- Erber, M.; Tress, M.; Mapesa, E. U.; et al. *Macromolecules* **2010**, *43*, 7729.
- Fukao, K. *Eur. Phys. J. E* **2003**, *12*, 119.
- Fukao, K.; Koizumi, H. *Phys. Rev. E* **2008**, *77*, 021503.
- Fukao, K.; Miyamoto, Y. *Europhys. Lett.* **1999**, *46*, 649.
- Fukao, K.; Miyamoto, Y. *Phys. Rev. E* **2000**, *61*, 1743.
- Fukao, K.; Miyamoto, Y. *J. Phys. IV* **2000**, *10*, 243.
- Fukao, K.; Miyamoto, Y. *Phys. Rev. E* **2001**, *64*, 011803.
- Fukao, K.; Uno, S.; Miyamoto, Y.; et al. *Phys. Rev. E* **2001**, *64*, 051807.
- Fukao, K.; Uno, S. B.; Miyamoto, Y.; et al. *J. Non-Cryst. Solids* **2002**, *307*, 517.
- Hartmann, L.; Kremer, F.; Pouret, P.; Leger, L. *J. Chem. Phys.* **2003**, *118*, 6052.
- Jeon, S.; Granick, S. *Macromolecules* **2001**, *34*, 8490.
- Kojio, K.; Jeon, S.; Granick, S. *Eur. Phys. J. E* **2002**, *8*, 167.
- Kremer, F.; Hartmann, L.; Serghei, A.; et al. *Eur. Phys. J. E* **2003**, *12*, 139.
- Labardi, M.; Prevosto, D.; Nguyen, K. H.; et al. *J. Vac. Sci. Technol., B* **2010**, *28*, C4D11.
- Lupascu, V.; Picken, S. J.; Wubbenhorst, M. *J. Non-Cryst. Solids* **2006**, *352*, 5594.
- Mapesa, E. U.; Erber, M.; Tress, M.; et al. *Eur. Phys. J. Special Topics* **2010**, *189*, 173.
- Martin, J.; Mijangos, C.; Sanz, A.; et al. *Macromolecules* **2009**, *42*, 5395.
- Napolitano, S.; Wubbenhorst, M. *Polymer* **2010**, *51*, 5309.
- Peter, S.; Napolitano, S.; Meyer, H.; et al. *Macromolecules* **2008**, *41*, 7729.
- Priestley, R. D.; Broadbelt, L. J.; Torkelson, J. M.; Fukao, K. *Phys. Rev. E* **2007**, *75*, 061806.
- Russell, E. V.; Israeloff, N. E. *Nature* **2000**, *408*, 695.
- Serghei, A.; Hartmann, L.; Kremer, F. *J. Non-Cryst. Solids* **2007**, *353*, 4330.
- Serghei, A.; Hartmann, L.; Pouret, P.; et al. *Colloid. Polym. Sci.* **2004**, *282*, 946.
- Serghei, A.; Kremer, F. *Phys. Rev. Lett.* **2003**, *91*, 165702.
- Serghei, A.; Kremer, F. *Rev. Sci. Instrum.* **2006**, *77*, 116108.
- Serghei, A.; Kremer, F. *Macromol. Chem. Phys.* **2008**, *209*, 810.
- Serghei, A.; Lutkenhaus, J. L.; Miranda, D. F.; et al. *Small* **2010**, *6*, 1822.
- Serghei, A.; Mikhailova, Y.; Eichhorn, K. J.; et al. *J. Polym. Sci., Part B: Polym. Phys.* **2006**, *44*, 3006.
- Serghei, A.; Mikhailova, Y.; Huth, H.; et al. *Eur. Phys. J. E* **2005**, *17*, 199.
- Serghei, A.; Tress, M.; Kremer, F. *Macromolecules* **2006**, *39*, 9385.
- Serghei, A.; Tress, M.; Kremer, F. *J. Chem. Phys.* **2009**, *131*, 154904.
- Sharp, J. S.; Forrest, J. A. *Phys. Rev. E* **2003**, *67*, 031805.
- Svanberg, C. *Macromolecules* **2007**, *40*, 312.
- Daoukaki, D.; Barut, G.; Pelster, R.; et al. *Phys. Rev. B* **1998**, *58*, 5336.

104. Haralampus, N.; Argiriadi, P.; Gilchrist, A.; *et al.* *J. Non-Cryst. Solids* **1998**, *235*, 428.
105. Kremer, F.; Huwe, A.; Schonhals, A.; Rozanski, S. A. In *Broadband Dielectric Spectroscopy*; Kremer, F.; Schonhals, A., Eds.; Springer: Berlin, Germany, 2003, p 171.
106. Alba-Simionesco, C.; Dosseh, G.; Dumont, E.; *et al.* *Eur. Phys. J. E* **2003**, *12*, 19.
107. Ward, I. M. *Mechanical Properties of Solid Polymers*, 2nd ed.; Wiley: New York, NY, 1983.
108. Akionis, J. J.; MacKnight, W. J. *Introduction to Polymer Viscoelasticity*, 2nd ed.; Wiley: New York, NY, 1983.
109. Ray, S. S.; Okamoto, M. *Prog. Polym. Sci.* **2003**, *28*, 1539.
110. Priya, L.; Jog, J. P. *J. Polym. Sci., Part B: Polym. Phys.* **2002**, *40*, 1682.
111. Agag, T.; Koga, T.; Takeichi, T. *Polymer* **2001**, *42*, 3399.
112. Bogoslovov, R. B.; Roland, C. M.; Ellis, A. R.; *et al.* *Macromolecules* **2008**, *41*, 1289.
113. Peng, Z.; Kong, L. X.; Li, S. D. *Synth. Met.* **2005**, *152*, 25.
114. Lu, H. B.; Nutt, S. *Macromolecules* **2003**, *36*, 4010.
115. Mortezaei, M.; Hossein, M.; Famili, N.; Kokabi, M. *J. Appl. Polym. Sci.* **2010**, *115*, 969.
116. Liu, Z. J.; Chen, K. Q.; Yan, D. Y. *Eur. Polym. J.* **2003**, *39*, 2359.
117. Tsagaropoulos, G.; Eisenberg, A. *Macromolecules* **1995**, *28*, 6067.
118. Arrighi, V.; McEwen, I. J.; Qian, H.; Prieto, M. B. S. *Polymer* **2003**, *44*, 6259.
119. Ratna, D.; Divekar, S.; Samui, A. B.; *et al.* *Polymer* **2006**, *47*, 4068.
120. Robertson, C. G.; Lin, C. J.; Rackaitis, M.; Roland, C. M. *Macromolecules* **2008**, *41*, 2727.
121. Tjong, S. C.; Meng, Y. Z.; Hay, A. S. *Chem. Mater.* **2002**, *14*, 44.
122. Koppensteiner, J.; Schranz, W.; Puica, M. R. *Phys. Rev. B* **2008**, *78*, 054203.
123. Akabori, K.; Tanaka, K.; Nagamura, T.; *et al.* *Macromolecules* **2005**, *38*, 9735.
124. Hu, H. W.; Carson, G. A.; Granick, S. *Phys. Rev. Lett.* **1991**, *66*, 2758.
125. Granick, S. *Science* **1991**, *253*, 1374.
126. Hu, H. W.; Granick, S. *Science* **1992**, *258*, 1339.
127. Reiter, G.; Demirel, A. L.; Granick, S. *Science* **1994**, *263*, 1741.
128. O'Connell, P. A.; McKenna, G. B. *Science* **2005**, *307*, 1760.
129. O'Connell, P. A.; Hutcheson, S. A.; McKenna, G. B. *J. Polym. Sci., Part B: Polym. Phys.* **2008**, *46*, 1952.
130. Meyer, E.; Hug, H. J.; Bennewitz, R. *Scanning Probe Microscopy: The Lab on a Tip*; Springer: New York, NY, 2004.
131. Birdi, K. S. *Scanning Probe Microscopes: Applications in Science and Technology*; CRC Press: Boca Raton, FL, 2003.
132. Magonov, S. N.; Reneker, D. H. *Annu. Rev. Mater. Sci.* **1997**, *27*, 175.
133. Dinelli, F.; Buenviaje, C.; Overney, R. M. *J. Chem. Phys.* **2000**, *113*, 2043.
134. Overney, R. M.; Buenviaje, C.; Luginbuhl, R.; Dinelli, F. *J. Therm. Anal. Calorim.* **2000**, *59*, 205.
135. Sills, S.; Overney, R. M.; Chau, W.; *et al.* *J. Chem. Phys.* **2004**, *120*, 5334.
136. Kajiyama, T.; Tanaka, K.; Takahara, A. *Macromolecules* **1997**, *30*, 280.
137. Kajiyama, T.; Tanaka, K.; Takahara, A. *Polymer* **1998**, *39*, 4665.
138. Tanaka, K.; Hashimoto, K.; Kajiyama, T.; Takahara, A. *Langmuir* **2003**, *19*, 6573.
139. Tanaka, K.; Takahara, A.; Kajiyama, T. *Macromolecules* **1998**, *31*, 863.
140. Satomi, N.; Takahara, A.; Kajiyama, T. *Macromolecules* **1999**, *32*, 4474.
141. Satomi, N.; Tanaka, K.; Takahara, A.; *et al.* *Macromolecules* **2001**, *34*, 8761.
142. Tanaka, K.; Takahara, A.; Kajiyama, T. *Macromolecules* **2000**, *33*, 7588.
143. Tanaka, K.; Takahara, A.; Kajiyama, T. *Macromolecules* **1997**, *30*, 6626.
144. Tsui, O. K. C.; Wang, X. P.; Ho, J. Y. L.; *et al.* *Macromolecules* **2000**, *33*, 4198.
145. Wang, X. P.; Xiao, X. D.; Tsui, O. K. C. *Macromolecules* **2001**, *34*, 4180.
146. Ge, S.; Pu, Y.; Zhang, W.; *et al.* *Phys. Rev. Lett.* **2000**, *85*, 2340.
147. Pu, Y.; Ge, S. R.; Rafailovich, M.; *et al.* *Langmuir* **2001**, *17*, 5865.
148. Buenviaje, C.; Ge, S. R.; Rafailovich, M.; *et al.* *Langmuir* **1999**, *15*, 6446.
149. Hammerschmidt, J. A.; Gladfelter, W. L.; Haugstad, G. *Macromolecules* **1999**, *32*, 3360.
150. Kajiyama, T.; Tanaka, K.; Ge, S. R.; Takahara, A. *Prog. Surf. Sci.* **1996**, *52*, 1.
151. Fu, J.; Li, B. Y.; Han, Y. C. *J. Chem. Phys.* **2005**, *123*, 064713.
152. Tocha, E.; Schonherr, H.; Vancso, J. *Soft Matter* **2009**, *5*, 1489.
153. Fryer, D. S.; Nealey, P. F.; de Pablo, J. J. *Macromolecules* **2000**, *33*, 6439.
154. Zhou, J.; Berry, J.; Douglas, J. F.; *et al.* *Nanotechnology* **2008**, *19*, 495703.
155. Soles, C. L.; Yee, A. F. *J. Polym. Sci., Part B: Polym. Phys.* **2000**, *38*, 792.
156. Tseng, K. C.; Turro, N. J.; Durning, C. J. *Polymer* **2000**, *41*, 4751.
157. Tseng, K. C.; Turro, N. J.; Durning, C. J. *Phys. Rev. E* **2000**, *61*, 1800.
158. Frank, B.; Gast, A. P.; Russell, T. P.; *et al.* *Macromolecules* **1996**, *29*, 6531.
159. Hall, D. B.; Miller, R. D.; Torkelson, J. M. *J. Polym. Sci., Part B: Polym. Phys.* **1997**, *35*, 2795.
160. Lin, E. K.; Wu, W. L.; Satija, S. K. *Macromolecules* **1997**, *30*, 7224.
161. Lin, E. K.; Kolb, R.; Satija, S. K.; Wu, W. L. *Macromolecules* **1999**, *32*, 3753.
162. Kuhlmann, T.; Kraus, J.; Muller-Buschbaum, P.; *et al.* *J. Non-Cryst. Solids* **1998**, *235*, 457.
163. Kawaguchi, D.; Tanaka, K.; Kajiyama, T.; *et al.* *Macromolecules* **2003**, *36*, 1235.
164. Zheng, X.; Sauer, B. B.; Vanalsten, J. G.; *et al.* *Phys. Rev. Lett.* **1995**, *74*, 407.
165. Pu, Y.; Rafailovich, M. H.; Sokolov, J.; *et al.* *Phys. Rev. Lett.* **2001**, *87*, 206101.
166. Lin, H. C.; Tsai, I. F.; Yang, A. C. M.; *et al.* *Macromolecules* **2003**, *36*, 2464.
167. Roe, R. J. *Methods of X-ray and Neutron Scattering in Polymer Science*; Oxford University Press: New York, NY, 2000.
168. Schwarz, S. A.; Wilkens, B. J.; Puzenzi, M. A. A.; *et al.* *Mol. Phys.* **1992**, *76*, 937.
169. Zheng, X.; Rafailovich, M. H.; Sokolov, J.; *et al.* *Phys. Rev. Lett.* **1997**, *79*, 241.
170. Vogt, B. D.; Soles, C. L.; Jones, R. L.; *et al.* *Langmuir* **2004**, *20*, 5285.
171. Vogt, B. D.; Soles, C. L.; Lee, H. J.; *et al.* *Polymer* **2005**, *46*, 1635.
172. Vogt, B. D.; Soles, C. L.; Lee, H. J.; *et al.* *Langmuir* **2004**, *20*, 1453.
173. Jackle, J. J. *Phys.: Condens. Matter.* **1998**, *10*, 7121.
174. Wyard, F. B.; Daillant, J. *Can. J. Phys.* **1990**, *68*, 1084.
175. Milchev, A.; Binder, K. *J. Chem. Phys.* **1997**, *106*, 1978.
176. Xie, R.; Karim, A.; Douglas, J. F.; *et al.* *Phys. Rev. Lett.* **1998**, *81*, 1251.
177. Reiter, G. *Phys. Rev. Lett.* **1992**, *68*, 75.
178. Dalnoki-Veress, K.; Nickel, B. G.; Roth, C.; Dutcher, J. R. *Phys. Rev. E* **1999**, *59*, 2153.
179. Masson, J. L.; Green, P. F. *Phys. Rev. E* **2002**, *65*, 031806.
180. Kerle, T.; Lin, Z. Q.; Kim, H. C.; Russell, T. P. *Macromolecules* **2001**, *34*, 3484.
181. Fakhraei, Z.; Forrest, J. A. *Science* **2008**, *319*, 600.
182. Ding, Y. F.; Ro, H. W.; Douglas, J. F.; *et al.* *Adv. Mater.* **2007**, *19*, 1377.
183. Hamdorf, M.; Johannsmann, D. *J. Chem. Phys.* **2000**, *112*, 4262.
184. Peng, H. G.; Kong, Y. P.; Yee, A. F. *Macromolecules* **2010**, *43*, 409.
185. Reiter, G. *Macromolecules* **1994**, *27*, 3046.
186. Higgins, A. M.; Sierrazza, M.; Jones, R. A. L.; *et al.* *Eur. Phys. J. E* **2002**, *8*, 137.
187. Ding, Y. F.; Ro, H. W.; Germer, T. A.; *et al.* *ACS Nano* **2007**, *1*, 84.
188. Petersen, K.; Johannsmann, D. *J. Non-Cryst. Solids* **2002**, *307*, 532.
189. Roth, C. B.; Dutcher, J. R. *Phys. Rev. E* **2005**, *72*, 021803.
190. Ding, Y. F.; Ro, H. W.; Alvine, K. J.; *et al.* *Adv. Funct. Mater.* **2008**, *18*, 1854.
191. Brochardwyart, F.; Degennes, P. G.; Hervet, H.; Redon, C. *Langmuir* **1994**, *10*, 1566.
192. Tolan, M.; Seeck, O. H.; Schlomka, J. P.; *et al.* *Phys. Rev. Lett.* **1998**, *81*, 2731.
193. de Gennes, P. G. *Rev. Mod. Phys.* **1985**, *57*, 827.
194. Debregeas, G.; Martin, P.; Brochardwyart, F. *Phys. Rev. Lett.* **1995**, *75*, 3886.
195. BrochardWyart, F.; Debregeas, G.; Fondcave, R.; Martin, P. *Macromolecules* **1997**, *30*, 1211.
196. Bodiguel, H.; Fretigny, C. *Phys. Rev. Lett.* **2006**, *97*, 266105.
197. Kim, H.; Ruhm, A.; Lurio, L. B.; *et al.* *Phys. Rev. Lett.* **2003**, *90*, 068302.
198. Buck, E.; Petersen, K.; Hund, M.; *et al.* *Macromolecules* **2004**, *37*, 8647.
199. Yang, Z. H.; Fujii, Y.; Lee, F. K.; *et al.* *Science* **2010**, *328*, 1676.
200. Tsui, O. K. C.; Wang, Y. J.; Lee, F. K.; *et al.* *Macromolecules* **2008**, *41*, 1465.
201. Yang, F. Z.; Wornyo, E.; Gall, K.; King, W. P. *Scanning* **2008**, *30*, 197.
202. Roth, C. B.; Dutcher, J. R. *J. Polym. Sci., Part B: Polym. Phys.* **2006**, *44*, 3011.
203. Saulnier, F.; Raphael, E.; de Gennes, P. G. *Phys. Rev. Lett.* **2002**, *88*, 196101.
204. Saulnier, F.; Raphael, E.; de Gennes, P. G. *Phys. Rev. E* **2002**, *66*, 061607.
205. Al Akhrass, S.; Reiter, G.; Hou, S. Y.; *et al.* *Phys. Rev. Lett.* **2008**, *100*, 178301.
206. Reiter, G.; Hamieh, M.; Damman, P.; *et al.* *Nat. Mater.* **2005**, *4*, 754.
207. Gabriele, S.; Damman, P.; Sclavons, S.; *et al.* *J. Polym. Sci., Part B: Polym. Phys.* **2006**, *44*, 3022.
208. Reiter, G.; de Gennes, P. G. *Eur. Phys. J. E* **2001**, *6*, 25.
209. Prest, W. M.; Luca, D. J. *J. Appl. Phys.* **1980**, *51*, 5170.
210. Lu, H. Y.; Chen, W.; Russell, T. P. *Macromolecules* **2009**, *42*, 9111.
211. Shin, K.; Obukhov, S.; Chen, J. T.; *et al.* *Nat. Mater.* **2007**, *6*, 961.
212. Rowland, H. D.; King, W. P.; Pethica, J. B.; Cross, G. L. W. *Science* **2008**, *322*, 720.
213. Srivastava, S.; Kandar, A. K.; Basu, J. K.; *et al.* *Phys. Rev. E* **2009**, *79*, 021408.
214. Li, C. H.; Koga, T.; Jiang, J.; *et al.* *Macromolecules* **2005**, *38*, 5144.
215. Jiang, Z.; Kim, H.; Jiao, X.; *et al.* *Phys. Rev. Lett.* **2007**, *98*, 227801.
216. Lumma, D.; Lurio, L. B.; Mochrie, S. G. J.; Sutton, M. *Rev. Sci. Instrum.* **2000**, *71*, 3274.
217. Wang, J.; Tolan, M.; Seeck, O. H.; *et al.* *Phys. Rev. Lett.* **1999**, *83*, 564.
218. Tolan, M.; Seeck, O. H.; Wang, J.; *et al.* *Physica B* **2000**, *283*, 22.
219. Soles, C. L.; Lin, E. K.; Lenhart, J. L.; *et al.* *J. Vac. Sci. Technol., B* **2001**, *19*, 2690.
220. Soles, C. L.; Douglas, J. F.; Wu, W. L.; Dimeo, R. M. *Phys. Rev. Lett.* **2002**, *88*, 037401.
221. Soles, C. L.; Douglas, J. F.; Lin, E. K.; *et al.* *J. Appl. Phys.* **2003**, *93*, 1978.
222. Soles, C. L.; Douglas, J. F.; Wu, W. L.; Dimeo, R. M. *Macromolecules* **2003**, *36*, 373.
223. Soles, C. L.; Douglas, J. F.; Wu, W. L. *J. Polym. Sci., Part B: Polym. Phys.* **2004**, *42*, 3218.
224. Soles, C. L.; Douglas, J. F.; Wu, W. L.; *et al.* *Macromolecules* **2004**, *37*, 2890.
225. Inoue, R.; Kanaya, T.; Nishida, K.; *et al.* *Phys. Rev. E* **2009**, *80*, 031802.

226. Frick, B.; Dalnoki-Veress, K.; Forrest, J. A.; *et al.* *Eur. Phys. J. E* **2003**, *12*, S93.
227. Inoue, R.; Kanaya, T.; Nishida, K.; *et al.* *Phys. Rev. E* **2008**, *77*, 032801.
228. Kanaya, T.; Miyazaki, T.; Inoue, R.; *et al.* In *Slow Dynamics in Complex Systems*; Tokuyama, M.; Oppenheim, I., Eds.; Springer: New York, NY, 2004; Vol. 708, p 197.
229. Inoue, R.; Kanaya, T.; Nishida, K.; *et al.* *Phys. Rev. E* **2006**, *74*, 021801.
230. Inoue, R.; Kanaya, T.; Nishida, K.; *et al.* *Phys. Rev. Lett.* **2005**, *95*, 056102.
231. Kanaya, T.; Inoue, R.; Kawashima, K.; *et al.* *J. Phys. Soc. Jpn.* **2009**, *78*, 041004.
232. Inoue, R.; Kanaya, T.; Nishida, K.; *et al.* *Eur. Phys. J. E* **2007**, *24*, 55.
233. Lagrene, K.; Zanotti, J. M. *Eur. Phys. J. Special Topics* **2007**, *141*, 261.
234. Krutyeva, M.; Martin, J.; Arbe, A.; *et al.* *J. Chem. Phys.* **2009**, *131*, 174901.
235. Kusmin, A.; Gruener, S.; Henschel, A.; *et al.* *Macromolecules* **2010**, *43*, 8162.
236. Lagrene, K.; Zanotti, J. M.; Daoud, M.; *et al.* *Phys. Rev. E* **2010**, *81*, 060801.
237. Lagrene, K.; Zanotti, J. M.; Daoud, M.; *et al.* *Eur. Phys. J. Special Topics* **2010**, *189*, 231.
238. Martin, J.; Krutyeva, M.; Monkenbusch, M.; *et al.* *Phys. Rev. Lett.* **2010**, *104*, 197801.
239. Rittigstein, P.; Priestley, R. D.; Broadbelt, L. J.; Torkelson, J. M. *Nat. Mater.* **2007**, *6*, 278.
240. Rittigstein, P.; Torkelson, J. M. *J. Polym. Sci., Part B: Polym. Phys.* **2006**, *44*, 2935.
241. Campbell, C. G.; Vogt, B. D. *Polymer* **2007**, *48*, 7169.
242. Ellison, C. J.; Kim, S. D.; Hall, D. B.; Torkelson, J. M. *Eur. Phys. J. E* **2002**, *8*, 155.
243. Ellison, C. J.; Mundra, M. K.; Torkelson, J. M. *Macromolecules* **2005**, *38*, 1767.
244. Ellison, C. J.; Ruzskowski, R. L.; Fredin, N. J.; Torkelson, J. M. *Phys. Rev. Lett.* **2004**, *92*, 095702.
245. Ellison, C. J.; Torkelson, J. M. *J. Polym. Sci., Part B: Polym. Phys.* **2002**, *40*, 2745.
246. Ellison, C. J.; Torkelson, J. M. *Nat. Mater.* **2003**, *2*, 695.
247. Hall, D. B.; Deppe, D. D.; Hamilton, K. E.; *et al.* *J. Non-Cryst. Solids* **1998**, *235*, 48.
248. Hall, D. B.; Dhinojwala, A.; Torkelson, J. M. *Phys. Rev. Lett.* **1997**, *79*, 103.
249. Hall, D. B.; Hamilton, K. E.; Miller, R. D.; Torkelson, J. M. *Macromolecules* **1999**, *32*, 8052.
250. Hall, D. B.; Hooker, J. C.; Torkelson, J. M. *Macromolecules* **1997**, *30*, 667.
251. Hall, D. B.; Torkelson, J. M. *Macromolecules* **1998**, *31*, 8817.
252. Kim, S.; Mundra, M. K.; Roth, C. B.; Torkelson, J. M. *Macromolecules* **2010**, *43*, 5158.
253. Kim, S.; Roth, C. B.; Torkelson, J. M. *J. Polym. Sci., Part B: Polym. Phys.* **2008**, *46*, 2754.
254. Kim, S. D.; Torkelson, J. M. *Macromolecules* **2002**, *35*, 5943.
255. Mundra, M. K.; Donthu, S. K.; Dravid, V. P.; Torkelson, J. M. *Nano Letters* **2007**, *7*, 713.
256. Mundra, M. K.; Ellison, C. J.; Behling, R. E.; Torkelson, J. M. *Polymer* **2006**, *47*, 7747.
257. Mundra, M. K.; Ellison, C. J.; Rittigstein, P.; Torkelson, J. M. *Eur. Phys. J. Special Topics* **2007**, *141*, 143.
258. Priestley, R. D.; Broadbelt, L. J.; Torkelson, J. M. *Macromolecules* **2005**, *38*, 654.
259. Priestley, R. D.; Ellison, C. J.; Broadbelt, L. J.; Torkelson, J. M. *Science* **2005**, *309*, 456.
260. Priestley, R. D.; Rittigstein, P.; Broadbelt, L. J.; *et al.* *J. Phys.: Condens. Matter* **2007**, *19*, 205120.
261. Roth, C. B.; McNerny, K. L.; Jager, W. F.; Torkelson, J. M. *Macromolecules* **2007**, *40*, 2568.
262. Royal, J. S.; Torkelson, J. M. *Macromolecules* **1993**, *26*, 5331.
263. Jeon, S.; Bae, S. C.; Granick, S. *Macromolecules* **2001**, *34*, 8401.
264. Reichert, D. In *Annual Reports on NMR Spectroscopy*; Webb, G. A., Eds.; Elsevier: Amsterdam, The Netherlands, 2005; Vol. 55, p 159.
265. Schmidt-Rohr, K. S.; Spiess, H. W. *Multidimensional Solid-State NMR and Polymers*; Academic Press: London, UK, 1994.
266. Bloembergen, N.; Purcell, E. M.; Pound, R. V. *Phys. Rev.* **1948**, *73*, 679.
267. Bovey, F. A.; Mirau, P. A. *NMR of Polymers*, 1st ed.; Academic Press: San Diego, CA, 1996.
268. Dosseh, G.; Xia, Y. D.; Alba-Simionesco, C. *J. Phys. Chem. B* **2003**, *107*, 6445.
269. Nair, S.; Dimeo, R. M.; Neumann, D. A.; *et al.* *J. Chem. Phys.* **2004**, *121*, 4810.
270. Wong, S.; Vasudevan, S.; Vaia, R. A.; *et al.* *J. Am. Chem. Soc.* **1995**, *117*, 7568.
271. Jelinski, L. W. *Annu. Rev. Mater. Sci.* **1985**, *15*, 359.
272. Lin, W. Y.; Blum, F. D. *Macromolecules* **1997**, *30*, 5331.
273. Zeghal, M.; Deloche, B.; Albouy, P. A.; Auroy, P. *Phys. Rev. E* **1997**, *56*, 5603.
274. Lin, W. Y.; Blum, F. D. *Macromolecules* **1998**, *31*, 4135.
275. Rivillon, S.; Auroy, P.; Deloche, B. *Phys. Rev. Lett.* **2000**, *84*, 499.
276. Primak, S. V.; Jin, T.; Dagger, A. C.; *et al.* *Phys. Rev. E* **2002**, *65*, 031804.
277. Blum, F. D.; Lin, W. Y.; Porter, C. E. *Colloid Polym. Sci.* **2003**, *281*, 197.
278. Metin, B.; Blum, F. D. *J. Chem. Phys.* **2006**, *125*, 054707.
279. Okumo, M. O.; Metin, B.; Blum, F. D. *Langmuir* **2008**, *24*, 2539.
280. Metin, B.; Blum, F. D. *Langmuir* **2010**, *26*, 5226.
281. Gedat, E.; Schreiber, A.; Albrecht, J.; *et al.* *J. Phys. Chem. B* **2002**, *106*, 1977.
282. Manias, E.; Kuppa, V.; Yang, D. K.; Zax, D. B. *Colloids Surf., A* **2001**, *187*, 509.
283. Rivillon, S.; Auroy, P.; Deloche, B. *J. Phys. IV* **2000**, *10*, 233.
284. Kimmich, R. *NMR Tomography, Diffusometry, Relaxometry*; Springer-Verlag: Berlin, Germany, 1997.
285. Stapf, S.; Kimmich, R. *J. Chem. Phys.* **1995**, *103*, 2247.
286. Mattea, C.; Fatkullin, N.; Fischer, E.; *et al.* *Appl. Magn. Reson.* **2004**, *27*, 371.
287. Kimmich, R. *Chem. Phys.* **2002**, *284*, 253.
288. Kausik, R.; Mattea, C.; Fatkullin, N.; Kimmich, R. *J. Chem. Phys.* **2006**, *124*, 114903.
289. Ayalur-Karunakaran, S.; Blumich, B.; Stapf, S. *Langmuir* **2009**, *25*, 12208.
290. Ayalur-Karunakaran, S.; Blumich, B.; Stapf, S. *Eur. Phys. J. E* **2008**, *26*, 43.
291. Kimmich, R. *C. R. Phys.* **2010**, *11*, 149.
292. Kimmich, R.; Fatkullin, N. *Macromolecules* **2010**, *43*, 9821.
293. Kausik, R.; Mattea, C.; Kimmich, R.; Fatkullin, N. *Eur. Phys. J. Special Topics* **2007**, *141*, 235.
294. Chavez, F. V.; Saalwachter, K. *Phys. Rev. Lett.* **2010**, *104*, 198305.
295. Jagadeesh, B.; Demco, D. E.; Blumich, B. *Chem. Phys. Lett.* **2004**, *393*, 416.
296. Ok, S.; Steinhart, M.; Serbescu, A.; *et al.* *Macromolecules* **2010**, *43*, 4429.
297. Wang, M. F.; Bertmer, M.; Demco, D. E.; *et al.* *Macromolecules* **2003**, *36*, 4411.
298. Briggs, A. *Acoustic Microscopy*; Clarendon Press: Oxford, UK, 1992.
299. Mutti, P.; Bottani, C. E.; Ghisloti, G.; *et al.* In *Advances in Acoustic Microscopy*; Briggs, A., Eds.; Plenum Press: New York, NY, 1995; Vol. 1, p 249.
300. Farnell, G. W.; Adler, E. L. In *Physical Acoustics: Principles and Methods*; Mason, W. P.; Thurston, R. N., Eds.; Academic Press: New York, NY, 1972; Vol. IX, p 35.
301. Forrest, J. A.; Dalnoki-Veress, K.; Dutcher, J. R. *Phys. Rev. E* **1997**, *56*, 5705.
302. Forrest, J. A.; Dalnoki-Veress, K.; Dutcher, J. R. *Phys. Rev. E* **1998**, *58*, 6109.
303. Mattsson, J.; Forrest, J. A.; Borjesson, L. *Phys. Rev. E* **2000**, *62*, 5187.
304. Forrest, J. A.; Mattsson, J. *Phys. Rev. E* **2000**, *61*, R53.
305. Forrest, J. A.; Mattsson, J. *J. Phys. IV* **2000**, *10*, 251.
306. Cheng, W.; Sainidou, R.; Burgardt, P.; *et al.* *Macromolecules* **2007**, *40*, 7283.
307. Gomopoulos, N.; Cheng, W.; Efremov, M.; *et al.* *Macromolecules* **2009**, *42*, 7164.
308. Urbas, A. M.; Thomas, E. L.; Krieger, H.; *et al.* *Phys. Rev. Lett.* **2003**, *90*, 108300.
309. Tommaseo, G.; Penciu, R. S.; Fytas, G.; *et al.* *Macromolecules* **2004**, *37*, 5006.
310. Hotz, R.; Kruger, J. K.; Possart, W.; Tadros-Morgane, R. *J. Phys.: Condens. Matter* **2001**, *13*, 7953.
311. Cheng, W.; Gorishnyy, T.; Krikorian, V.; *et al.* *Macromolecules* **2006**, *39*, 9614.
312. Cheng, W.; Gomopoulos, N.; Fytas, G.; *et al.* *Nano Lett.* **2008**, *8*, 1423.
313. Sui, L.; Huang, L.; Podsiadlo, P.; *et al.* *Macromolecules* **2010**, *43*, 9541.
314. Penciu, R. S.; Fytas, G.; Economou, E. N.; *et al.* *Phys. Rev. Lett.* **2000**, *85*, 4622.
315. Still, T.; D'Acunzi, M.; Vollmer, D.; Fytas, G. *J. Colloid Interface Sci.* **2009**, *340*, 42.
316. Still, T.; Mattarelli, M.; Kiefer, D.; *et al.* *J. Phys. Chem. Lett.* **2010**, *1*, 2440.
317. Hartschuh, R.; Ding, Y.; Roh, J. H.; *et al.* *J. Polym. Sci., Part B: Polym. Phys.* **2004**, *42*, 1106.
318. Hartschuh, R. D.; Kisliuk, A.; Novikov, V.; *et al.* *Appl. Phys. Lett.* **2005**, *87*, 173121.
319. Johnson, W. L.; Kim, S. A.; Geiss, R.; *et al.* *Nanotechnology* **2010**, *21*, 075703.
320. Sandercock, J. A. *Phys. Rev. Lett.* **1972**, *29*, 1735.
321. Glotzer, S. C.; Paul, W. *Ann. Rev. Mater. Res.* **2002**, *32*, 401.
322. Baschnagel, J.; Binder, K.; Doruker, P.; *et al.* In *Advances in Polymer Science: Viscoelasticity, Atomistic Models, Statistical Chemistry*; Abe, A.; Albertsson, A. C.; Cantow, H. J., Eds.; Springer: New York, NY, 2000; Vol. 152, p 41.
323. Barrat, J.-L.; Baschnagel, J.; Lyulin, A. *Soft Matter* **2010**, *6*, 3430.
324. Peter, C.; Kremer, K. *Soft Matter* **2009**, *5*, 4357.
325. Daoulas, K. C.; Theodorou, D. N.; Harmandaris, V. A.; *et al.* *Macromolecules* **2005**, *38*, 7134.
326. Blum, F. D.; Young, E. N.; Smith, G.; Sittin, O. C. *Langmuir* **2006**, *22*, 4741.
327. Borodin, O.; Smith, G. D.; Bandyopadhyaya, R.; Bytner, E. *Macromolecules* **2003**, *36*, 7873.
328. Smith, G. D.; Bedrov, D.; Borodin, O. *Phys. Rev. Lett.* **2003**, *90*, 226103.
329. Smith, J. S.; Borodin, O.; Smith, G. D.; Kober, E. M. *J. Polym. Sci., Part B: Polym. Phys.* **2007**, *45*, 1599.
330. Cifra, P.; Bleha, T. *Macromol. Theory Simul.* **1999**, *8*, 603.
331. Serghei, A.; Kremer, F.; Kob, W. *Eur. Phys. J. E* **2003**, *12*, 143.
332. Muller, M. *J. Chem. Phys.* **2002**, *116*, 9930.
333. Baschnagel, J.; Varnik, F. *J. Phys.: Condens. Matter* **2005**, *17*, R851.
334. Varnik, F.; Baschnagel, J.; Binder, K.; Mareschal, M. *Eur. Phys. J. E* **2003**, *12*, 167.
335. Chen, Z.; Escobedo, F. A. *Macromolecules* **2001**, *34*, 8802.
336. Baschnagel, J.; Binder, K. *J. Phys. J* **1996**, *6*, 1271.
337. Ngai, K. L. *Eur. Phys. J. E* **2003**, *12*, 93.

338. Ngai, K. L. *J. Phys. IV* **2000**, 10, 21.
339. Fehr, T.; Lowen, H. *Phys. Rev. E* **1995**, 52, 4016.
340. Riggleman, R. A.; Yoshimoto, K.; Douglas, J. F.; de Pablo, J. J. *Phys. Rev. Lett.* **2006**, 97, 045502.
341. Ngai, K. L. *J. Polym. Sci., Part B: Polym. Phys.* **2006**, 44, 2980.
342. Jain, T. S.; de Pablo, J. J. *Phys. Rev. Lett.* **2004**, 92, 155505.
343. Yoshimoto, K.; Jain, T. S.; Nealey, P. F.; de Pablo, J. J. *J. Chem. Phys.* **2005**, 122, 144712.
344. Varnik, F.; Baschnagel, J.; Binder, K. *J. Phys. IV* **2000**, 10, 239.
345. Torres, J. A.; Nealey, P. F.; de Pablo, J. J. *Phys. Rev. Lett.* **2000**, 85, 3221.
346. Manias, E.; Kuppa, V. *Eur. Phys. J. E* **2002**, 8, 193.
347. Mischler, C.; Baschnagel, J.; Binder, K. *Adv. Colloid Interface Sci.* **2001**, 94, 197.
348. Varnik, F.; Baschnagel, J.; Binder, K. *Phys. Rev. E* **2002**, 65, 021507.
349. Peter, S.; Meyer, H.; Baschnagel, J.; Seemann, R. *J. Phys.: Condens. Matter.* **2007**, 19, 205119.
350. Varnik, F.; Baschnagel, J.; Binder, K. *Eur. Phys. J. E* **2002**, 8, 175.
351. Mischler, C.; Baschnagel, J.; Dasgupta, S.; Binder, K. *Polymer* **2002**, 43, 467.
352. Peter, S.; Meyer, H.; Baschnagel, J. *J. Polym. Sci., Part B: Polym. Phys.* **2006**, 44, 2951.
353. Papakonstantopoulos, G. J.; Doxastakis, M.; Nealey, P. F.; *et al.* *Phys. Rev. E* **2007**, 75, 031803.
354. Hackett, E.; Manias, E.; Giannelis, E. P. *Chem. Mater.* **2000**, 12, 2161.
355. Starr, F. W.; Schroder, T. B.; Glotzer, S. C. *Phys. Rev. E* **2001**, 64, 021802.
356. Papakonstantopoulos, G. J.; Yoshimoto, K.; Doxastakis, M.; *et al.* *Phys. Rev. E* **2005**, 72, 031801.
357. Desai, T.; Koblinski, P.; Kumar, S. K. *J. Chem. Phys.* **2005**, 122, 134910.
358. Kim, K.; Yamamoto, R. *Phys. Rev. E* **2000**, 61, R41.
359. Buchner, S.; Heuer, A. *Phys. Rev. E* **1999**, 60, 6507.
360. Scheidler, P.; Kob, W.; Binder, K. *Europhys. Lett.* **2000**, 52, 277.
361. Mansfield, K. F.; Theodorou, D. N. *Macromolecules* **1991**, 24, 4295.
362. Mansfield, K. F.; Theodorou, D. N. *Macromolecules* **1990**, 23, 4430.
363. Bitsanis, I. A.; Tenbrinke, G. J. *J. Chem. Phys.* **1993**, 99, 3100.
364. Doruker, P.; Mattice, W. L. *Macromolecules* **1999**, 32, 194.
365. Harmandaris, V. A.; Daoulas, K. C.; Mavrantzas, V. G. *Macromolecules* **2005**, 38, 5796.
366. Mansfield, K. F.; Theodorou, D. N. *Macromolecules* **1991**, 24, 6283.
367. Baschnagel, J.; Binder, K. *Macromolecules* **1995**, 28, 6808.
368. Binder, K.; Milchev, A.; Baschnagel, J. *Annu. Rev. Mater. Sci.* **1996**, 26, 107.
369. Lee, S.; Chang, J.; Jaffe, R. L.; Yoon, D. Y. *Macromolecules* **2007**, 40, 7407.
370. Theodorou, D. N. *Macromolecules* **1989**, 22, 4589.
371. Theodorou, D. N. *Macromolecules* **1989**, 22, 4578.
372. Gao, J. P.; Luedtke, W. D.; Landman, U. *Phys. Rev. Lett.* **1997**, 79, 705.
373. Scheidler, P.; Kob, W.; Binder, K. *J. Phys. Chem. B* **2004**, 108, 6673.
374. Bennemann, C.; Donati, C.; Baschnagel, J.; Glotzer, S. C. *Nature* **1999**, 399, 246.
375. Ngai, K. L.; Rizos, A. K.; Plazek, D. J. *J. Non-Cryst. Solids* **1998**, 235, 435.
376. Ngai, K. L. *Eur. Phys. J. E* **2002**, 8, 225.
377. Buchner, S.; Heuer, A. *Phys. Rev. Lett.* **2000**, 84, 2168.
378. Jerome, B. *J. Phys.: Condens. Matter* **1999**, 11, A189.
379. de Gennes, P. G. *Eur. Phys. J. E* **2000**, 2, 201.
380. Dalnoki-Veress, K.; Forrest, J. A.; Murray, C.; *et al.* *Phys. Rev. E* **2001**, 63, 031801.
381. Lai, S. L.; Guo, J. Y.; Petrova, V.; *et al.* *Phys. Rev. Lett.* **1996**, 77, 99.
382. Bitsanis, I.; Hadziioannou, G. *J. Chem. Phys.* **1990**, 92, 3827.
383. Giessen, A. E. v.; Szleifer, I. *J. Chem. Phys.* **1995**, 102, 9069.
384. Kumar, S. K.; Vacatello, M.; Yoon, D. Y. *J. Chem. Phys.* **1988**, 89, 5206.
385. Novotny, V. J.; Hussla, I.; Turlet, J. M.; Philpoit, M. R. *J. Chem. Phys.* **1989**, 90, 5861.
386. Silberberg, A. *J. Colloid Interface Sci.* **1982**, 90, 86.
387. Shuto, K.; Oishi, Y.; Kajiyama, T.; Han, C. C. *Macromolecules* **1993**, 26, 6589.
388. Ho, D. L.; Briber, R. M.; Jones, R. L.; *et al.* *Macromolecules* **1998**, 31, 9247.
389. Jones, R. L.; Kumar, S. K.; Ho, D. L.; *et al.* *Nature* **1999**, 400, 146.
390. Jones, R. L.; Kumar, S. K.; Ho, D. L.; *et al.* *Macromolecules* **2001**, 34, 559.
391. Jones, R. L.; Soles, C. L.; Starr, F. W.; *et al.* In *Advances in Resist Technology and Processing XIX, Pts 1 and 2*; Fedynshyn, T. H., Eds.; SPIE-Int Soc Optical Engineering: Bellingham, UK, 2002; Vol. 4690, p 342.
392. Wei, G.; Eichinger, B. E. *Macromolecules* **1990**, 23, 4845.
393. Brown, H. R.; Russell, T. P. *Macromolecules* **1996**, 29, 798.
394. Soles, C. L.; Ding, Y. F. *Science* **2008**, 322, 689.
395. Si, L.; Massa, M. V.; Dalnoki-Veress, K.; *et al.* *Phys. Rev. Lett.* **2005**, 94, 127801.
396. O'Connell, P. A.; McKenna, G. B. *Eur. Phys. J. E* **2006**, 20, 143.
397. Adam, G.; Gibbs, J. H. *J. Chem. Phys.* **1965**, 43, 139.
398. Donth, E.; Huth, H.; Beiner, M. *J. Phys.: Condens. Matter* **2001**, 13, L451.
399. Hempel, E.; Hempel, G.; Hensel, A.; *et al.* *J. Phys. Chem. B* **2000**, 104, 2460.
400. Saiter, A.; Saiter, J. M.; Grenet, J. *Eur. Polym. J.* **2006**, 42, 213.
401. Yamamuro, O.; Tsukushi, I.; Lindqvist, A.; *et al.* *J. Phys. Chem. B* **1998**, 102, 1605.
402. Qiu, X. H.; Ediger, M. D. *J. Phys. Chem. B* **2003**, 107, 459.
403. Reinsberg, S. A.; Heuer, A.; Doliwa, B.; *et al.* *J. Non-Cryst. Solids* **2002**, 307, 208.
404. Reinsberg, S. A.; Qiu, X. H.; Wilhelm, M.; *et al.* *J. Chem. Phys.* **2001**, 114, 7299.
405. Tracht, U.; Wilhelm, M.; Heuer, A.; *et al.* *Phys. Rev. Lett.* **1998**, 81, 2727.
406. Dalnoki-Veress, K.; Forrest, J. A.; de Gennes, P. G.; Dutcher, J. R. *J. Phys. IV* **2000**, 10, 221.
407. Fakhraai, Z.; Forrest, J. A. *Phys. Rev. Lett.* **2005**, 95, 025701.
408. Giannelis, E. P.; Krishnamoorti, R.; Manias, E. In *Polymers in Confined Environments*; Granick, S., Eds.; Springer: New York, NY, 1999; Vol. 138, p 107.
409. Krishnamoorti, R.; Vaia, R. A.; Giannelis, E. P. *Chem. Mater.* **1996**, 8, 1728.
410. Linares, A.; Nogales, A.; Sanz, A.; *et al.* *Phys. Rev. E, Stat. Nonlinear Soft Matter Phys.* **2010**, 82, 031802.
411. Pye, J. E.; Rohald, K. A.; Baker, E. A.; Roth, C. B. *Macromolecules* **2010**, 43, 8296.
412. Sauer, B. B.; Avakian, P. *Polymer* **1992**, 33, 5128.
413. Vaia, R. A.; Sauer, B. B.; Tse, O. K.; Giannelis, E. P. *J. Polym. Sci., Part B: Polym. Phys.* **1997**, 35, 59.
414. Donati, C.; Douglas, J. F.; Kob, W.; *et al.* *Phys. Rev. Lett.* **1998**, 80, 2338.
415. Donati, C.; Glotzer, S. C.; Poole, P. H.; *et al.* *Phys. Rev. E* **1999**, 60, 3107.
416. Kob, W.; Donati, C.; Plimpton, S. J.; *et al.* *Phys. Rev. Lett.* **1997**, 79, 2827.
417. Giovambattista, N.; Buldyrev, S. V.; Starr, F. W.; Stanley, H. E. *Phys. Rev. Lett.* **2003**, 90, 085506.
418. Stevenson, J. D.; Schmalen, J.; Wolynes, P. G. *Nat. Phys.* **2006**, 2, 268.
419. Merabia, S.; Sotta, P.; Long, D. *Eur. Phys. J. E* **2004**, 15, 189.
420. Long, D.; Lequeux, F. *Eur. Phys. J. E* **2001**, 4, 371.
421. Merabia, S.; Long, D. *Eur. Phys. J. E* **2002**, 9, 195.
422. Besancon, B. M.; Green, P. F. *J. Chem. Phys.* **2007**, 126, 224903.
423. Chung, J. Y.; Chastek, T. Q.; Fasaloka, M. J.; *et al.* *ACS Nano* **2009**, 3, 844.
424. Shuto, K.; Oishi, Y.; Kajiyama, T. *Polymer* **1995**, 36, 549.
425. Bhattacharya, M.; Sanyal, M. K.; Geue, T.; Pietisch, U. *Phys. Rev. E* **2005**, 71, 041801.
426. Efremov, M. Y.; Soofi, S. S.; Kiyanova, A. V.; *et al.* *Rev. Sci. Instrum.* **2008**, 79, 043903.
427. Kanaya, T.; Miyazaki, T.; Watanabe, H.; *et al.* *Polymer* **2003**, 44, 3769.
428. Soles, C. L.; Douglas, J. F.; Jones, R. L.; Wu, W. L. *Macromolecules* **2004**, 37, 2901.
429. Huang, Y.; Paul, D. R. *J. Membr. Sci.* **2004**, 244, 167.
430. Smith, B. A. *Macromolecules* **1982**, 15, 469.
431. Tate, R. S.; Fryer, D. S.; Pasqualini, S.; *et al.* *J. Chem. Phys.* **2001**, 115, 9982.
432. Al-Assaad, R. M.; Regonda, S.; Tao, L.; *et al.* *J. Vac. Sci. Technol., B* **2007**, 25, 2396.
433. Bodiguel, H.; Fretigny, C. *Eur. Phys. J. E* **2006**, 19, 185.
434. Damman, P.; Gabriele, S.; Coppee, S.; *et al.* *Phys. Rev. Lett.* **2007**, 99, 036101.
435. Rowland, H. D.; King, W. P.; Cross, G. L. W.; Pethica, J. B. *ACS Nano* **2008**, 2, 419.
436. Vilmin, T.; Raphael, E. *Europhys. Lett.* **2005**, 72, 781.
437. Vilmin, T.; Raphael, E.; Damman, P.; *et al.* *Europhys. Lett.* **2006**, 73, 906.

Biographical Sketches

Dr. Huagen Peng is a senior research associate in the Polymers Division of the National Institute of Standards and Technology. He received his PhD in Materials Science and Engineering from the University of Michigan in 2004, followed by a postdoctoral research fellowship at the University of California, Irvine. He has deep expertise in positron annihilation lifetime spectroscopy and inelastic neutron scattering and is interested in leveraging these techniques to study solid polymer electrolytes for lithium ion batteries.



Dr. Ryan Nieuwendaal received his PhD in Chemistry from Washington University in St. Louis in 2008 before joining the Polymers Division at the National Institute of Standards and Technology as a NRC Postdoctoral Research Fellow. His research interests include the development of solid-state NMR techniques for materials science, elucidating morphology and structure via solid-state NMR methods, solid-state NMR characterization of heterogeneous polymer blend systems, and the characterization of polymer dynamics via solid-state NMR methods. He is currently applying these solid-state NMR methods to understand the physics of organic semiconducting materials and photovoltaic devices.



Dr. Christopher Soles leads the Energy and Electronics Materials Research Group in the Polymers Division of the National Institute of Standards and Technology (NIST). In 1998 he received his PhD in Materials Science and Engineering from the University of Michigan and first came to NIST as a NRC Postdoctoral Research Fellow. His research interests include thin films and polymers under confinement, polymer dynamics, lithographic patterning, porous materials, organic semiconducting materials, and ion containing polymers for energy storage and delivery. He has published over 110 peer-reviewed publications and received several awards, including the Presidential Early Career Award for Science and Engineering (2006) and the United States Department of Commerce Bronze (2006, 2008) and Silver (2006) Medals, and the Arthur S. Flemming Award from George Washington University (2010). From 2007 to 2010 Dr. Soles served as a Technical Program Chair for the Polymeric Material: Science & Engineering (PMSE) Division of the American Chemical Society.